

Evaluation of 1D/2D river flood simulation with HEC-RAS 5.0.3 considering change of boundary conditions

Maryellen Hearn

August 2017

Supervisor: Professor Dr. Jochen Schanze

Advisor: Dipl. Hydr. Verena Maleska

External Advisor: Associate Professor Ir. Ioana Popescu PhD. Msc.



University of Ljubljana



**UNIVERSITAT POLITÈCNICA
DE CATALUNYA
BARCELONATECH**

For administrative purposes:

TU Dresden Matriculation Number: 4564504

IHE Delft MSc. Number: WSE-FRM.17-07

IHE Delft Student Number: 1005432

This research is completed for the partial fulfilment of requirements for the Master of Science degree at Technische Universität Dresden. The work presented in this thesis was conducted independently and without other sources, other than those attributed. The findings, interpretations, and conclusions expressed in this thesis do not necessarily reflect the views of Technische Universität Dresden, IHE Delft Institute for Water Education, Universitat Politècnica de Catalunya, The University of Ljubljana, or the individual members of the MSc. committee.

Abstract

Amid rising global temperatures, there is a need to better understand changes to flood hazard, and the degree of uncertainty of flood hazard, in the future. To accomplish this, it is necessary to employ, evaluate, combine, and continue to improve the modelling tools and methodologies currently available.

The objectives of this thesis include: 1) an evaluation of a HEC-RAS 5.0.3 1D/2D model with respect to past flood events, 2) the creation of tools and assessment of methodology for running many simulations in HEC-RAS with changing boundary conditions, 3) an assessment of the sensitivity of flood extent and flood depth to changing upstream boundary conditions, 4) an assessment of stability and computation time during these many simulations, and 5) an exploration of how to present flood hazard uncertainty in maps.

A HEC-RAS 1D/2D unsteady flow model was set up for Bennewitz, Germany and subsequently calibrated and validated with past flood events (Task 1). The validated model was used to produce 81 simulations of flood events under climate change conditions, represented by changes to the flow hydrograph at the upstream boundary (Task 2). The display of the uncertainty of flood characteristics were explored using mapping techniques (Task 3).

As a result of Task 1, the model achieved a flood extent Critical Success Indicator (CSI) of 0.844 for the validation event (1 indicates perfect match; 0 indicates no match). Task 2 produced results which indicate that, while flood extent appears relatively insensitive in this particular investigation area, flood depth appears to be quite sensitive to the changing boundary conditions. Task 3 produced two sets of maps highlighting the effect of the classification of flood extent uncertainty and the visual scale of flood depth uncertainty.

Combining the work from all three tasks, this research takes a modest but valuable step toward a better understanding of uncertainty in flood inundation modelling, and how to analyse and represent it in a spatially distributed manner. In addition, it presents the first known example of a HEC-RAS 1D/2D model used as part of a model chain. The results of from this HEC-RAS model will eventually feed into the next module of the model chain, focused on flood damage and vulnerability.

Keywords: Flood hazard, 1D/2D HEC-RAS flood modelling, uncertainty, model chain, climate change, flood hazard mapping

Abstrakt

Durch weltweit steigende Temperaturen ist es notwendig, die Veränderungen der Hochwassergefährdung und den Grad der Unsicherheit der Hochwassergefährdung in Zukunft besser zu verstehen. Um dies zu erreichen, ist es nötig, derzeit verfügbare Modellierungswerkzeuge und -methoden anzuwenden, zu bewerten, zu kombinieren und weiter zu verbessern.

Die Ziele dieser Forschungsarbeit beinhalten: 1) eine Evaluation von ein HEC-RAS 5.0.3 1D/2D Modell in Bezug auf vergangene Hochwasserereignisse, 2) die Erstellung von Werkzeugen und Bewertung von Methoden zur Simulation zahlreicher Hochwasserereignisse mit HEC-RAS unter sich ändernden Randbedingungen, 3) eine Einschätzung der Sensitivität des Ausmaßes der Überflutungsflächen und der Überschwemmungstiefen infolge sich ändernder Randbedingungen, 4) die Bewertung der Stabilität und der Rechenzeit während zahlreicher Simulationen, und 5) eine Untersuchung, wie man Unsicherheiten von Hochwasserereignissen in Karten darstellt.

Für Bennewitz wurde ein HEC-RAS 1D / 2D instationäres Strömungsmodell aufgebaut und anschließend an vergangenen Hochwasserereignissen kalibriert und validiert (Aufgabe 1). Das validierte Modell wurde verwendet, um 81 Simulationen von Hochwasserereignissen unter den Randbedingungen des Klimawandels anzutreiben (Aufgabe 2). Die Abbildung von Unsicherheiten der Hochwassermerkmale wurde anhand verschiedener Darstellungstechniken untersucht (Aufgabe 3).

Als Ergebnis von Aufgabe 1 erreichte das Modell einen Critical Success Indicator (CSI) von 0,844 für das Validierungsergebnis (1 bedeutet perfekte Übereinstimmung, 0 bedeutet keine Übereinstimmung). Aufgabe 2 ergab Ergebnisse, die darauf hindeuten, dass die Hochwassertiefe, während die Hochwasserausdehnung in diesem speziellen Untersuchungsgebiet relativ unempfindlich erscheint, sehr empfindlich gegenüber den sich ändernden Randbedingungen ist. Aufgabe 3 resultierte in zwei Kartensätzen, die den Effekt der Klassifizierung der Hochwasserschutzunsicherheit und der visuellen Skala der Überschwemmungstiefenunsicherheit hervorheben.

Durch die Kombination der Arbeit von allen drei Aufgaben, liefert diese Forschungsarbeit einen bescheidenen, aber wertvollen Schritt hin zu einem besseren Verständnis der Unsicherheit in der Hochwassergefährdungmodellierung und wie man sie in einer räumlich verteilten Weise analysiert und repräsentiert. Darüber hinaus präsentiert sie die erste bekannte Anwendung des HEC-RAS 1D/2D Modells, das als Teil einer Modellkette verwendet wird. Die Ergebnisse dieses HEC-RAS Modells werden schließlich in das nächste Modul der Modellkette übertragen, das auf Hochwasserschäden und Vulnerabilität fokussiert ist.

Stichwörter: Hochwassergefährdung, 1D/2D HEC-RAS Hochwassermodellierung, Unsicherkeit, Modelkaskade, Klimawandel, Hochwassergefährdungskarten.

Acknowledgements

This research would not have been possible without the guidance and support of a great number of people, to whom I would like to express my gratitude. Professor Dr. Jochen Schanze always approached my ideas with optimism and an open mind, but also a critical eye, to guide this work to its full potential. Ms. Verena Maleska has been an invaluable mentor and advisor. Beyond her role in navigating the greater project, she provided a supportive sounding board when my thoughts were flowing and promising suggestions when prospects appeared bleak. Associate Professor Ioana Popescu brought a fresh perspective in her guidance and review of my work. Dr.-Ing. Torsten Heyer provided valuable support for the set up of the 1D/2D HEC-RAS model. Alex Konis and Eklavyya Popat, fellow master's students working on the same greater project, joined me in tackling the day-to-day challenges of data collection, processing, and analysis. They, along with Ms. Maleska and our officemate Ms. Xiaotong Ren, joined me for countless lunches, which served as much-needed breaks from the workday.

I consider myself very lucky to have received technical and motivational support from my fellow Flood Risk Management students, though we have been scattered throughout Europe for our thesis period. I would also like to express my thanks to my dear family and friends, both here in Dresden and around the world, for the various forms of support and encouragement they continue to provide. Lastly, I am grateful to the Erasmus Mundus Flood Risk Management program, and all of the individuals and organisations who have made this experience possible.

Contents

Abstract	iv
Abstrakt	vi
Acknowledgements	viii
1 Introduction	1
1.1 Problem Statement	1
1.2 Research Objectives and Questions	2
1.3 Approach	3
1.4 Limitations	5
1.5 Structure of Thesis	6
2 State of the Art	9
2.1 Hydrodynamic Modelling	9
2.2 Uncertainty in Flood Inundation Modelling	10
2.2.1 Knowledge Uncertainty	10
2.2.2 Inherent Uncertainty	11
2.3 Flood Hazard Maps and Visual Representation of Uncertainty	12
3 Case Study Area and Past Flood Events	15
3.1 Bennewitz, Germany on the Mulde River	15
3.2 Boundary of the Investigation Area	16
3.3 Past Flood Events in the Region	17
3.3.1 Pre-21st Century Flood Events	17
3.3.2 Recent Floods	17
4 Data and Methods	21
4.1 Theoretical Background of HEC-RAS	21
4.1.1 Assumptions	21
4.1.2 1D Unsteady Flow	22
4.1.3 2D Unsteady Flow	22
4.2 Task 1: Model Set Up, Calibration, and Conditional Validation	23
4.2.1 Data Selection, Preparation, and Sources	23
4.2.2 HEC-RAS Software, 1D/2D Approach, and Solvers	26
4.2.3 1D Geometry	27
4.2.4 2D Geometry and Connection to 1D	28
4.2.5 Initial and Boundary Conditions	29
4.2.6 Spacing and Timestep Selection	30
4.2.7 Roughness Sensitivity and Calibration	31
4.2.7.1 Calibration of 1D Component	31
4.2.7.2 Calibration of 2D Component	32
4.2.8 Sensitivity Analysis	33

4.2.9	Model Validation and Simulations for Evaluation	33
4.3	Task 2: Repeated Simulation with Changing Boundary Conditions	34
4.3.1	Overview of Task 2	34
4.3.2	Data Selection, Preparation, and Sources	35
4.3.3	Adjustments to the Geometry of the Model	37
4.3.4	Steps for Preparing and Running Multiple Simulations with Changing Boundary Conditions	38
4.4	Task 3: Visualisation and Display	39
4.4.1	Representation of Uncertainty in Flood Extent	39
4.4.2	Representation of Uncertainty in Flood Depth	39
5	Results	41
5.1	Task 1: Model Set Up, Calibration, and Conditional Validation	41
5.1.1	Model Set Up and Intermediate Model Calibration Results	41
5.1.2	Calibrated Model Results	42
5.1.3	Model Sensitivity	49
5.2	Task 2: Repeated Simulation with Changing Boundary Conditions	51
5.2.1	Extent of Automation of the Process of Changing Boundary Conditions	51
5.2.2	Sensitivity of Simulated Future Flood Characteristics to Changing Boundary Conditions	52
5.2.3	Uncertainty of Flood Extent	54
5.2.4	Uncertainty in Maximum Water Depth	57
5.2.5	HEC-RAS Stability and Computation Effort	60
5.3	Task 3: Visualisation and Display	61
5.3.1	Mapping Uncertainty in Flood Extent	61
5.3.2	Mapping Uncertainty in Flood Depth	61
6	Discussion	63
6.1	Task 1: Model Set Up, Calibration, and Conditional Validation	63
6.1.1	Model Set Up	63
6.1.2	Accuracy	64
6.1.3	Stability, Computational Effort, and Volume Accounting	66
6.1.4	Output Consistency	67
6.1.5	Model Sensitivity	67
6.1.6	Sources of Uncertainty	68
6.2	Task 2: Repeated Simulation with Changing Boundary Conditions	69
6.2.1	Assessment of Automation Tools and Methods for Modelling Changing Boundary Conditions	69
6.2.2	Assessment of Sensitivity of Flood Characteristics to Changing Boundary Conditions	70
6.2.2.1	Flood Extent	70
6.2.2.2	Flood Depth	71
6.2.3	Evaluation of HEC-RAS Model under Changing Boundary Conditions	71
6.2.4	Sources of Uncertainty	71
6.3	Task 3: Visualisation and Display	72
7	Conclusions and Recommendations	75
8.	References	77

Appendices	83
A Geometric Data	85
B Extracting and Processing Data from HEC-RAS	87
C Data Sources for Task 1	91
D Additional Results from Task 1	97
E Additional Discussion Regarding the Influence of DEM Uncertainty on Flood Extent Results from Task 1	111
F Data Sources for Task 2	113
G Python Tools for Task 2	115
H Additional Results from Task 2	117

List of Tables

Table 1.1 WEREX V ensembles which provide simulated future climate time series for the Free State of Saxony	4
Table 3.1 Observed peak discharge at Golzern gauge for calibration and validation events	18
Table 4.1 Manning's n values for 1D calibration of 1D/2D HEC-RAS unsteady flow model	31
Table 4.2 Contingency table for calculating the flood extent using the Critical Success Indicator (CSI)	32
Table 4.3 Manning's n values for 2D calibration of 1D/2D HEC-RAS unsteady flow model	33
Table 4.4 Descriptive statistics of maximum discharge at Golzern for highest peak flood events simulated by HBV hydrologic model under simulated future climate conditions	36
Table 4.5 Points of interest (POIs) for investigation of sensitivity of flood depth to changing upstream boundary conditions under simulated future climate conditions	37
Table 5.1 Calibrated Manning's n values for 1D/2D unsteady flow HEC-RAS model .	42
Table 5.2 Calibration and validation of 1D/2D unsteady flow HEC-RAS model based on peak discharge (Q) at Golzern	43
Table 5.3 Calibration and validation of 1D/2D unsteady flow HEC-RAS model based on CSI	43
Table 5.4 Maximum water surface elevation error for calibrated 1D/2D unsteady flow model at high water marks	47
Table 5.5 Stability, computational effort, and volume accounting for calibrated 1D/2D HEC-RAS unsteady flow model	48
Table 5.6 Output consistency of calibrated 1D/2D HEC-RAS unsteady flow model, for the 2002 event	48
Table 5.7 Sensitivity of calibrated 1D/2D HEC-RAS unsteady flow model to equation sets and boundary conditions, for the 2002 event (1)	50
Table 5.8 Sensitivity of calibrated 1D/2D HEC-RAS unsteady flow model to equation sets and boundary conditions, for the 2002 event (2)	51
Table 5.9 Sensitivity of calibrated 1D/2D HEC-RAS unsteady flow model to equation sets and boundary conditions, for the 2002 event (3)	51
Table 5.10 Descriptive statistics of extent and of maximum water depth for future highest peak flood events simulated by 1D/2D HEC-RAS unsteady flow model under simulated future climate conditions	52
Table C.1 Observed high water marks in Bennewitz from the flood event of 2002	93
Table D.1 Roughness value ranges for 1D/2D HEC-RAS unsteady flow model calibration	98
Table D.2 1D/2D HEC-RAS model performance under varying mesh size	99
Table D.3 1D/2D HEC-RAS model performance under varying timestep (1)	100

Table D.4 1D/2D HEC-RAS model performance under varying timestep (2)	100
Table D.5 1D/2D HEC-RAS unsteady flow model 1D calibration intermediate results, Stage 1	101
Table D.6 1D/2D HEC-RAS unsteady flow model 1D calibration intermediate results, Stage 2 (1)	102
Table D.7 1D/2D HEC-RAS unsteady flow model 1D calibration intermediate results, Stage 2 (2)	103
Table D.8 1D/2D HEC-RAS unsteady flow model 2D calibration Manning's values for Stage 1	104
Table D.9 1D/2D HEC-RAS unsteady flow model 2D calibration intermediate results, Stage 1 (1)	105
Table D.10 1D/2D HEC-RAS unsteady flow model 2D calibration intermediate results, Stage 1 (2)	106
Table D.11 1D/2D HEC-RAS unsteady flow model 2D calibration Manning's n values for Stages 2 and 3	107
Table D.12 1D/2D HEC-RAS unsteady flow model 2D calibration intermediate results, Stage 2	108
Table D.13 1D/2D HEC-RAS unsteady flow model 2D calibration intermediate results, Stage 3	109
Table F.1 Optimal parameter sets for HBV hydrologic model	113

List of Figures

Figure 3.1 Location of Bennewitz, Germany	15
Figure 3.2 The Mulde River and its tributaries	16
Figure 3.3 Boundary of the primary investigation area for assessment of 1D/2D flood inundation for past and future events, including the communities of Bennewitz and Schmölen	17
Figure 3.4 Observed discharge at Golzern gauge for events in 2002, 2006, 2010, 2011, and 2013	19
Figure 4.1 Location of observed high water marks in the main community of Bennewitz for the 2002 event	25
Figure 4.2 2D flow area boundary for 1D/2D HEC-RAS model of Bennewitz, Germany .	28
Figure 4.3 Lateral structure connecting the Mulde River to Bennewitz in HEC-RAS 1D/2D model	29
Figure 4.4 Model combinations, realisations, and parameter sets to simulate future discharge hydrographs	35
Figure 4.5 Simulated 1000 hour future discharge hydrographs from HBV model under simulated future climate conditions, using nine distinct HBV parameter sets .	36
Figure 4.6 Location of points of interest (POIs) for investigation of sensitivity of flood depth to changing upstream boundary conditions under simulated future climate conditions	37
Figure 5.1 Maximum water surface elevation and maximum water depth in investigation area for 2002 event, simulated by calibrated 1D/2D unsteady flow HEC-RAS model	44
Figure 5.2 Maximum water surface elevation and maximum water depth in investigation area for 2013 event, simulated by calibrated 1D/2D unsteady flow HEC-RAS model	45
Figure 5.3 Flood extent of 2002 event simulated by 1D/2D unsteady flow HEC-RAS model compared to observed flood extent	46
Figure 5.4 Flood extent of 2013 event simulated by 1D/2D unsteady flow HEC-RAS model compared to observed flood extent	46
Figure 5.5 Water surface elevation at the high water marks in the 2D flow area throughout the 2002 event, as simulated by 1D/2D HEC-RAS model	47
Figure 5.6 Histograms of maximum water depth at each of the points of interest (POIs) in the 2D flow area of 1D/2D HEC-RAS model under changing boundary conditions	53
Figure 5.7 Sensitivity of flood extent to the upstream boundary condition for all 81 1D/2D HEC-RAS unsteady flow simulations	54
Figure 5.8 Sensitivity of flood extent to the upstream boundary condition for the 27 model combination 8 1D/2D HEC-RAS unsteady flow simulations	55
Figure 5.9 Sensitivity of flood extent to the upstream boundary condition for the 27 model combination 9 1D/2D HEC-RAS unsteady flow simulations	56

Figure 5.10 Sensitivity of flood extent to the upstream boundary condition for the 27 model combination 9 1D/2D HEC-RAS unsteady flow simulations	57
Figure 5.11 Descriptive statistics of maximum water depth for all 81 1D/2D HEC-RAS unsteady flow simulations	58
Figure 5.12 Standard deviation per pixel of maximum water depth for all 81 1D/2D HEC-RAS unsteady flow simulations	59
Figure 5.13 Standard deviation per pixel of maximum water depth for model combination 8 1D/2D HEC-RAS unsteady flow simulations	60
Figure 5.14 Comparison of means of representing flood extent based on results from 1D/2D HEC-RAS unsteady flow model	61
Figure 5.15 Comparison of means of representing flood extent based on results from 1D/2D HEC-RAS unsteady flow model	62
 Figure A.1 HEC-RAS 1D/2D model geometric data for Task 1	85
Figure A.2 HEC-RAS 1D/2D model geometric data for Task 2	86
 Figure B.1 ArcGIS ModelBuilder tool to convert TIFs to polygons	88
Figure B.2 ArcGIS ModelBuilder tool to fill gaps and clip to 2D area	89
Figure B.3 ArcGIS ModelBuilder tool to calculate hits, misses, and false positives to support the CSI calculation	89
Figure B.4 ArcGIS ModelBuilder tool to extract tables for CSI calculation	90
 Figure C.1 DEM of Bennewitz from 2009, with building footprints added	91
Figure C.2 DEM of Bennewitz adjusted to better represent elevation during the flood event of 2002	92
Figure C.3 DEM of Bennewitz adjusted to better represent elevation during the flood event of 2002	92
Figure C.4 Shift of the location of the LS6 observed high water mark	94
Figure C.5 Observed 2002 flood extent for calibration of 1D/2D HEC-RAS unsteady flow model	94
Figure C.6 Observed 2013 flood extent for calibration of 1D/2D HEC-RAS unsteady flow model, with no gaps filled.	95
Figure C.7 Observed 2013 flood extent for calibration of 1D/2D HEC-RAS unsteady flow model, with gaps filled.	95
 Figure D.1 Simulated maximum water surface elevation in 2D flow area of 1D/2D HEC-RAS unsteady flow model for flood event in 2006	110
Figure D.2 Simulated maximum water surface elevation in 2D flow area of 1D/2D HEC-RAS unsteady flow model for flood event in 2010	110
Figure D.3 Simulated maximum water surface elevation in 2D flow area of 1D/2D HEC-RAS unsteady flow model for flood event in 2011	110
 Figure H.1 1D/2D HEC-RAS unsteady flow model effect of wall along Wurzen on simulated maximum water surface elevation	118

List of Abbreviations

1D/2D	1 Dimensional-2 Dimensional, here referring to the dimensionality of a coupled hydrodynamic model
AR4	IPCC Fourth Assessment Report (2007)
AR5	IPCC Fifth Assessment Report (2013/2014)
ATKIS	Amtlichen Topographisch-Kartographischen Informationssystems (Official Topographical-Cartographical Information System)
CSI	Critical Success Indicator
CSV	Comma-Separated Value file format
DEM	Digital Elevation Model
DLM	Digitales Landschaftsmodell (Digital Landscape Model)
FEMA	U.S. Federal Emergency Management Agency
GCM	Global Circulation Model
HBV	Hydrologiska Byråns Vattenbalansavdelning (Hydrological Agency's Water Balance Department)
HEC-RAS	Hydraulic Engineering Center's River Analysis System
HTAB	Hydraulic Table, here referring to one of the tables of hydraulic parameters in the HEC-RAS geometry editor
HWSK	Hochwasserschutzkonzept (Flood Protection Concept) is a project to assess all of the rivers in Saxony regarding flood hazard and flood protection.
IPCC	Intergovernmental Panel on Climate Change
LfULG	Sächsisches Landesamt für Umwelt, Landwirtschaft, und Geologie (Saxony's Agency for Environment, Agriculture, and Geology)
LHWZ	Landeshochwasserzentrum (Saxon Flood Center)
LTV	Landestalsperrenverwaltung des Freistaates Sachsen (State Reservoir Administration of Saxony)

MAE	Mean Absolute Error
POI	Point of Interest
RCM	Regional Climate Model
RMSE	Root Mean Square Error
SRES	Special Report on Emissions Scenarios (2000)
TAR	IPCC Third Assessment Report (2001)
TIF	Tagged Image File Format, here referring to a particular format in which raster data is produced by the HEC-RAS model
TXT	Text file format
UNISDR	United Nations International Strategy for Disaster Reduction
WEREX V	A version of the statistical method WETTREG focused on the Free State of Saxony
WETTREG	A statistical method for the calculation of climatic variables developed in Germany
WSEL	Water Surface Elevation

1. Introduction

1.1. Problem Statement

Flooding is one of the most significant hazards experienced worldwide (Opperman *et al.*, 2009; Tingsanchali, 2012; Di Baldassarre *et al.*, 2013; Traver, 2014). Particularly amid rising global temperatures, there is a need to increase our understanding of changing flood hazard and risk in the future. This sentiment was clearly indicated in the Sendai Framework for Disaster Risk Reduction 2015-2030 (UNISDR, 2015). According to a study focused on river flooding under varying projected climate conditions, there is a clear positive relationship between global temperature increase and the increase in flood risk, with the largest increases in Asia, the U.S., and Europe (Alfieri *et al.*, 2016).

Flood modelling and the resulting flood hazard maps support the development, planning, and implementation of flood risk reduction measures and policy. The 2007 adoption of the EU Floods Directive (2007/60/EC), which includes a requirement for flood hazard and flood risk maps, is one example of a high-level policy shift toward a flood risk management approach, as opposed to traditional flood protection (de Moel *et al.*, 2009). Flood risk can be defined as the probability of negative consequences due to flooding (Schanze, 2006). It emerges at the intersection of 1) flood hazard, the probability of a potentially harmful event, and 2) flood vulnerability, those characteristics of elements which determine the potential to be harmed (Schanze, 2006; Blanco-Vogt & Schanze, 2014). This intersection is referred to as exposure, and thus flood risk depends on the exposure of vulnerable elements to a flood hazard (Schanze, 2006). Wood (2011) claims that risk is not only a function of exposure, but also a function of the choices made by individuals and societies. Given that water infrastructure has a typical lifetime of 30-200 years, adaptive, long-term planning and management approaches are needed in the design and operation of flood- and other water-related infrastructure (Gersonius *et al.*, 2013).

As part of the process of understanding potential changes to flood hazard in the long-term future, there is an ongoing need for development, expansion, and evaluation of hydrodynamic modelling tools and how they can incorporate potential climate change at the local level. In September 2016, the most recent version (5.0.3) of the Hydrologic Engineering Center's River Analysis System (HEC-RAS) software was released. HEC-RAS is a free, publicly available tool developed and supported by the United States Army Corps of Engineers. In February 2016, the official release of HEC-RAS 5.0 expanded the software package to include for 2D and 1D/2D capabilities, as only 1D was previously available. HEC-RAS is a well-respected tool in the industry, and there is a wealth of research evaluating and employing previous versions of the software in river and flood modelling. Given its recent release, HEC-RAS 5.0.3 capabilities, have been used for and examined through relatively few research publications to date, particularly the 1D/2D capabilities.

1. Introduction

Like most if not all hydrodynamic modelling software, a HEC-RAS model requires certain input data and computational decisions from the modeller and produces a single simulation result file. This aligns with the traditional use of hydrodynamic model simulations, when practitioners are presented with a single or small number of deterministic output data sets. However, in recent decades there has been an increase of interest, both from scientists and decision-makers, for the representation of uncertainty modelling. Pappenberger & Beven (2006) discuss the primary reasons for resistance to introducing uncertainty representation in water resources research in general, concluding that all said reasons are ultimately untenable. According to their research and discussions with scientists and practitioners alike, there is an overwhelming need and responsibility to address uncertainty in the basic process of modelling and the communication of results.

There are numerous sources of uncertainty in flood modelling, and climate change has been added to the list. This source of inherent uncertainty about the future of the planet, and how it manifests itself at the local level, requires further examination. In some systems, climate change, and the modelling process used to project future climate characteristics, will play a significant role in understanding the range of potential future flood hazard levels. In other systems, the influence of changing climate characteristics will play a less prominent role than other sources of uncertainty.

This research presents an early example of evaluating HEC-RAS 5.0.3 1D/2D with respect to past flood events. This research also presents the first known example of HEC-RAS 5.0.3 1D/2D as part of a model chain, incorporating the flow hydrographs produced from a climate model and hydrologic model cascade into the upstream boundary conditions of the HEC-RAS model.

1.2. Research Objectives and Questions

This research project includes five objectives, guided by the associated questions.

Objective 1: Set up a 1D/2D HEC-RAS model for the study area, calibrate the model, and perform conditional validation for a past event. Research question 1: *How accurately does the calibrated HEC-RAS 1D/2D model represent the flood extent and water surface elevation from recent flooding events?*

Objective 2: Identify and assess a method for automating HEC-RAS simulations and post-processing for medium-large numbers (20-1000) of artificial flood events, each with a unique discharge hydrograph for the upstream boundary condition. Research question 2: *How might one automate the simulation and/or post-processing of large numbers of flood events with changing upstream boundary conditions, and how efficient would it be to automate these processes?*

Objective 3: Assess the sensitivity of flood characteristics (flood extent and depth) to different climate conditions within the A1B scenario (see Section 1.3 for clarification of these scenarios). Research question 3: *How sensitive are flood characteristics (flood extent and depth) to different simulated climate conditions within the A1B scenario?*

Objective 4: Assess HEC-RAS model performance when conducting numerous simulations with changing boundary conditions. Research question 4: *How does the simulation of changing boundary conditions affect stability and computational effort of HEC-RAS?*

Objective 5: Produce flood hazard maps which represent the spatial distribution of flood extent and depth uncertainty. Research question 5: *How can the uncertainty of flood extent and depth be represented in a spatially distributed manner?*

1.3. Approach

There are three principle tasks of this research: 1) model set up, calibration, and conditional validation, 2) repeated simulation with changing boundary conditions, 3) visualisation and display. Task 1 addresses objective 1; Task 2 addresses objectives 2, 3, and 4; and Task 3 addresses objective 5. Before introducing the tasks and the case study to which the methodology was applied, the following subsection describes the context of this research within a greater, external research effort.

Context within Model Chain

This research is affiliated with a project underway at the Competence Center for Scalable Data Services and Solutions Dresden/Leipzig (ScaDS), a collaboration between the Technical University of Dresden, Leipzig University, Max Planck Institute for Molecular Cell Biology and Genetics, and the Leibniz Institute of Ecological Urban and Regional Development. One primary goal of the greater project is to create a model chain from climate change ensembles to flood impacts. The project incorporates the WEREX V regional climate projections for the Free State of Saxony. Given data and climate projections available at the time, the two climate scenarios used for the WEREX V project were the A1B scenario from the 2000 Special Report on Emissions Scenarios (SRES) (Nakicenovic *et al.*, 2000) and the E1 scenario from the ENSEMBLES project (van der Linden & Mitchell, 2009). The WEREX V projections include downscaled meteorological characteristics from Global Circulation Models (GCMs) and Regional Climate Models (RCMs), using a version of the statistical method WETTREG (Kreienkamp *et al.*, 2011). Table 1.1 presents the 12 combinations of GCM and RCM ensembles fed into the WEREX V empirical statistical downscaler (ESD), and the scenario on which each model combination was run. Additional information regarding the GCMs is available from the IPCC Data Distribution Centre (Intergovernmental Panel on Climate Change, 2016). Each of the 12 GCM/RCM combinations produced ten distinct realisations of climate characteristics. The total of 120 climatological data sets are known as the WEREX V ensemble climate data. As part of the greater project under ScaDS, these WEREX V data are currently being fed into a hydrologic model called Hydrologiska Byråns Vattenbalansavdelning (HBV) (Swedish Meteorological and Hydrological Institute, 2017). The HBV model produced flow hydrographs for the upstream boundary conditions of the HEC-RAS model at Golzern. The hydrologic component of this model chain is ongoing, performed by Ms. Verena Maleska, and only early results from the HBV model were available for incorporation in the research presented in this thesis. The HBV model and first optimisation run results were selected for testing HEC-RAS as one member for the hydrodynamic module within the model chain.

1. Introduction

Table 1.1.: WEREX V ensembles which provide simulated future climate time series for the Free State of Saxony

ID	Type	GCM	RCM	ESD	Scenario
1	GCM → ESD	ECHAM5 (Run 1)	-	WEREX V	E1
2	GCM → ESD	HadCM3C (Run 1)	-	WEREX V	E1
3	GCM → ESD	HadGEM2 (Run 1)	-	WEREX V	E1
4	GCM → ESD	ECHAM5 (Run 1)	-	WEREX V	A1B
5	GCM → ESD	ECHAM5 (Run 2)	-	WEREX V	A1B
6	GCM → ESD	ECHAM5 (Run 3)	-	WEREX V	A1B
7	GCM → ESD	HadCM3C (Run 1)	-	WEREX V	A1B
8	GCM → ESD	HadGEM2 (Run 1)	-	WEREX V	A1B
9	GCM → RCM → ESD	ECHAM5 (Run 3)	RACMO	WEREX V	A1B
10	GCM → RCM → ESD	ECHAM5 (Run 3)	REMO	WEREX V	A1B
11	GCM → RCM → ESD	ECHAM5 (Run 1)	CLM	WEREX V	A1B
12	GCM → RCM → ESD	ECHAM5 (Run 2)	CLM	WEREX V	A1B

Each of the 12 model combinations produced ten distinct realisations of downscaled climate data to be fed into the hydrologic model.

The SRES scenario families are referenced in the International Panel on Climate Change (IPCC) Third Assessment Report (TAR, 2001) and Fourth Assessment Report (AR4, 2007), while the 2010 Representative Concentration Pathways (RCP) were adopted in the most recent Fifth Assessment Report (AR5, 2013/2014). The SRES details four storylines: A1, A2, B1, and B2; each storyline contains at least one Scenario Group: A1F1, A1T, A1B, A2, B1, and B2; and each Scenario Group has two scenarios (Nakicenovic *et al.*, 2000). The storylines describe social and economic shifts bundled with emission projections. The RCPs, on the other hand, are focused on the concentration levels in the atmosphere and the radiative forcing (e.g. change of energy in the atmosphere, global temperature increase). In an effort to provide continuity, the following pairs are typically considered to be similar: SRES A1F1 and RCP 8.5; SRES A1B and RCP 6.0; SRES B1 and RCP 4.5 (Melillo *et al.*, 2014). The lowest RCP scenario, RCP 2.6, is much lower than any of the SRES scenarios, as it includes strategies for negative carbon dioxide emissions before 2100 (Melillo *et al.*, 2014). The E1 scenario was introduced as part of the European Commission's ENSEMBLES project. It is described as a mitigation scenario, representing a future in which atmospheric concentrations are stabilised at 450 parts per million carbon dioxide equivalent after 2100 (specifically by 2140) (van der Linden & Mitchell, 2009). Therefore, the methodology for developing the E1 scenario is more similar to that of the RCPs than of the SRES.

For the purposes of this thesis, only model combinations 8, 9, and 10 (bolded) in Table 1.1 were considered, all of which are based on the A1B SRES scenario. With regard to the WEREX V data sets, Bernhofer *et al.* (2016) found that these three combinations, along with that which includes CLM (see Table 1.1) best reproduced the statistical characteristics (magnitude, exceedance days, and periodicity) of heavy precipitation in the past.

Task 1: Model Set Up, Calibration, and Conditional Validation

The study area is represented in an unsteady HEC-RAS 5.0.3 model, using a coupled 1D/2D approach. HEC-GeoRAS 10.2 was used in combination with ArcGIS for Desktop 10.4.1 for the creation of the HEC-RAS geometry data. Roughness values for the 1D channel and overbanks were calibrated using observed stage, discharge, and high water marks. Roughness values for the 2D flow area were calibrated using observed high water marks and flood extent. Validation was based on observed discharge values in the 1D component of the model and flood extent in the

1. Introduction

2D area.

Task 1 addresses Objective 1.

Task 2: Repeated Simulation with Changing Upstream Boundary Conditions

Once the model was calibrated and validated, the upstream boundary conditions were adjusted to represent a variety of possible discharge values, based on the climate ensembles and subsequent hydrologic model realisations delivered by the model chain. No other boundary conditions or other inputs were adjusted for these repeated simulations. This task includes the development of support tools, principally using Python 2.7, to aid in the creation and processing of input and output files to and from HEC-RAS. Hydrodynamic simulations were performed in HEC-RAS for an 8 day period around the maximum peak discharge event for each 101 year simulation, producing a total of 81 simulation result files.

Task 2 addresses Objectives 2, 3, and 4.

Task 3: Visualisation and Display

The results from Task 2 were used to examine three components of the visual representation of uncertainty of flood characteristics in maps. This task is viewed as an initial exploratory exercise. It did not incorporate a thorough analysis of end-user groups and needs, though it was guided by findings from recent studies in flood uncertainty map design. The two components of map making briefly explored in this task are:

- Representation of the number of times each cell is wetted by a simulation
- The effect of water depth scale in comparing standard deviation of maximum water depth for the 27 simulations from one model combination compared to the full 81 simulations

Task 3 addresses Objective 5.

1.4. Limitations

The limitations of this research and methodology are organised by task.

Task 1: Model Set Up, Calibration, and Conditional Validation

The following limitations must be taken into consideration with regard to the HEC-RAS 1D/2D unsteady flow model produced and evaluated in Task 1:

- The calibration effort for the model produced by Task 1 was particularly limited in terms of access to observed data.
- The model is applicable only to the case study area and conditional validation refers to its validation for the 2013 event. There is, of course, no way to validate the model for future events.
- In order to follow the methodology used for this research effort, this task requires not only HEC-RAS 5.0.3, but also ArcGIS 10.4.1, Python 2.7, and DSSVue 2.0.1 (for visualisation of simulated results compared to observed discharge during calibration).
- A list of the principle sources of uncertainty for this model can be found in Section 6.1.6.

1. Introduction

Task 2: Repeated Simulation with Changing Boundary Conditions

The following limitations must be taken into consideration with regard to the methodology and analysis from Task 2:

- This task depends on access to a calibrated model of the catchment in question, such as that produced by Task 1.
- In order to follow the methodology used for this research effort, this task requires access to HEC-RAS 5.0.3, Python 2.7, and ArcGIS 4.0.1.
- The methodology developed for changing boundary conditions is not directly transferable to changing other components of the model, such as the Manning's n value. The scripts could likely be adapted to manage other components (which may require the creation of and editing of HDF files through Python, perhaps through the h5py package), though this was not proven as part of this research effort.
- The methodology developed and employed in this task is a combination of functional components, but these components have not been integrated into a polished whole or a fully automated process. The user is still needed to run the scripts individually and monitor intermediate results.
- Given that HEC-RAS can hold no more than 99 unique plans at any given time, the process would need to be repeated multiple times if more than 99 simulations are required. This barrier could be overcome with additional automation tools, such as the HECRASController API. However, engaging the HEGRASController API, either through Python or VBA, was not selected for this particular effort, given the scale of the project.
- The results from this task are limited by the available climatological data sets available from upstream on the model chain. For example, only model combinations using the A1B scenario were available for introduction into the HEC-RAS model.
- The results from this task are not comparable to past events, as they represent future conditions. In addition, the model for Task 2 differs slightly from Task 1, as described in Section 4.3.3.

Task 3: Visualisation and Display

The following limitations must be taken into consideration with regard to the exploration of presenting the spatial distribution of uncertainty in Task 3:

- This task has no systematic external review or evaluation component. The purpose of this task is to provide a dedicated space for exploring techniques for displaying the results from Task 2 in a distributed manner. In order to provide recommendations based on this task, a future evaluation of the various techniques and their effectiveness for communication to specific audiences must first be performed.
- This task is limited to components of map symbology and how it may shift the viewer's focus or otherwise change his or her perception of the data. This task does not investigate questions of the colour palette, selection of what data to include on a map, or how different sources of uncertainty might be combined in a map.

1.5. Structure of Thesis

This work is divided into seven chapters, followed by eight appendices. Section 1 of this thesis introduces the research effort and selected approach. Section 2 provides a review of the state of

1. Introduction

the art in terms of hydrodynamic modelling, types of uncertainty in hydrodynamic modelling, and the representation of uncertainty in hydrodynamic models. Section 3 provides introduces the case study area and past flood events. Section 4 details the data acquired for this research and the methodology followed. Section 5 presents the results of the research. Section 6 discusses the results, including challenges experienced throughout the process. Section 7 presents a distillation of research conclusions and offers recommendations for future research.

2. State of the Art

2.1. Hydrodynamic Modelling

Hydrodynamic modelling is a principle tool employed for assessing and managing flood hazard. Compared to other computer-based models used in environmental sciences, hydrodynamic models require relatively little input data (Bates *et al.*, 2014). Models require physical information about the riverbed, banks, and floodplain (often derived from a digital elevation model, along with friction parameter values); upstream and downstream boundary conditions (such as discharge hydrographs, stage hydrographs, or normal depth); and initial conditions (water levels). For flood hazard estimation, a model is expected to output at least water surface elevation (and/or depth) and flood extent. Many models also output flow velocity, duration of inundation, and other variables.

The level of complexity of hydrodynamic models varies greatly depending on the specific purpose, the skill set of the modeller, and available data. Numerous publications discuss selection of the most appropriate model approach, such as 1D, 2D, or coupled 1D/2D, for a particular application (Kalyanapu *et al.*, 2011; Falter *et al.*, 2013; Bates *et al.*, 2014). Along with selecting the model's dimensionality, the modeller will typically opt for additional simplifications of the fluid dynamics equations. In making decisions about the complexity of the model, experts seek to follow Occam's razor, proposed by William of Occam in the 14th century (Young *et al.*, 1996). As it relates to environmental modelling, the guidance suggests that a model should be as simple as possible without omitting a crucial component of the system of study. The general concept has resonated under many names, such as the Keep It Simple Stupid (KISS) principle and the principle of parsimony, but the avoidance of unnecessary complexity in problem-solving underscores all of them.

Among a host of available hydrodynamic modelling software, HEC-RAS 5.0.3 was selected for this study. Previous versions of HEC-RAS have been thoroughly represented in hydrodynamic modelling studies, including those with a strong focus on quantifying model uncertainty (Smemoë *et al.*, 2007; Elmer *et al.*, 2012; Jung *et al.*, 2014; Jung & Merwade, 2015; Faghih *et al.*, 2017). A study by Quiroga *et al.* (2016) presents one of the first studies using the HEC-RAS 2D capabilities (pre-release version), simulating flooding in the Bolivian Amazon region in 2014. In 2015, the authors of this study led a session to present a tool to automate HEC-RAS input data for considering uncertainties in flood modelling at the IAHR World Congress (Quiroga *et al.*, 2015). Given the recent release of the HEC-RAS 5, relatively few studies have been published with the new software. Along with the new version of the software, HEC released the results of the benchmarking study, which demonstrates that HEC-RAS 2D modelling capabilities perform to a similar level as the 2D models evaluated in the U.K. Environmental Agency research report from August 2013 (Brunner, 2016a). The tests for benchmarking, used in both of these reports,

2. State of the Art

were developed by the U.K. Joint Department for Environment Food and Rural Affairs (Defra), under Defra's Flood and Coastal Erosion Risk Management Research and Development program (Brunner, 2016a). Though publications using HEC-RAS 5.0.3 are limited, this version was used to compare 1D vs 2D prototype models of a portion of the Mississippi Delta with regard to hydraulics and sediment transport characteristics under multiple sea level conditions in the Gulf of Mexico (Olivier, 2017).

2.2. Uncertainty in Flood Inundation Modelling

The U.S. National Research Council provides a relatively broad definition of uncertainty: "Uncertainty is a general concept that reflects our lack of sureness about something or someone, ranging from just short of complete sureness to an almost complete lack of conviction about an outcome" (National Research Council, 2000; HR Wallingford, 2002). Sources of uncertainty in modelling are frequently categorised into those which could theoretically be measured versus those which are inherently unknowable, unmeasurable, irreducible. However, different authors have labelled these categories with a number of different terms over time.

One of the early authors to propose this distinction in written form was Frank H. Knight, writing within the context of economics. Knight used the terms "measurable uncertainty" and "risk proper" to refer to the first category, and "unmeasurable uncertainty" and "true uncertainty" to refer to the second category (Knight, 1921). In 2002, HR Wallingford employed the terms "knowledge uncertainty" and "natural variability" for these two categories, respectively (HR Wallingford, 2002). The same publication also includes a list of other terms used for the categories around the turn of the 21st century. The terms "epistemic uncertainty" and "aleatoric (or aleatory) uncertainty" have been adopted for the respective categories by a number of authors (Hall & Strutt, 2003; Apel *et al.*, 2004; Der Kiureghian & Ditlevsen, 2009). In their interpretation of these concepts, Apel *et al.* (2004) specify that aleatory uncertainty includes both natural and anthropogenic variability.

For this work, the first category will be referred to as "knowledge uncertainty." The second category will be referred to as "inherent uncertainty." The term "inherent" is often used to describe the second group, though not often chosen as the categorical title. It was selected as the title of the category for this work so as to avoid the implication that all sources of uncertainty within this category are based on chance, on probability, as might be understood from the term "aleatory" or "natural variability." Rather, the heart of this category is the fact that, no matter how much you know about the present and past, the future is *inherently* uncertain.

These two categories are not rigid, and thus can become blurred and difficult to distinguish, as demonstrated by Der Kiureghian & Ditlevsen (2009). For example, uncertainty around weather and climate is typically treated as inherent uncertainty (specifically natural or anthropogenically-influenced variability) within the discipline of flood risk management, but knowledge uncertainty within the discipline of climate simulation (Gouldby & Samuels, 2005). The sources of uncertainty addressed in Section 2.2.1 are considered primarily in the category of knowledge uncertainty, and those in Section 2.2.2 primarily in that of inherent uncertainty. However, both include components that could be argued as belonging to the other category, depending on the context.

2.2.1. Knowledge Uncertainty

The four major categories of knowledge uncertainty sources in hydrodynamic modelling identified by Bates *et al.* (2014) include: 1) input data, 2) observed data for estimating parameters and simulation likelihoods, 3) simplifications of the model structure, and 4) conceptual model uncertainty, given that validation data is usually sparse, and different model classes may fit this data equally well (a phenomenon known as equifinality). According to Faghih *et al.* (2017), uncertainty analyses around flood inundation modelling tend to focus

2. State of the Art

primarily on the parameters, model structure, and assumptions, but the component with the largest impact is instead the flood frequency analysis (which determines the upstream boundary condition). Jung & Merwade (2015) demonstrated that the relative influence of variables depends in part on the valley shape and can also depend on particular sub-ranges of other variables. In their study, the U-shaped valley was most sensitive to uncertainty from topography, whereas the V-shaped valley was most sensitive to uncertainty of the upstream boundary condition (discharge).

It is good modelling practice to perform a sensitivity analysis as a prerequisite to calibration so as to identify the appropriate calibration parameters (van Waveren *et al.*, 1999). Likewise the uncertainty analysis may be conducted after calibration, as an attempt to quantify remaining uncertainties from a variety of sources (van Waveren *et al.*, 1999). The body of literature around uncertainty continues to grow, and with it new techniques arise and old techniques evolve (Faghih *et al.*, 2017). Many of these techniques employ Monte Carlo methods, Bayesian probabilities, the Generalised Likelihood Uncertainty Estimation (GLUE, which incorporates Monte Carlo and Bayesian theory), the Gaussian process, fuzzy sets, and other mathematical and statistical techniques for managing likelihood (Jung *et al.*, 2014; Faghih *et al.*, 2017).

Quantification of knowledge uncertainty of hydrodynamic models has been explored in a variety of capacities. Many analyses focus on the uncertainty of the hydrodynamic model input values, most often the Manning's n, discharge, and topography (Jung *et al.*, 2014). For example, Aronica *et al.* (2002) and Weichel *et al.* (2007) use the Monte Carlo method to sample from a distribution of feasible roughness values; Smemoë *et al.* (2007), Kalyanapu *et al.* (2011) and Faghih *et al.* (2017) explore the effects of changing upstream discharge, the first by varying the Curve Number (in the hydrologic modelling process), the second based on a Monte Carlo sampling from a uniform distribution, and the third using a bootstrap analysis for peak-streamflow frequency curves; Cook & Merwade (2009) examine differences in accuracy based on LiDAR versus other topographical approaches, as well as differences in the geometric description and modelling approach. Yan *et al.* (2015) examine the spatial resolution and vertical accuracy of a number of low-cost sources of elevation data, particularly focused on its influence in flood modelling. Some analyses examine the combined effects of multiple sources of uncertainty within the hydrodynamic model, such as Jung *et al.* (2014) and Jung & Merwade (2015), which stress the interdependence of the input variables.

2.2.2. Inherent Uncertainty

As discussed in Section 2.2, inherent uncertainty is that which is irreducible. A typical example is the natural variability associated with the timing of extreme events, often represented by a recurrence interval (e.g. a flood expected to occur on average once every 100 years) or annual probability (e.g. 1% annual chance flood). However, there are also non-probabilistic, inherent uncertainties. For example, it is inherently uncertain when and how a flood risk system will change in the future due to external drivers (climate change, land use change, etc.). As this research is focused on the influence of climate change on flood hazard, this section will focus heavily on climate change as a source of inherent uncertainty.

It is widely accepted in the scientific community that the climate, on a global scale, is experiencing unprecedented change (Hartmann *et al.*, 2013; Milly *et al.*, 2015). However, when it comes to incorporating climate change into modelling and decision-making processes, opinions are diverse. Since the publication of Milly *et al.* (2008), titled *Stationarity is Dead: Whither Water Management?*, there has been healthy academic conversation around stationary models versus non-stationary models and how to consider climate change as a source of uncertainty for water resources modelling and management (Milly *et al.*, 2008; Lins, 2012; Serinaldi & Kilsby, 2015; Milly *et al.*, 2015). For the purposes of this study, climate change is incorporated into the modelling process specifically through the influence of climate projections on upstream boundary conditions.

2. State of the Art

Relatively few studies are designed to propagate future climate change from GCMs and RCMs, through hydrologic models, and all the way to hydrodynamic models. Lehner *et al.* (2006) and New *et al.* (2007) incorporate global model data for producing discharge levels in Europe (126 drainage basins and sub-basins) and the River Thames, respectively, but these publications do not extend to hydrodynamic modelling. Muis *et al.* (2015) present an example of propagating global climate ensembles through the hydrologic and hydrodynamic components of GLOFRIS to produce low-resolution river-induced inundation results for all of Indonesia. Schanze *et al.* (2015) explore the changing future of flood risk in the Elbe River basin, including discussion of potential future scenarios, downscaling methods, coupled hydrologic-hydrodynamic modelling techniques, and changes to flood damage and risk. Also applied to the Elbe River basin, Merz *et al.* (2016) present a model chain consisting of a hydrologic model, a 1D/2D hydrodynamic model, and a flood loss model.

Potential climate change is not the only external factor which affects long-term planning in flood risk management, and it is not necessarily the dominant driver affecting the flood risk system for any given locale. Population change and land use change play a significant role in determining flood risk, not to mention other socioeconomic conditions, technological advances, and current policy (Schanze, 2012). When combining climate projections with projections of other relevant trends, researchers and practitioners can explore a much more comprehensive view of possible futures and possible flood risk estimations. For example, Nicholls *et al.* (1999) explore the effect of combined simultaneous changes in global sea-level rise and subsidence, increasing coastal population, and improving flood defence standards on flooding due to storm surge and wetland loss due to sea level rise. The importance of any given external factor in influencing the flood risk system will be different over time and space, and further research, both on the impact of individual external factors and on combinations of external factors, is needed.

From a study comparing the relative influence of external factors on flood risk in the Mulde basin, which is also the study area examined in this thesis, findings suggest that climate-induced changes to the flood hazard are important, but not a dominant factor in changes to flood risk (Elmer *et al.*, 2012). Rather, in this study, land use change, particularly urban sprawl, is found to be the main driver of flood risk change (Elmer *et al.*, 2012). It should be noted that this particular study a) was focused on the influence of drivers on flood *risk* rather than specifically on flood *hazard*, b) it includes only one climate scenario (based on SRES emission scenario A1B) compared to a reference scenario, and c) the combined effects of different drivers were not considered.

2.3. Flood Hazard Maps and Visual Representation of Uncertainty

According to the European Exchange Circle on Flood Mapping (EXCIMAP), often multiple recurrence intervals are included on the same flood hazard map, depending on the purpose and resources available (Martini & Loat, 2007). Under the Floods Directive (Directive 2007/60/EC), flood hazard maps are required for all member states of the European Union (European Union, 2007). According to Article 6, the hazard maps must include: "a) floods with a low probability, or extreme event scenarios; b) floods with medium probability (likely return period of ≥ 100 years); c) floods with a high probability, where appropriate" (European Union, 2007). However, beyond the recognition of uncertainty around the timing of flood events (represented by the recurrence interval), rarely is uncertainty represented in flood hazard maps designed for practical use.

Some studies have begun to examine the potential benefits and barriers to including a visual representation of uncertainty in a flood map for practical use. The basic technology and knowledge required to explore such maps for practical use exists, and this is demonstrated by the numerous quality examples in the academic literature (Aronica *et al.*, 2002; Romanowicz & Beven, 2003; Smemo *et al.*, 2007; Kalyanapu *et al.*, 2011; Jung *et al.*, 2014; Faghih *et al.*,

2. State of the Art

2017). Smemoe *et al.* (2007) demonstrate a technique for incorporating flood model uncertainty within the context of the U.S. Federal Emergency Management Agency (FEMA) flood maps. While recognising institutional barriers to adoption, the study is particularly geared toward enabling the creation of graduated flood insurance rates (Smemoe *et al.*, 2007). Vause (2013) focuses on how to design the most effective uncertainty-inclusive flood hazard maps based on end-user needs. This approach is in line with the sentiment voiced by Morss *et al.* (2005), which encourages increased incorporation of decision-making needs into scientific research and development process. Morss *et al.* (2005) also highlight the diversity among potential users of flood hazard and flood risk tools, and particularly their unique needs and constraints with respect to implementing those tools.

Despite the advancements in flood hazard uncertainty quantification in academia, the distributed (i.e. per pixel) representation of uncertainty in a flood hazard map has not found its way into mainstream practical application. Traditionally, and usually still today, flood hazard maps present deterministic flood model results (Smemoe *et al.*, 2007; Merwade *et al.*, 2008; de Moel *et al.*, 2009). This means that, for a particular flood recurrence interval, there is one hard boundary representing where the flood is estimated to reach (flood extent), and each pixel within that boundary may represent one result value for depth, velocity, or other characteristics of the flood.

3. Case Study Area and Past Flood Events

3.1. Bennewitz, Germany on the Mulde River

The approach in Section 1.3 was applied to a study area along the Mulde River in the Free State of Saxony, Germany. The Mulde River, Elbe River, and tributaries of both were the rivers worst affected by flooding in the Osterzgebirge (East Ore Mountains) region during the 2002 regional flooding (Walther, 2004). The principle area of focus is the main community of Bennewitz and the neighboring community of Schmölen, as discussed in Section 3.2.

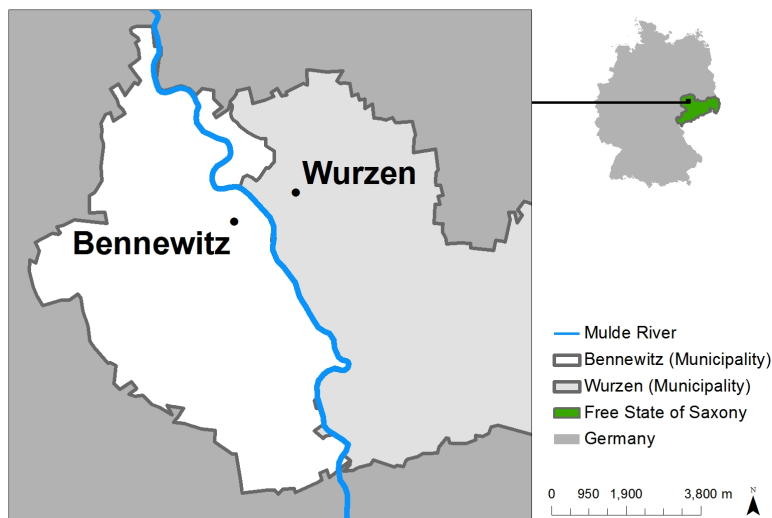


Figure 3.1.: Location of Bennewitz, Germany

Bennewitz (Germany) Bennewitz is a municipality (Gemeinde Bennewitz) in Leipzig County (Landkreis Leipzig), within the Free State of Saxony (Freistaat Sachsen). Bennewitz is located just across the Mulde River from Wurzen, about 40 minutes driving east of the city of Leipzig, and roughly 100 kilometres (as the crow flies) northwest of the border between Germany and the Czech Republic. The 2014 population of Gemeinde Bennewitz is estimated at 4,920 residents, according to a 2016 regional publication (Statistisches Landesamt des Freistaat Sachsen, 2016a). In line with the population of the entire Free State of Saxony, the population has experienced a steady decline, at least as far back as 1990 (Statistisches Landesamt des Freistaat Sachsen,

3. Case Study Area and Past Flood Events

2014, 2016a). In 2014, 14.8% of the Gemeinde Bennewitz population was under 20, 61.2% was at least 20 and less than 65 years old, and 24.0% was 65 or older (Statistisches Landesamt des Freistaat Sachsen, 2016a). The state as a whole is largely agricultural. According to a 2016 publication, 78.3% of the Free State of Saxony is farmland, 21.1% is permanent grassland, and 0.6% is permanent cultural land (including houses and gardens) (Statistisches Landesamt des Freistaat Sachsen, 2016b). Figure 3.1 presents the location and boundary of the municipality of Bennewitz.

Mulde River The Mulde River is a left tributary of the Elbe River. It originates in the East Ore Mountains (Osterzgebirge) in the Free State of Saxony, near the Czech border. There are two major tributaries, the Zwickauer Mulde (left) and the Freiberger Mulde (right), which meet to form the Vereinigte Mulde (which translates to the United Mulde). The confluence of these two occurs just after the communities of Großermuth (on the Zwickauer Mulde) and Erln (on the Freiberger Mulde), before continuing on to the city of Grimma, Bennewitz and Wurzen, Eilenburg, and Bad Düben. After Bad Düben, the Vereinigte Mulde crosses into Saxony's neighbour to the north, Saxony Anhalt, where it joins the Elbe River along its journey to the North Sea. At Bennewitz, the bed slope of the Mulde is not very steep, roughly 0.0011 (i.e. a drop of 1.10 m height per distance in kilometres), based on elevation data from 2009 (see Section 4.2.1). Figure 3.2 presents the location of the Mulde River, flowing south to north.

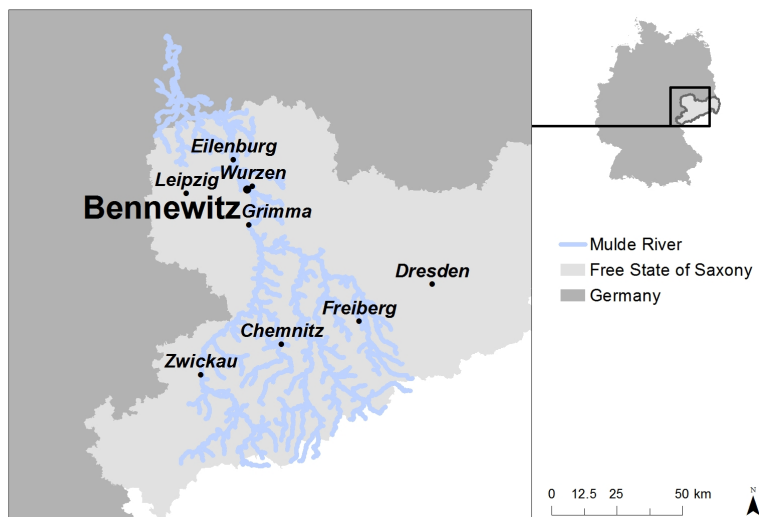


Figure 3.2.: The Mulde River and its tributaries

3.2. Boundary of the Investigation Area

The boundary of the investigation area for all three tasks is a sub-region within the 2D flow area (see Section 4, Figure 4.2) and presented in Figure 3.3. The investigation area was set to include the buildings of the main community of Bennewitz (northern portion of investigation area), the buildings in Schmölen (southern portion of investigation area), the train station, and any elevation lower than 119.50 m upstream of the train bridge that intersects these two communities. The investigation area was created after Task 1 was complete, and thus the 119.50 m threshold was selected because it is 1 m higher than the highest maximum water surface elevation result for any pixel in the 2D area for the 2002 flood event. The investigation area does not have any influence on the computations of the HEC-RAS model, but is rather a boundary within which the results are considered most important.

3. Case Study Area and Past Flood Events

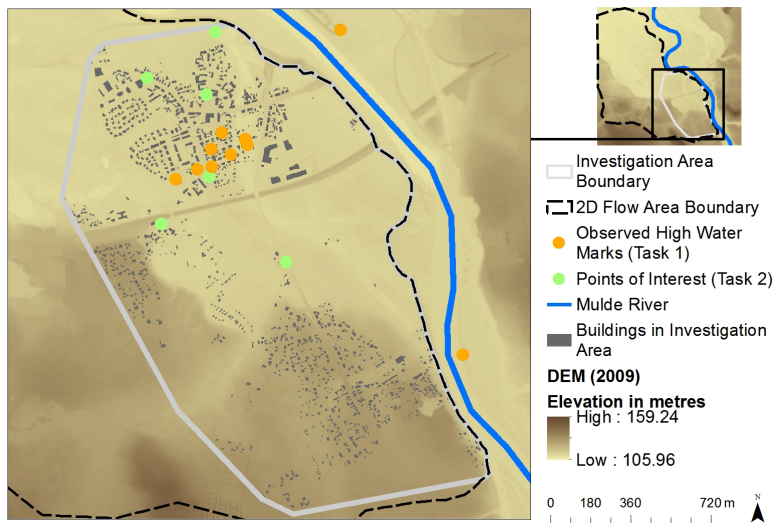


Figure 3.3.: Boundary of the primary investigation area for assessment of 1D/2D flood inundation for past and future events, including the communities of Bennewitz and Schmölen

3.3. Past Flood Events in the Region

3.3.1. Pre-21st Century Flood Events

*The following details are available in a 2002 *Leipziger Volkszeitung* article regarding the history of flooding in the Mulde Valley (LVZ [author unknown], 2002).* The recorded history of flooding in Mulde River dates back as far as 1017. The years 1439, 1587, 1629, 1665, 1689, 1673, and 1749 brought notable flood events, the last of which resulted in a significant change of the riverbed. In 1771, the river left grasslands and fields covered in sludge after three attempts to escape its banks. In 1796, the dike near Schmölen was breached by floodwaters, leading to the drowning of many cattle in Deuben. The flood of 1854 rose as high as 4 m, broke Grimmatische Strasse, as well as a bridge. Four years later, the flood of 1858 broke the Schmölen dike yet again, and proceeded to tear down the train bridge. The worst flood of the 19th century occurred in 1897, causing the dike to break in four locations. Floods were reported in 1899, 1907, and 1915, but the worst flood of the 20th century was in 1954. However, with the help of 4,900 volunteers, 810 soldiers, 290 policemen, 1,405 firefighters, and 30,000 sandbags, only the dike in Walzig broke during the flood of '54.

3.3.2. Recent Floods

August 2002 Flood The 2002 event was a major regional affair, meteorologically connected to a number of floods in Central Europe, and the most significant flood event in recent history in Saxony. Torrential rains on August 12 and 13 caused flash floods in the mountains, sending great volumes of water down the Mulde and Elbe Rivers with devastating consequences (Sächsisches Landesamt für Umwelt und Geologie, 2004). The event was classified as an extreme event, estimated to have a 0.2%-1.0% annual chance of occurrence (100-500 year statistical recurrence period) in some catchments. However, the event analysis showed that it was not an event of greatest possible magnitude, and thus more severe events may occur in the future (Sächsisches Landesamt für Umwelt und Geologie, 2004). Throughout cities and towns along the Mulde and Elbe Rivers, residents and visitors can still see placards on some private and public buildings, marking the maximum height of the 2002 flood waters. In Bennewitz, there were a series of dike overtoppings and/or breaches, one or two near Schmölen, as well as multiple breaches downstream

3. Case Study Area and Past Flood Events

of the bridges. A significant portion of Gemeinde Bennewitz was flooded, including all of the main community of Bennewitz, which is the area of focus for this study. In this research, the 2002 event was used for calibration of the 1D and 2D portions of the model.

March-April 2006 Flood This high water event is the smallest of those considered in this study. The peak at the Golzern gauge, roughly 14 kilometres upstream of Bennewitz, in 2006 was 25% of the recorded peak at the same gauge during the 2002 flood. The observed hydrographs at Großsermuth, Erln, and Golzern show two principle peaks during the event, the first of which is higher than the second, and a number of smaller pulses throughout the event. In this research, the 2006 event was only used for the calibration of the 1D portion of the model.

September-October 2010 Flood The magnitude of this event was not much greater than the 2006 event, reaching 27% of the peak at Golzern, compared to the 2002. The observed hydrographs at Colditz (Zwickauer Mulde, just upstream of Großsermuth), Leisnig (Freiberger Mulde, just upstream of Erln), and Golzern show only one noticeable pulse just before the primary flood wave. In this research, the 2010 event was only used for the calibration of the 1D portion of the model.

January 2011 Flood The 2011 flood, like the 2006 flood, was a series of two peaks, though only the higher of the two (the second) was used in this research. The magnitude of the event reached 31% of the 2002 flood peak at Golzern. In this research, the 2011 event was only used for the calibration of the 1D portion of the model.

June 2013 Flood Similar to 2002, 2013 is remembered throughout the region as a significant flood year. Comparatively, the 2013 magnitude was 79% as great as 2002 at the Golzern gauge. As it took place eleven years after the 2002 event, many of the lessons learned had fortunately translated into additional mitigation measures by 2013. In the municipality of Bennewitz, the area upstream of the train bridge, including Schmölen, was inundated in 2013. However, the tunnels under the train bridge were closed off, keeping the main community of Bennewitz dry throughout the event. The dike was overflowed near Schmölen, though it is not classified as a breach, given that it did not break (Koehler, 2016). The only official breach near to the main community of Bennewitz was just downstream, near the community named Nepperwitz (Koehler, 2016). The statistical recurrence interval of the magnitude of the 2013 event at Golzern is estimated at 200 years, when analysing only time series data up to 2011, and at 100 years when analysing the time series including the 2013 event (Bilinski *et al.*, 2015). In this research, the 2013 event was used for model validation.

Figure 3.4 presents the hourly discharge hydrograph from each of the five events used in the calibration and validation of this model, and Table 3.1 provides the peak discharge for each of the five events. Golzern is the nearest gauge to the study area for which data is available for all of the events.

Table 3.1.: Observed peak discharge at Golzern gauge for calibration and validation events

Year	Peak Discharge [m ³ /s]	Date	Time
2002	2604	13 August	19:00
2006	658	28 March	13:00
2010	697	28 September	16:00
2011	816	15 January	6:00
2013	2060	3 June	9:00

Hourly discharge data provided by LfULG.

3. Case Study Area and Past Flood Events

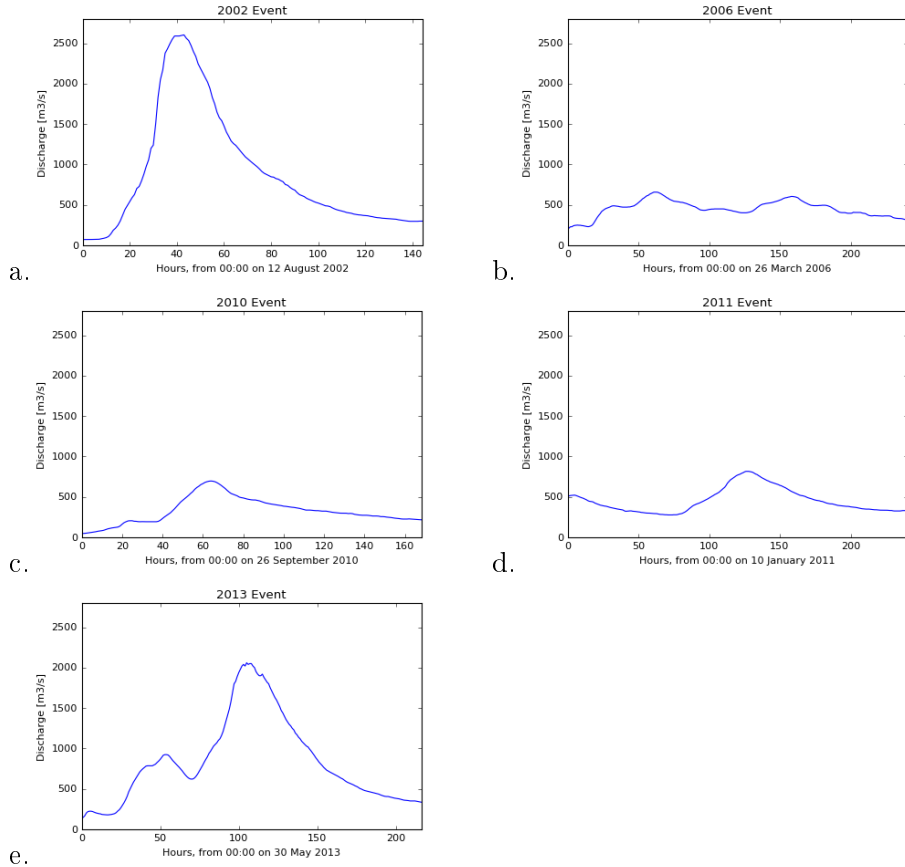


Figure 3.4.: Observed discharge at Golzern gauge for events in 2002, 2006, 2010, 2011, and 2013
Hourly discharge hydrographs for Golzern gauge from 2002 (a), 2006 (b), 2010 (c), 2011 (d), and 2013 (e). Data provided by LfULG.

4. Data and Methods

This research is organised into three principle tasks. The first task, Model Set Up, Calibration, and Conditional Validation, generates and assesses a model for use at the end of the model chain described in Section 1.3. The second task, Repeated Simulations with Changing Upstream Boundary Conditions, creates tools to take advantage of the many climate data sets available through the model chain. The third task, Visualisation and Display, explores possibilities for compiling and presenting the results. Occasional references to the "project team" indicate activities performed by the author along with a fellow PhD and two Masters students involved in the project. Before discussing the data and methods by task, the theoretical background of HEC-RAS and the methodology for creating the Investigation Area are presented.

4.1. Theoretical Background of HEC-RAS

4.1.1. Assumptions

In hydrodynamic modelling, the continuity equation (conservation of mass) and conservation of momentum are the two principle laws which govern unsteady flow (Brunner, 2016b). They provide the foundation for the Navier-Stokes equations as well as the St. Venant shallow water equations. HEC-RAS is grounded on the St. Venant shallow water equations. As is evident from the name, these equations are intended for application in situations where vertical flow is much less significant than longitudinal and lateral flow. They do not account for vertical water movement. Specifically, the St. Venant shallow water equations are based on the following assumptions (Brunner, 2016b):

- Vertical length scale is much smaller than horizontal length scale.
- Flow is incompressible.
- Flow has uniform density.
- Flow has uniform hydrostatic pressure.
- Eddy viscosity can approximate turbulent motion (i.e. the equations are Reynolds averaged).

4. Data and Methods

4.1.2. 1D Unsteady Flow

The 1D St. Venant continuity equation can be expressed as follows (Brunner, 2016b).

$$\frac{\partial A_T}{\partial t} + \frac{\partial Q}{\partial x} - q_l = 0 \quad (4.1)$$

Where:

x = distance along the channel

t = time

Q = flow

A_T = total flow area

q_l = lateral inflow per unit length

The 1D St. Venant momentum equation can be expressed as follows (Brunner, 2016b).

$$\frac{\partial Q}{\partial t} + \frac{\partial QV}{\partial x} + gA \left(\frac{\partial z}{\partial x} + S_f \right) = 0 \quad (4.2)$$

Where:

x = distance along the channel

t = time

Q = flow

V = average flow velocity

g = acceleration of gravity

A = cross section area

$\frac{\partial z}{\partial x}$ = water surface slope

S_f = friction slope

HEC-RAS uses an implicit finite difference scheme for solving 1D unsteady flow equations (Brunner, 2016b). More information on the four-point implicit scheme is available in the HEC-RAS 5.0 Hydraulic Reference Manual (Brunner, 2016b).

4.1.3. 2D Unsteady Flow

For 2D unsteady flow in HEC-RAS 5.0.3, the modeller may select either the full St. Venant equations (referred to in HEC-RAS as the "full momentum" equations) or the simplified diffusion wave equations (Brunner, 2016b).

The 2D St. Venant shallow water continuity equation can be expressed as follows (Brunner, 2016b).

$$\frac{\partial H}{\partial t} + \frac{\partial(hu)}{\partial x} + \frac{\partial(hv)}{\partial y} + q = 0 \quad (4.3)$$

Where:

H = water surface elevation

h = water depth

u = depth-averaged velocity in x direction

v = depth-averaged velocity in y direction

q = source/sink flux term, representing external inflows (for example, precipitation)

4. Data and Methods

The 2D St. Venant shallow water momentum balances can be expressed as follows (Brunner, 2016b).

$$\frac{\partial u}{\partial t} + u \frac{\partial u}{\partial x} + v \frac{\partial u}{\partial y} = -g \frac{\partial H}{\partial x} + v_t \left(\frac{\partial^2 u}{\partial x^2} + \frac{\partial^2 u}{\partial y^2} \right) - c_f u + fv \quad (4.4)$$

$$\frac{\partial v}{\partial t} + u \frac{\partial v}{\partial x} + v \frac{\partial v}{\partial y} = -g \frac{\partial H}{\partial y} + v_t \left(\frac{\partial^2 v}{\partial x^2} + \frac{\partial^2 v}{\partial y^2} \right) - c_f v + fu \quad (4.5)$$

Where:

H = water surface elevation

v_t = eddy viscosity coefficient

c_f = bottom friction coefficient

f = Coriolis parameter

u = depth-averaged velocity in x direction

v = depth-averaged velocity in y direction

The first term from the left of the above equations concerns unsteady acceleration, the second two concern convective acceleration, and each of the next terms, continuing left to right, concern barotropic pressure, eddy diffusion, bottom friction, and the Coriolis effect.

The full 2D shallow water equations are simplified further still into what are called the diffusion wave equations. The diffusion wave equations disregard the inertial terms (unsteady and convective acceleration, eddy diffusion, and Coriolis effect) from the original 2D St. Venant shallow water equations, assuming that gravity and bottom friction terms are dominant for the particular study area (Brunner, 2016b).

The 2D solver uses an implicit finite volume solution algorithm so as to manage subcritical, supercritical, and mixed flow regimes (Brunner, 2016b). Additional detail regarding computational equations and assumptions in HEC-RAS can be found in the HEC-RAS 5.0 Hydraulic Reference Manual (see Brunner 2016b).

4.2. Task 1: Model Set Up, Calibration, and Conditional Validation

4.2.1. Data Selection, Preparation, and Sources

Digital Elevation Model (DEM) The DEM for the study area was acquired in ASCII format, at 2 m resolution. The spatial reference is ETRS89 / UTM Zone 33, and this reference was adopted for the research project. The model area covers multiple tiles, the data for all of which were collected between 2008-2010 (most tiles in 2009). The original 50 GB ASCII file was clipped to a manageable size, just larger than that required to cover the extent of the 1D portion of the model, using R and gdal. As the original elevation data was provided in centimetres, it was converted to metres using the Raster Calculator in ArcGIS. The same process was performed to create a smaller subset of this dataset, just large enough to cover the extent to be modelled in 2D, focused on Bennewitz and Wurzen. As the original DEM did not include buildings, the building data was converted from a building footprint shapefile to a raster of 2 m cell size. All buildings were set at 165 m elevation. The 2009 DEM was adjusted slightly to better represent elevation data during the calibration and validation years. Two sections of the dike, one near Schmölen and one just after the B6 bridge, were shifted after the 2006 event and before the 2010 event. Based on maps and AutoCAD drawings, the project team adjusted the 2009 DEM to match the estimated alignment and elevation of the previous dike. This adjusted DEM was used during the calibration of the 2D portion of the model (2002 event). Given that the data to make these adjustments were not available until after the calibration of the 1D component of the model,

4. Data and Methods

the original 2009 DEM was used for calibrating the 1D component of the model for the 2002 and 2006 events. This was considered acceptable, as the principle point of calibration for the 1D component of the model is at the Golzern gauge, more than 14 km upstream from the locations where the dikes were moved. In 2013, the tunnels under the train bridge were successfully closed off by the community, in preparation for the flood. Therefore, the 2009 DEM was adjusted to seal off the train bridge tunnels. This adjusted DEM was used for 1D calibration events of 2010 and 2011 as well as the validation event of 2013. Additional information regarding these minor adjustments to the DEM are available in Section 4.2.7, as well as Figures C.1, C.2, and C.3 in Appendix C.

Bridge Measurements As bridge and cross section survey data were not available, the project team took rough estimates of bridge dimensions during a visit to Bennewitz and Wurzen (23 May 2017). These estimates are incorporated into the two bridges included in the 1D portion of the HEC-RAS model (the train bridge and the B6 bridge). Dimensions not feasible for direct measurement during the on-site visit (e.g. width of bridge deck) were estimated using Google Earth aerial imagery, terrain profiles from the DEM, and photos from the on-site visit.

High Water Marks There were only two high water marks available in digital format for this research, both of which were located in the 1D region of the model, and both for the 2002 event. They were accessed in March 2017 from the Free State of Saxony's geodata download section for water data (Saechsisches Landesamt fuer Umwelt, Landwirtschaft und Geologie, 2017). These marks are located near the citizen protection centre (Bürger-Schützengilde) in Wurzen and one just upstream, near the ferry house (Fährhaus) in Dehnitz. The digital feature representing the high water mark located near the citizen protection centre was moved roughly 2 m to the southeast, as the original location of the mark was located directly on top of a building in the DEM. A picture of this shift is presented in Appendix C, Figure C.4. Within Bennewitz, there were no high water marks available in digital format for this research. However, the project team collected photos and measurements, where possible, of high water marks from the 2002 flood in Bennewitz, as recorded on public and private buildings (23 May 2017). The project team collected eight high water marks in this manner. Of these eight, the project team had sufficient access to measure four of them with a measuring tape. The other four were on private land with no owner present to grant closer access to the mark, and so were estimated from a distance of 5-15 m. The list of high water marks collected during this site visit can be found in Table C.1 in Appendix C. Figure 4.1 presents the locations of the 2002 high water marks.

4. Data and Methods

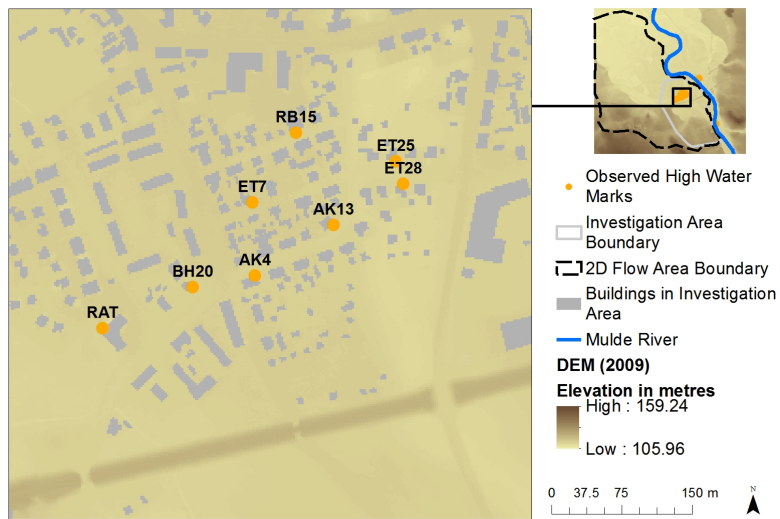


Figure 4.1.: Location of observed high water marks in the main community of Bennewitz for the 2002 event

The address for each high water mark is available in Appendix C, Table C.1.

Flood Extent Shapefiles The 2002 and 2013 flood extent data were available in shapefile format from the Free State of Saxony's geographic information download site (Sächsisches Landesamt fuer Umwelt, Landwirtschaft und Geologie, 2017). In addition, the project team had the opportunity to view a printed outline of the 2002 flood extent for display during the visit to the Bennewitz town hall. For comparison to the flood extent generated by model simulations, the extent was limited to the boundary of the model's 2D area. The observed flood extent shows as wet certain locations within the area known to have been dry during the 2002 event (such as the top of the elevated train tracks). Therefore, it was assumed that dry locations between the river and the outer extent were filled in (i.e. represented as wet) in the process of generating the observed extent file. In the 2013 flood extent shapefile, however, such gaps do not appear to have been filled (evidenced by the three pockets of land surrounded by water near the downstream end of the 2D area). The original observed flood extent data for 2002 and 2013 are available in Appendix C, Figures C.5 and C.6. The gaps-filled version of the 2010 observed flood extent is available in Figure C.7.

Land Cover Data CORINE Land Cover (CLC) 2012 data was available in shapefile format from the Copernicus Programme (Copernicus Programme, 2017). CLC data are based on ortho-corrected, high spatial resolution satellite imagery, corrected and refined with topographic maps, orthophotos, and ground survey data (Copernicus Programme, 2017). As has been true for previous CLC updates, the database includes 44 CLC classes, 100 m positional accuracy, and a 25 hectare minimum mapping unit (Copernicus Programme, 2017). The alternative to the CLC 2012 data was the Amtlichen Topographisch-Kartographischen Informationssystems ATKIS (ATKIS) digital landscape model known as the DLM250 dataset, which also has 100 m positional accuracy (Federal Agency for Cartography and Geodesy (Bundesamt fuer Kartographie und Geodäsie), 2017). In comparing the taxonomic nomenclature of ATKIS data to CLC data, author Ubbo Visser notes that the two differ based on their intended use, ATKIS being more focused on the administration of human activities, and CLC on the state of the environment and vegetation (Visser, 2005). Therefore, the ATKIS categories for urban areas and human activities in a more fine-grained manner, and are more general for natural and cultivated areas, whereas the opposite is true for CORINE. Given the that the landscape along the Mulde is heavily agricultural and

4. Data and Methods

natural, the CORINE dataset was selected for this study.

Hourly Observed Hydrographs Partial time series of observed stage and discharge data were provided by the Saxon Flood Centre (Landeshochwasserzentrum, or LHWZ), based on when the various gauges were in operation. Continuous discharge data for the Zwickauer Mulde were available from Großermuth for the 2002 and 2006 events, and from Colditz for the 2010, 2011, and 2013 events. Continuous discharge data for the Freiberger Mulde were available from Erln for the 2002 and 2006 event, and from Leisnig for the 2010, 2011, and 2013 events. The gauge at Golzern provided sufficient discharge data for all calibration and validation events.

Historical Maps and Photos A sampling of historical maps and photos were available from the Hochwasserschutzkonzept (HWSK) and the Bennewitz Library. Details regarding how map information was incorporated into the model is described in Section 4.2.7.2. Photos were limited to those of the 2002 event.

4.2.2. HEC-RAS Software, 1D/2D Approach, and Solvers

HEC-RAS 5.0.3 was officially released in September 2016. The software was selected for its reputation and the recent addition of 1D/2D capabilities. The portion of the Mulde River modelled for this research was represented by a 1D river connected to a 2D mesh for the community of Bennewitz. There were three reaches included in the 1D model: 1) a portion of the Zwickauer Mulde, from Colditz to the junction, 2) a portion of the Freiberger Mulde, from Leisnig to the junction, and 3) Vereinigte Mulde, from the junction to Groitsch. The 2D area was located on the left side of the Mulde at Bennewitz, reaching as far upstream as Schmölen and as far downstream as Nepperwitz. The coupled 1D/2D approach was selected for this area as only the populated hinterland is expected to experience significant 2D flow at this project's scale. The connection of 1D to 2D by lateral structure was selected given that the majority of the connection is dominated by a dike to the left of the river.

For the 1D portion of the model, the default Skyline/Gaussian equation solver was selected, rather than the Pardiso solver, as 1D Pardiso solver is intended for large, interconnected systems (Brunner, 2016c). For the 2D portion of the model, the diffusion wave equation set was selected, running all available (4) cores. As noted in Section 4.1, the 2D diffusion wave equations simplify the 2D full St. Venant equations by disregarding the inertial terms (unsteady and convection acceleration, turbulence, and Coriolis), assuming that gravity and bottom friction terms are dominant for the particular study area (Brunner, 2016b). HEC-RAS documentation recommends the diffusion wave equations rather than the 2D full St. Venant equations for many cases, as they will run faster and are inherently more stable (Brunner, 2016c). Diffusion wave equations are sufficient when flow velocity is expected to be determined largely by gravity and friction (Brunner, 2016b). In a presentation by the creators of HEC-RAS, the 2D full St. Venant equations were recommended for more detailed applications, such as those in which the model is expected to capture the detailed movement around bridges, walls, and other structures, whereas flood extent applications, such as the research described in this thesis, were listed as one of those for which the diffusion wave equations would be sufficient (Brunner *et al.*, 2016).

The lateral structure connecting the 1D and 2D components of the model used the Standard Weir equation for overflow computation, with a weir coefficient of 1.1 (SI units). As weir coefficient calibration data was not available, Table 3-1 in the HEC-RAS User Manual 5.0 was used to estimate an appropriate weir coefficient. Given that the physical dike on which the modelled lateral structure runs is over a metre in height, the weir coefficient was expected to fall between 0.83 to 1.43 (SI units). Therefore, the default, given in English units, was converted to SI units to reach a value of 1.1.

4.2.3. 1D Geometry

The river centreline, banks, flowpaths, levees, storage area, lateral structure, and ineffective areas were originally created using HEC-GeoRAS 10.2 in ArcGIS for Desktop 10.4.1 and imported into HEC-RAS 5.0.3. The total 1D river centreline length was about 66.2 kilometres (6.7 km along the Zwickauer Mulde, 13.5 along the Freiberger Mulde, and 46.0 km along the Vereinigte Mulde), intersected by 388 manually placed cross sections. The average distance between cross sections was 170.7 m. Cross sections represent the entire floodplain for the Zwickauer Mulde, Freiberger Mulde, and the portions of the Vereinigte Mulde before and after the 2D flow area. At the 2D flow area, cross sections ended at the levee on the left side of the channel, but they extended to the full floodplain on the right side of the channel (including Wurzen). For the purpose of this work, the term "levee" will be used specifically to refer to the feature within HEC-RAS cross sections, while the term "dike" will be used to refer to the actual physical feature or its representation in a DEM.

As recommended in the HEC Hydraulic Reference Manual, cross sections were designed to lie perpendicular to the channel and floodplain flowpath lines. The original target for cross section spacing was roughly 200 m, according to the guidance equations proposed by P.G. Samuels in 1989 and Dr. Danny Fread in 1993 (Brunner, 2016b). Cross sections were added to better capture certain components of river geometry, which reduced the average spacing of cross sections over the entire channel.

The Cross Section Points Filter tool was used to limit each cross section to 480 points, while minimising area change. The cross sections near and alongside Bennewitz included levees, where applicable. Levee elevations were based on the dike elevation in the Digital Elevation Model (DEM). Just before Bennewitz, levees were included (at the high point of the terrain) to avoid water flowing from the Mulde into the small Lache tributary, as the inflow to the Mulde from this small stream was incorporated as lumped lateral inflow (see Section 4.2.5). The cross sections near the highway (B6) and train bridges between Bennewitz and Wurzen included ineffective flow areas. These ineffective flow areas were not permanent, which means that if the height is exceeded, the full area becomes a regular, effective flow area. The slopes leading up to the bridges are relatively shallow, and thus a permanent ineffective flow area would not be appropriate. The height of the ineffective flow areas were set halfway between the high and low chords of the corresponding bridges, for those cross sections nearest to the bridges (considered cross sections 2 and 3 when considering bridge calculations in HEC-RAS). Ineffective flow area heights for cross sections beyond these are slightly decreased. In the Hydraulic Table (HTAB) parameters for cross sections, the starting elevation of vertical discretisation was set to the channel minimum (using the "Copy Invert" option). The increment was set to 0.3, and the number of vertical discretisation points set to 120.

The two bridges were added directly in the HEC-RAS geometry editor. Judging by the guidance in Chapter 6 of the HEC-RAS User's Manual, the expansion ratio was expected to be between 1.5-2.0 for the highway bridge and between 1.0-2.0 for the train bridge. The expansion ratio guides the length of the expansion reach, and therefore the spacing of the cross sections downstream of each bridge. Given the unique layout of the bridges, the shape of the channel and floodplains, and the fact that the two bridges are quite close together, options for cross section placement were limited. Nevertheless, the guidance was followed to the extent possible. Guided by the HEC-RAS Hydraulic Reference Manual, the contraction and expansion coefficients were maintained at 0.1 and 0.3, respectively, throughout the model. The only exceptions were those cross sections adjacent to the bridges, for which the contraction coefficient was 0.3 and the expansion coefficient 0.5.

Storage areas and additional ineffective flow areas upstream of Bennewitz were considered in building the model. The original intent of adding these features was to capture any loss in water volume upstream, especially due to levee breaches. However, when adding storage areas, informed by limited information of the levee breaches for the 2002 event, the resulting reduction

4. Data and Methods

in discharge at Golzern was unreasonably severe. The use of ineffective flow areas to address storage upstream did not appear to have a great impact on the discharge, however they did reduce model stability. Without including upstream storage areas or ineffective flow areas, two of the four calibration events (2002 and 2006) were already slightly low in terms of discharge at Golzern. Therefore, with the understanding that the upstream storage areas and upstream ineffective flow areas did not appear to improve the accuracy of the model, and as they were causing issues with stability, the upstream storage areas and upstream ineffective flow areas were eliminated from the model.

A screenshot of the geometric data is available in the appendices, Figure A.1.

4.2.4. 2D Geometry and Connection to 1D

Figure 4.2 presents the boundary of the 2D flow area.

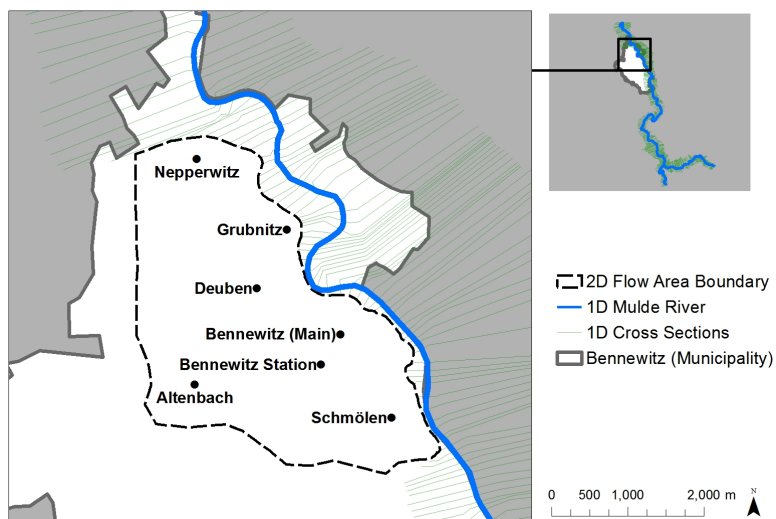


Figure 4.2.: 2D flow area boundary for 1D/2D HEC-RAS model of Bennewitz, Germany

As required by HEC-RAS, the 2D computational mesh was unstructured, meaning not all of the cells are quadratic and regular. Each cell could have up to eight sides, and the bottom face of the cell (the face that lies on the ground) matched the terrain layer (the DEM), which is of much higher resolution. For each simulation timestep, the water surface elevation for each cell would be computed, and any area below this elevation would be filled with water within the cell. This HEC-RAS feature allows for a computational mesh that is significantly lower in resolution, and therefore less computationally expensive, without losing the resolution of the available DEM. To create a computational mesh in HEC-RAS, the user selects the desired spacing in each direction (dx and dy), then HEC-RAS generates a grid accordingly, with adjustments around the edges and along any user-entered breaklines within the model. Breaklines are entered when the user wants to ensure that the mesh captures a particular topographic feature. In this model, breaklines were added along the raised elevation of the train tracks, roads, and other features, with particular emphasis on those within the main community of Bennewitz (the primary area of focus). Breaklines reduce the possibility that a cell would straddle such a feature, which would allow water to "leak" from one side of the raised feature to the other. The model was computational mesh size selected for the model was 25 metres in each direction (see Section 4.2.6 regarding methodology for this selection).

In HEC-RAS, a lateral structure was required for connecting 1D and 2D components of the model. Elevation data for the lateral structure in this model was originally based on the DEM. HEC-RAS does not allow for any portion of a lateral structure to lie below the 2D mesh cell to

4. Data and Methods

which it is connected. The lateral structure is located along the real dike, and therefore most of the lateral structure did not require elevation adjustment. However, small portions of the lateral structure were located near 2D mesh cells of slightly higher elevation (for example, 2D cells crossing the road leading up to the bridge). These portions required that the levee elevation be raised slightly to just above the 2D cell elevation. The location of the lateral structure, as visible in the HEC-RAS geometry editor, is presented in Figure 4.3. The lateral structure is modelled as a broad-crested weir, using the standard weir equation.

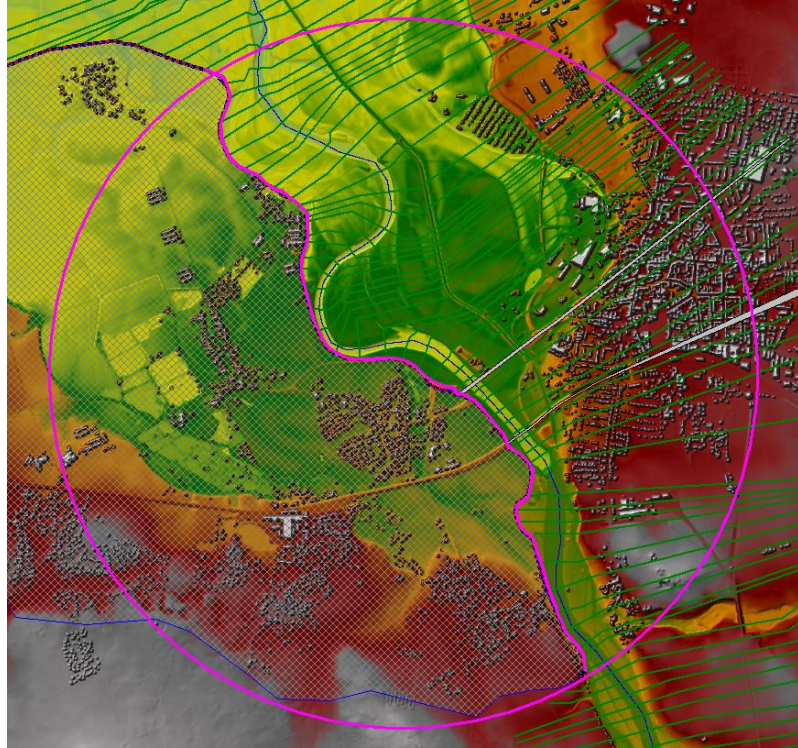


Figure 4.3.: Lateral structure connecting the Mulde River to Bennewitz in HEC-RAS 1D/2D model

The lateral structure (fuschia) is aligned with the dike on the left side of the Mulde River, according to the alignment in the 2009 DEM. Green lines represent HEC-RAS cross sections and grey hatched area represents the 2D flow area.

To the south and southwest, the boundary of the 2D flow area was located well beyond the observed flood extent of 2002 near the main community of Bennewitz. To the north and northwest, the boundary was set roughly 3 km downstream of the northern edge of the main community of Bennewitz. Along the river (i.e. to the east or northeast), the boundary was aligned with the dike in the 2009 DEM. This new dike (rather than the adjusted dike for the 2002 and 2006 events) was selected for the alignment of the 2D mesh, given that the simulations in Task 2 will be focused on future flood hazard, and therefore the current dike alignment is most appropriate. The small distance between the 2D flow area boundary and the dike adjustment for 2002 is visible in the the appendices, Figure C.2.

4.2.5. Initial and Boundary Conditions

By default in HEC-RAS, initial conditions for the 1D river reaches are set according to the first timestep of the boundary condition data. The 2D area started dry.

There are seven boundary conditions included in this unsteady model. At the upstream end of the 1D component of the model, there are two discharge hydrographs, one at the gauge in

4. Data and Methods

Colditz and one at the gauge in Leisnig. As noted in Section 4.2.1, the time series fed into these two upstream boundary conditions actually came from the gauges at Colditz and Leisnig only for the 2010, 2011, and 2013 events. The 2002 and 2006 event time series came from the downstream neighbours of Großermuth and Erln, respectively.

In addition to the upstream flow hydrographs, there are two lateral inflow hydrographs. The first enters the model at river station 28468.52, just before Golzern, representing the inflow from the Golzern catchment, but excluding that already accounted for at the upstream gauges. The second enters the model at river station 16268.82, roughly 2 kilometres before the start of the 2D area. This second gauge represents inflow from the catchment area at Bennewitz/Wurzen, excluding that already accounted for in the Golzern and upstream gauges. The discharge hydrographs generated for these lateral inflows are estimated based on the hourly discharge at Golzern for each event. The relative catchment size was calculated for each portion of catchment area to be accounted for, and the Golzern discharge was scaled accordingly. For those events using upstream discharge data from Erln and Großermuth, the lateral inflow near Golzern is 1.64% of observed discharge at Golzern. For those events using upstream discharge data from Leisnig and Colditz, the lateral inflow at Golzern is 4.21% of observed discharge at Golzern. For all events, the lateral inflow near Bennewitz/Wurzen is 2.85% of observed discharge at Golzern.

The 1D model has a downstream boundary condition of normal depth, with a friction slope of 0.0004. This friction slope was estimated using the slope of the channel in the lower end of the reach (a local sample of roughly 2.78 kilometres). This very low slope appears reasonable, given the meandering nature of the channel at this stretch of the river. In addition, this downstream boundary condition is located more than 8 kilometres downstream from the connection to the downstream end of the 2D study area. This placement was chosen so as to reduce the influence of the downstream boundary on the results in Bennewitz.

There are two boundary condition lines for the 2D computational mesh. One lies along the northern border of the mesh. The second lies along the northwestern border. These were added so as to allow water to freely exit the 2D mesh. Originally this downstream portion of the 2D mesh was represented by a lateral structure to allow the water to flow back into the 1D river. However, this original strategy caused water to flow into the 2D area from downstream, and also effectively trapped water in the 2D study region (as the lateral structure is required by HEC-RAS to be higher than the tailwater 2D cells to which it is connected). Therefore, the two boundary condition lines were selected in order to best represent the flow and water levels in the 2D region. The line along the northern border is represented by normal depth, with a friction slope of 0.0125, derived from the local slope. The line along the northwestern border lies along variable terrain, some of which is sloping upward. It is represented by a very small friction slope 0.0001.

4.2.6. Spacing and Timestep Selection

All Task 1 simulations were run on an Intel (R) Core (TM) i5-6400 CPU with four cores and 8.0 GB RAM. The selection of appropriate spacing and timesteps included changes to the computational timestep, cross section spacing, mesh size, and, when needed, adjustment of bridges, levees or other model components to ensure sufficient model stability. The criteria for this process were:

- The full simulation (2002) must run without going unstable.
- Minimise computation effort (i.e. computation time).
- Maximise accuracy to the degree possible without having yet calibrated the model.

The timestep was first estimated by calculating the Courant condition, based on the equation provided in the HEC-RAS 5.0 Reference Manual (converted to metric units).

4. Data and Methods

$$C = \frac{V_w \Delta T}{\Delta X} \leq 1$$

Where:

C = Courant number

ΔT = Timestep in seconds

ΔX = Distance step in metres

V_w = Wave speed in metres/second

Once all geometric model components were added and edited in order to successfully complete simulations, a series of ten simulations were run only varying the timestep (0.5, 1, 2, 3, 4, 5, 6, 10, 12, 15 s), to identify the most appropriate timestep for this model. The results of this test are available in Appendix D, Tables D.3 and D.4.

No adjustments were needed in terms of cross section spacing on a global scale. However, local adjustments were required in portions of the model near the bridges and near sharp bends in the river.

The appropriate 2D computational mesh size was determined principally by the effect on computation time and on maximum depth error as compared to the 2002 observed high water marks in the 2D area. This event was selected as it is the only event for which water elevation/depth data was available in the 2D region. A series of seven different mesh sizes were tested, ranging from 10 to 40 m in 5 m increments.

4.2.7. Roughness Sensitivity and Calibration

4.2.7.1. Calibration of 1D Component

The 1D component of calibration considered the Manning's n values in the channel and overbanks. The events for calibration included 2002, 2006, 2010, and 2011. These were the peaks over the threshold of 650 m³/s (25% of the 2002 event) at the Golzern gauge in the time series available (years available include 2002, 2006, and 2007-2015). The 2002 and 2006 events were simulated using the original 2009 DEM (as this was completed before information about the old dike alignment was available). The 2010, 2011, and 2013 events were simulated using an edited version of the DEM, in which the tunnels under the overland train bridge are sealed off.

Calibration of the 1D component was conducted in two stages, the first to identify an appropriate Manning's n value for the channel, the second to identify Manning's n values for the overbanks in the tributaries and the Vereinigte Mulde. In all cases, the left and right overbanks maintained the same Manning's n value, and in all cases, the Zwickauer and Freiberger Mulde tributaries maintained the same Manning's n value. Table 4.1 presents the Manning's n values selected for 1D calibration.

Table 4.1.: Manning's n values for 1D calibration of 1D/2D HEC-RAS unsteady flow model

	Minimum		Maximum
Channel	0.0250	0.0316	–
Overbanks	0.0500	0.0632	0.1110*

A description of why these ranges were selected is available in Appendix D. A single asterisk () indicates a value that was only considered in Stage 2 of 1D calibration.*

In Stage 1, only channel-overbank pairs in which the overbank Manning's n value was greater than that of the channel n value were considered. Each result of seven trials (28 simulations) from Stage 1 was compared with each other result from Stage 1 in terms of accuracy of the peak

4. Data and Methods

discharge at the gauge at Golzern, time lag of peak discharge at Golzern, and error in terms of water surface elevation at the two high water marks located in the 1D component of the model. Accuracy in terms of peak discharge at Golzern was assessed in terms of mean absolute error (MAE) and root mean square error (RMSE). With only four events per trial, MAE and RMSE were not considered statistically valid indicators, but rather simple tools to aid in the digesting and comparing of data. In those cases where one trial had a lower MAE and the other had a lower RMSE, RMSE was favoured, given that it represents a more even distribution of error (given that it "punishes" extreme values more than the simple MAE).

In Stage 2, an intermediate value was added to the possible overbank values for comparison. In addition, Stage 2 included trials with different Manning's n overbank values upstream (in the Zwickauer Mulde and Freiberger Mulde) versus downstream (in the Vereinigte Mulde). Each result of the 16 trials (64 simulations) was assessed in terms of RMSE of the peak discharge at Golzern, highest time lag of peak discharge at Golzern, and maximum water surface elevation error at the two high water marks in the 1D component of the model.

4.2.7.2. Calibration of 2D Component

Calibration of the 2D component of the model was conducted using only the 2002 event, as this is the only event for which there are observed high water mark data available in the 2D area. The 2009 DEM used for this portion of calibration was adjusted to better represent the old dike alignment near Bennewitz. There are two portions of the dike which were edited. The first is just upstream of the train bridge, and the second is just downstream of the highway bridge. The upstream dike shift was based on the height along a remnant of the dike, visible in the 2009 DEM, as well as images of maps from before the dike was moved. The downstream dike shift was based on images of the old dike alignment, and heights of the surrounding portions of the dike, particularly the portion between the two bridges.

The calibration of the 2D component was based on the RMSE and MAE of maximum water surface elevation at the eight high water marks in the 2D area, as well as the Critical Success Index (CSI), representing the goodness of fit of the flood extent for the full 2D flow area. Again, given that there are so few values (8 per trial), these were considered not statistically valid indicators, but rather simple tools to aid in the comparison of the trial results. The CSI, also known as a threat score or, according to Aronica *et al.* (2002) the fraction F(2), is based on a contingency table, such as that in Table 4.2. The CSI provides a fraction between 0 and 1, indicating how well modelled values match observed values, penalising both misses and false alarms (Bennett *et al.*, 2013). A CSI value of 1 would indicate an exact match. The equation for the CSI is as in Equation 4.6 (Bennett *et al.*, 2013).

$$CSI = \frac{\text{hits}}{\text{hits} + \text{misses} + \text{false alarms}} \quad (4.6)$$

Table 4.2.: Contingency table for calculating the flood extent using the Critical Success Indicator (CSI)

		Observed	
		Yes (Wet)	No (Dry)
Modelled	Yes (Wet)	Hits	False Alarms
	No (Dry)	Misses	Correct Negatives

All results were extracted from HEC-RAS as TIF files representing maximum water surface elevation. The water surface elevation at each of the eight high water marks in Bennewitz

4. Data and Methods

were pulled from each TIF file using the ArcGIS Extract Multi Values to Points tool. The CSI calculation required first a conversion to shapefile format (to match the observed data), and also a filling of the "gaps" in the result file, as noted in Section 4.2.1. A series of ArcGIS tools were combined into a number of ArcGIS ModelBuilder tools to manage the conversion, filling of gaps, and clipping the result file to the extent of the 2D area. A detailed description of the process, Python tools, and ArcGIS tools used for extracting the data from HEC-RAS and processing the result files for calibration can be found in Appendix B.

This 2D calibration effort was again conducted in three stages, the first varying all three land cover categories across the full range of possibilities, the second varying only two of them and within a more focused range, and the third examining the effect of varying selected Manning's n values by 15% in each direction. Table 4.3 presents the Manning's n values selected for 2D calibration for urban (U), agricultural (A), and woodland (W) areas. A description of why these ranges were selected is available in Appendix D.

Table 4.3.: Manning's n values for 2D calibration of 1D/2D HEC-RAS unsteady flow model

	Min.										Max.
U	0.0100	0.0375	0.0773	0.0830	0.0910	0.0980	0.1050	0.1130	0.1200	0.1400	0.1600
A	0.0200	0.0470	0.0510	0.0550	0.0590	0.0630	0.0900	–	–	–	0.1600
W	0.0300	0.0625	0.0950	–	–	–	–	–	–	–	0.1600

A description of why these ranges were selected is available in Appendix D. Single asterisk () indicates values which were only considered in Stage 2 of 2D calibration. Double asterisk (**) indicates values which were only considered in Stage 3 of the 2D calibration.*

4.2.8. Sensitivity Analysis

The model's sensitivity to roughness values was explored in depth during the calibration process. However, the model was also examined in terms of sensitivity to the upstream and downstream boundary conditions, as well as the equation set used for 2D computations. This involved running the model exactly as it was run for the calibrated 2002 event, except for the variable of concern. For the upstream boundary conditions, this included an alteration of 15% above and below the discharge hydrograph for the 2002 event. There are three downstream boundary conditions, all controlled by normal depth with friction slopes based on local elevation changes. The friction slope for each of these boundary conditions was varied by 20% in both directions. Finally, the model was run for the 2002 event using full momentum equations rather than the diffusion wave equations.

4.2.9. Model Validation and Simulations for Evaluation

The model was conditionally validated based on the peak discharge error at Golzern and the CSI of the flood extent. The validation event was from June 2013. The DEM used was that from 2009 with tunnels under the overland train bridge blocked off. Other alterations made to the model (compared to the calibrated model for the 2002 event) include adjustment of the levee location and height (in 1D cross sections), update to the cross section elevations (to match the 2009 DEM, which required using the Cut From Terrain tool followed by a repeat of the Cross Section Points Filter tool in HEC-RAS), and adjustment of the lateral structure to align with the 2013 dike. Results of model validation can be found in Table 5.2.

The 2013 observed flood extent map does not appear to have gaps filled, contrary to the 2002 observed flood extent map. In order to maintain consistent methodology with the calibration runs, the CSI was calculated once with gaps filled in both the observed data and the simulated

4. Data and Methods

data for the 2013 event within the full 2D flow area. In addition, the CSI was recalculated using shapefiles without gaps removed. Therefore, for the no-gaps-removed CSI calculation, the Union tool in the process shown in Figure B.2 was omitted. This result was compared with the original observed shapefile, clipped to the boundary of the 2D extent. Both CSI calculations are available in Table 5.2. The CSI for both 2002 and 2013 was then re-calculated only for the investigation area (using the gaps-filled methodology for both) in order to assess the validity of the model for the primary area of interest, and also to remove the influence of concerns regarding the 2013 observed flood extent data (see Section 5.1.2).

The final model was re-run for each of the calibration events to produce the results presented in Table 5.2, and the 2002 event was run ten additional times in order to assess model output consistency (see Table 5.6). The maximum water surface elevation results from each of the ten additional simulations of the 2002 event were clipped by the 2D flow area boundary, and the 2002 calibration simulation was subtracted from each of these ten simulations to determine whether there was any difference in maximum water surface elevation results.

In order to examine the sensitivity of the model to friction slopes selected for the downstream boundary conditions, each was varied 20% in each direction. These results are available in Section 5.1.3. In addition, the calibrated model for 2002 was re-run using the full momentum equations for the 2D flow area, rather than the diffusion wave equations. These results are also available in Section 5.1.3.

4.3. Task 2: Repeated Simulation with Changing Boundary Conditions

4.3.1. Overview of Task 2

With a conditionally validated model and 81 flow hydrographs, each of which represents the peak event (8 days long) from a 101 year simulation of a unique future climate simulation, Task 2 includes a re-configuration of the model to represent these many upstream boundary conditions in HEC-RAS plans. The process of preparing and running this relatively large quantity of simulations is broken into four principle steps:

- Step 1: Transfer hydrograph data from TXT files into HEC-RAS unsteady flow files
- Step 2: Create plan files associated with each newly-created unsteady flow file
- Step 3: Import plan files and unsteady flow files into HEC-RAS
- Step 4: Run batched simulations
- Step 5: Extract and analyse results

Throughout this section, there are references to "unsteady flow files", "plan files", and the "project file". These are three types of files required for running a HEC-RAS unsteady flow simulation. The unsteady flow file (extension ".u##") contains information regarding boundary conditions (including upstream hydrographs) and initial conditions. The plan file (extension ".p##") contains information about which unsteady flow file and geometric data file should be used for a particular simulation, as well as information about the duration of the simulation, output settings, and more. The project file (extension ".prj" though this must not be confused with the *projection* file, which has the same file extension) indicates which unsteady flow files, geometric data files, map files, and other files are associated with a given project. If an unsteady flow file exists with the right name and is located in the right folder, but it is not listed in the project file, it will not be accessible through that HEC-RAS project. Unsteady flow files, plan files, and the project file can be edited with a text editor and treated similarly as a text file when being accessed with Python.

4. Data and Methods

The rest of this section covers the details regarding additional data for Task 2, adjustments to the model geometry, details of the five steps listed above, and limitations of this approach.

4.3.2. Data Selection, Preparation, and Sources

The only additional data required for Task 2 is the series of 81 discharge hydrographs to represent the upstream boundary conditions at Golzern. The optimisation algorithm used to calibrate the HBV model (calibrated to the events of 2002, 2011, and 2013) produced a Pareto front of nine parameter sets. The HBV model was run nine times (once for each optimal parameter set) for each realisation (three in total, denoted as 00, 11, and 22) of the three model combinations 8, 9, and 10 in Table 1.1. Figure 4.4 presents this flow as an organisational chart.

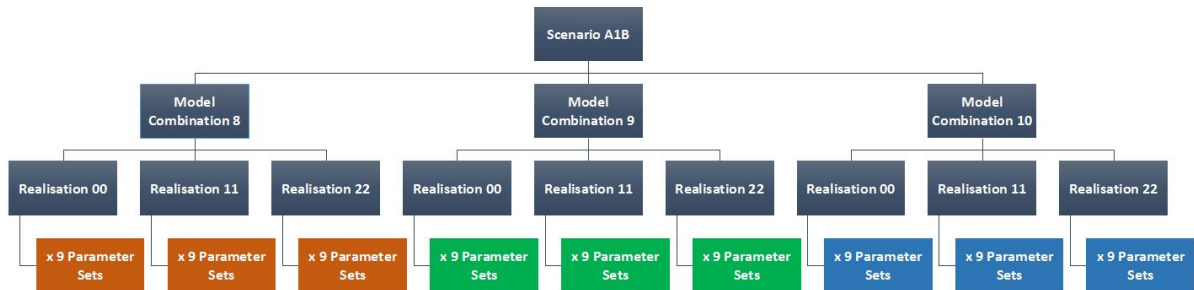


Figure 4.4.: Model combinations, realisations, and parameter sets to simulate future discharge hydrographs

Model combination 8 is HadGEM2 (GCM) combined with WEREX V (ESD). Model combination 9 is ECHAM5 (GCM) combined with RACMO (RCM) and WEREX V (ESD). Model combination 10 is ECHAM5 (GCM) combined with REMO (RCM) and WEREX V (ESD).

The highest peak event of each simulated discharge hydrograph (from a 101 year simulation, 2000 through 2100) was set to an arbitrary date in the middle of a 1000-hour artificial time series, shown in Figure 4.5. Of the nine parameter sets for each realisation, eight HBV simulations produced a maximum peak discharge that aligned with the same event compared to the other parameter sets for that realisation. However, parameter set 9 produced a peak discharge for an alternative event, compared to the other parameter sets. Additionally, the parameter values of parameter set 9 are further from the parameter values of parameter sets 1-8, compared to one another (see Appendix F, Table F.1). This is not visible in Figure 4.5, as the maximum peaks have all been set to the same artificial date, but it should be kept in mind for the analysis of results. Any discharge values that fell below 20 m³/s were changed to this threshold, as the HEC-RAS model becomes unstable under very low discharge conditions. This threshold was selected as it is high enough to avoid instability, but well below the average discharge value of observed data at Golzern (61.9 m³/s). Table 4.4 presents descriptive statistics for the maximum discharge of the 81 simulated events under future climate conditions, as well as the same for each model combination.

To reduce simulation time, the 1000-hour time series was shortened to 8 days, roughly straddling the peak. A visual analysis of Figure 4.5 confirms that the rise and fall of the flood wave is captured in this 8-day window (specifically, hour 408 to hour 600). The calibration and running of the HBV model were performed by Ms. Verena Maleska, as well as the identification of the highest peak event and the transfer of this event to an arbitrary 1000-hour time series. Additional details regarding the WEREX V and ScaDS projects upstream of the HBV model can be found in Section 1.3.

4. Data and Methods

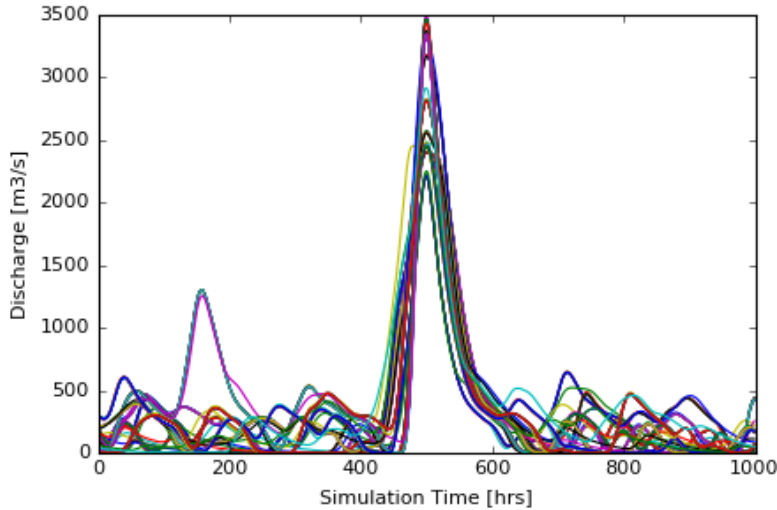


Figure 4.5.: Simulated 1000 hour future discharge hydrographs from HBV model under simulated future climate conditions, using nine distinct HBV parameter sets

Table 4.4.: Descriptive statistics of maximum discharge at Golzern for highest peak flood events simulated by HBV hydrologic model under simulated future climate conditions

Model Combination	Statistic	Max. Simulated Discharge at Golzern
All (81)	Min.	1982.47
	Max.	3491.82
	Range	1509.35
	Mean.	2765.50
	Std.	441.15
8, HadGEM2 (27)	Min.	1982.47
	Max.	2915.82
	Range	933.35
	Mean.	2597.96
	Std.	199.76
9, ECHAM5 + RACMO (27)	Min.	2204.42
	Max.	2484.95
	Range	280.54
	Mean.	2364.02
	Std.	109.22
10, ECHAM5 + REMO (27)	Min.	3169.31
	Max.	3491.82
	Range	322.51
	Mean.	3334.54
	Std.	119.10

All descriptive statistics are based on the maximum discharge at Golzern for each individual simulated flood event. The column titled “Model Combination.” indicates the model combination (8, 9, 10, or all), as well as the number of simulations included, in parentheses.

In addition, for Task 2, a series of six points of interest (POIs) were identified in the communities of Bennewitz (five) and Schmölen (one). The sites are intended to be community landmarks of geographically diverse distribution within the 2002 flood extent of these two

4. Data and Methods

communities. Ideally, the site selected would be a recognisable landmark, such as the fire department or a school. However, as no such landmark was available within the 2002 flood extent in Schmölen, a prominently located building was selected in its stead. Table 4.5 and Figure 4.6 present the POIs.

Table 4.5.: Points of interest (POIs) for investigation of sensitivity of flood depth to changing upstream boundary conditions under simulated future climate conditions

ID	Description	Name
POI1	House	Grimmaische Strasse 16
POI2	Bennewitz train station	Bahnhof Bennewitz
POI3	Bennewitz elementary school	Grundschule Bennewitz
POI4	Volunteer fire department	Freiwillige Feuerwehr Bennewitz
POI5	Post office	Deutsche Post Filiale
POI6	Sewage treatment plant	Klaerwerk

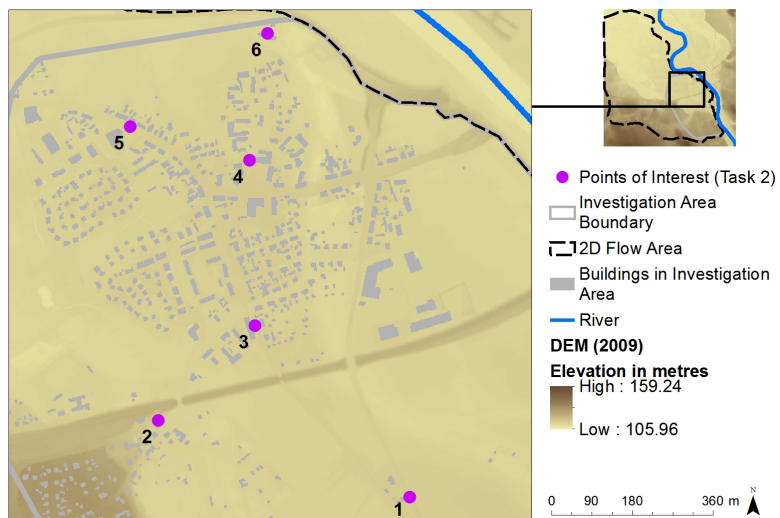


Figure 4.6.: Location of points of interest (POIs) for investigation of sensitivity of flood depth to changing upstream boundary conditions under simulated future climate conditions

4.3.3. Adjustments to the Geometry of the Model

The output of the hydrologic model is available for the Golzern gauge. This requires that the furthest upstream boundary of the HEC-RAS model for Task 2 is Golzern (river station 28195.3), and thus the Zwickauer Mulde, Freiberger Mulde, and the upper portion of the Vereinigte Mulde are removed from the 1D component of the Task 2 model. This leaves the upstream boundary condition of the model 14 kilometres upstream of the 2D flow area. To compare this shortened version of the model to the original model from Task 1, it was used to simulate the 2013 event using the simulated discharge at Golzern from the original model as an input to the shortened version of the model. The 2013 event was selected for this comparison given that the 2013 set up of the model would be used for the Task 2 simulations (with the exception that the tunnels under the train bridge are not blocked off for running Task 2 simulations, in addition to the change of the Wurzen levee, described below). The results for this comparison are available in Appendix H.

In an effort to isolate flooding in Bennewitz, the levee on the Wurzen side of the Mulde was artificially increased to eliminate the possibility of flooding in Wurzen. This decision came out of

4. Data and Methods

the recognition that the height of the Wurzen levee, based on the 2009 DEM, may have a strong impact on flooding in Bennewitz. The increasing of this levee in the model was not intended to create a more realistic representation of potential future events, but to remove the influence of the interaction between the height of the Wurzen levee and the varying of the upstream discharge. A description of and figure presenting the results from comparing the with- and without-wall versions of the Task 2 model are included in Appendix H.

An image of the geometric data for Task 2 is available in Appendix A, Figure A.2. The analysis of the results from Task 2 is focused on the investigation area, as this is the area for which the model in Task 1 has been conditionally validated.

4.3.4. Steps for Preparing and Running Multiple Simulations with Changing Boundary Conditions

Step 1: Transfer hydrograph data from TXT files into HEC-RAS unsteady flow files The purpose of Step 1 is to automate the process of creating HEC-RAS unsteady flow files. Step 1 is designed to reduce time but also likelihood of human error. This step requires the creation of a template unsteady flow file, including entry points for the inflow hydrographs. A program written in Python performs the following sub-steps on the TXT file for each climate realisation:

1. Open the TXT file.
2. Read in the hydrograph.
3. Populate the template unsteady flow file with the hydrographs and a unique title.
4. Save the file in the appropriate format (.u##) and location.

Step 2: Create plan files associated with each newly-created unsteady flow file The purpose of Step 2 is to avoid the need to manually transfer each of the unsteady flow files and save them as individual plans in HEC-RAS. Step 2 is designed to reduce time but also likelihood of human error. Very similar to Step 1, this step requires the creation of a template plan file, and entry points for the unsteady flow file name, a unique title, and a unique short ID. A program written in Python performs the following sub-steps for each climate realisation:

1. Open the plan file template.
2. Populate the template with the title, short ID, and unsteady flow file name
3. Create a new file and print the edited template into the new file
4. Save the file in the appropriate format (.p##) and location.

Step 3: Import plan files and unsteady flow files into HEC-RAS This requires a brief edit to the project file (.prj) using a simple text editor. The project file includes a list of all of the plan files, geometry files, and unsteady flow files that are associated with a project. Therefore, the user needs only to open the file, add in any missing plan or unsteady flow file numbers, and save the project file.

Step 4: Run batched simulations The Run Multiple Plans tool built into HEC-RAS suffices for this step. Assuming steps 1-3 were performed properly, the user must open HEC-RAS, navigate to the Run Multiple Plans tool, mark "Check all plans," and click "Run all checked plans."

Step 5: Extract and analyse results With minor adjustments, the tools developed in Task 1 (see Appendix B) serve to extract the results from HEC-RAS. Examples of minor adjustments include changing the path names and the number of characters to truncate from the names to maintain a unique name for each simulation.

4.4. Task 3: Visualisation and Display

Task 3 requires no additional data beyond the maximum water depth result files from Task 2. These files represent the maximum depth over the course of the entire 8 day HEC-RAS simulation. Each HEC-RAS simulation was fed by a unique discharge hydrograph at the upstream boundary. The discharge hydrographs were produced by the model chain described in Section 4.3. These simulations do not all represent an event of the same recurrence interval, but are rather the maximum peak event over the entire 101 year hydrologic model simulation.

4.4.1. Representation of Uncertainty in Flood Extent

The two maps created to represent flood extent uncertainty were produced using the following steps, implemented using Python, the ArcPy package, and basic ArcGIS tools:

- Apply a threshold to each of the maximum water depth simulation result files (for this thesis the threshold was held at 0.00 m, but the ability to apply a threshold was included in the script).
- Convert all cells with values above the threshold to a value of 1; all cells below the threshold to a value of 0.
- Add all files together, so each cell of the resulting file will represent the number of simulations which wetted the cell (above the threshold).
- Calculate the percent of simulations which wetted each cell (value of cell divided by total number of simulations multiplied by 100).
- Clip the file to the extent of the 2D flow area. *This produces Flood Extent Map 1.*
- Collapse the percentages into desired ranges (in this case 0-5%, 5-50%, 50-95%, and 95-100%). *This produces Flood Extent Map 2.*

4.4.2. Representation of Uncertainty in Flood Depth

This exploration was centred on the standard deviation of flood depth at each pixel, as standard deviation is one way of examining how spread out a series of values is. All of the 81 maximum water depth result files were fed into the Cell Statistics Tool in ArcGIS to so that the resulting file represents the standard deviation of maximum water depth at each cell. All 27 of the maximum water depth result files for model combination 8 (HadGEM2) were fed again into the Cell Statistics Tool to provide a map of the standard deviation of maximum water depth per cell only pertaining to one particular model combination. Both of these were presented in Section 5.2.4.

For Task 3, the additional map was created in the following manner by re-scaling the standard deviation map for model combination 8 to match the scale of the standard deviation map for all 81 simulations. *This produces Flood Depth Map 2. Flood Depth Map 1 is the same as Figure 5.13.*

5. Results

5.1. Task 1: Model Set Up, Calibration, and Conditional Validation

5.1.1. Model Set Up and Intermediate Model Calibration Results

In comparing the ten timestep-varied trials, the water surface elevation changed very slightly from simulation to simulation. As timestep decreased, so did computation effort. However, as timestep increased, the error in volume accounting (total water out of the system versus total water put into the system) increased as well. The selected timestep of 6 seconds was chosen in order to maintain volume accounting error under 1% for both the full model and the 2D area, while minimising computation time. Additional details regarding the selection of a 6 second timestep can be found in Appendix D, Table D.3.

In comparing the seven mesh size-varied trials, decreasing the computational mesh size correlated to decreasing volume accounting error, though even the maximum volume accounting error was well below 1%. There appeared to be no clear relation between mesh size maximum water surface elevation accuracy within this range of mesh size. Larger mesh sizes correlated to lower computation time. The selected mesh size of 25 metres was chosen in order to balance computation time and volume error. Additional details regarding the selection of a 25 metre mesh size can be found in Appendix D, Table D.2.

Stage 1 of 1D calibration produced a Manning's value of 0.0316 as the most suitable value for the channel. In comparing all of the trials, 58% of the comparisons showed a trial with 0.0316 in the channel to be preferable. Additional details regarding Stage 1 can be found in Appendix D, Table D.5.

Stage 2 of 1D calibration produced a Manning's value of 0.1580 for the overbanks along the Zwickauer Mulde and Freiberger Mulde, and a value of 0.0632 for the overbanks along the Vereinigte Mulde. Of the 16 trials, this combination was selected for its low peak discharge RMSE (ranking 2nd out of all of the trials) combined with decent maximum water surface elevation errors (ranking in 2nd place for the high water mark near the ferry house and 6th place near the civil protection building), in spite of a mediocre maximum time lag of peak discharge (6 hours for 2006). Additional details regarding Stage 2 can be found in Appendix D, Tables D.6 and D.7.

In the 64 trials of Stage 1 of 2D calibration, the RMSE ranged from 0.22 to 0.87, MAE from 0.18 to 0.79, and the CSI from 0.975 to 0.983. The results were pared down to the 11 trials which ranked in the top half for each of the comparative indicators. The value for woodland areas showed weak influence, which appeared reasonable given that the woodland areas are mostly on high elevation, and therefore don't overlap much with the flood extent. To address this value for Stage 2, the value of 0.1600 was selected, as it was the woodland area value present in these

5. Results

top 11 trials. For urban areas, the values of 0.0773 and 0.1600 were equally represented in the top 11 trials. As the gap between these values is significant, and as the urban area was located nearest to the principle study area of Bennewitz (the main community), three new Manning's n values were set to be tested for urban areas in Stage 2. No additional values were added for agricultural areas in Stage 2, but the values were limited to those present in the top 11 trials: 0.0550, 0.0900, and 0.1600. Additional detailed results of Stage 1 of 2D calibration can be found in Appendix D, Tables D.9 and D.10.

In the 15 trials of Stage 2 of 2D calibration, the RMSE ranged from 0.21 to 0.40, MAE from 0.16 to 0.34, and the CSI from 0.976 to 0.981. The trial with the lowest RMSE and MAE had the lowest maximum absolute error of all eight points (0.33 m at AK13). Given that all of the CSI values were quite good, including the CSI of this trial (0.979), this trial was selected as the base for the final stage of 2D calibration. The Manning's n values for this trial were 0.0980 for urban areas, 0.0550 for agricultural areas, and, as for all trials in this stage 0.1600 for woodland areas. Additional detailed results of Stage 2 can be found in Appendix D, Table D.12.

In the 25 trials of Stage 3 of 2D calibration (including the selected trial from Stage 2), the RMSE ranged from 0.21 to 0.23, MAE from 0.16 to 0.19, and the CSI from 0.977 to 0.979. The trial for which the highest absolute error of all the points was the lowest was that which consisted of the original values from Stage 2 (0.0980 for urban areas, 0.0550 for agricultural areas, 0.1600 in woodland areas). The values from this trial were selected for use in the validation of the model. Additional detailed results from Stage 3 of 2D calibration can be found in Appendix D, Table D.13.

5.1.2. Calibrated Model Results

The calibration efforts resulted in the Manning's n values presented in Table 5.1.

Table 5.1.: Calibrated Manning's n values for 1D/2D unsteady flow HEC-RAS model

Region	Manning's n
1D Channel	0.0316
1D Overbanks, Zwickauer and Freiberger Mulde	0.1580
1D Overbanks, Vereinigte Mulde	0.0632
2D Urban Areas	0.0980
2D Agricultural Areas	0.0550
2D Woodland Areas	0.1600

The Manning's value for the 1D channel was also used for a small body of water in the 2D area.

Tables 5.2 and 5.3 present results from the calibration and conditional validation of the HEC-RAS 1D/2D model. The largest absolute error of discharge at Golzern is for the 2013 validation event at 224.90 m³/s, which represents 10.92% deviation from the observed value. The largest error as a percent of the observed peak discharge is for the 2011 event, which simulates the peak 13.11% higher than the observed record. A discussion of the results can be found in Section 6.1. The largest time delay in hitting the peak is for the 2006 calibration event, as the simulated event peaks 6 hours after the observed peak discharge at Golzern.

5. Results

Table 5.2.: Calibration and validation of 1D/2D unsteady flow HEC-RAS model based on peak discharge (Q) at Golzern

Type	Event	Peak Q at Golzern			
		Simulated Q [m ³ /s]	Q Error	Q Error % of Obs.	Time Delay [hours]
Calibration	2002	2591.24	-12.34	-0.47	1
Calibration	2006	652.23	-5.67	-0.86	6
Calibration	2010	753.19	56.19	8.06	2
Calibration	2011	922.94	106.94	13.11	3
Validation	2013	2284.9	224.90	10.92	1

All errors are calculated as simulated minus observed.

Table 5.3.: Calibration and validation of 1D/2D unsteady flow HEC-RAS model based on CSI

Type	Event	CSI	
		2D Flow Area	Investigation Area
Calibration	2002	0.977	0.961
Validation	2013	0.564*; 0.671	0.844

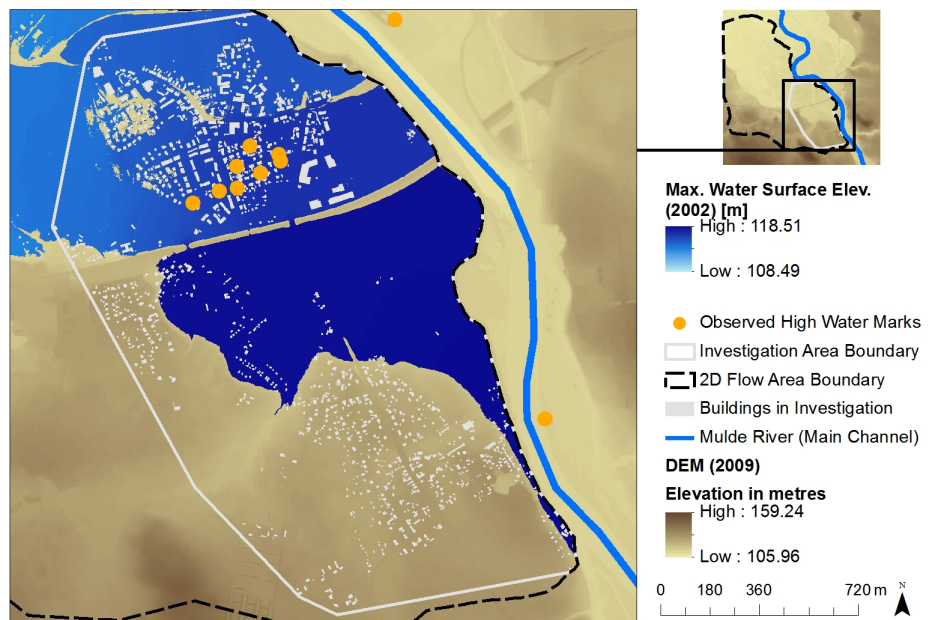
CSI values are not available for the 2006, 2010, and 2013 events, as there was no observed extent for comparison. Single asterisk indicates the CSI value calculated without filling the gaps in the observed and simulated extents.

For the CSI, a value of 1 represents a perfect match and 0 represents no overlap between the observed and simulated flood extents. The CSI for the 2002 event is 0.977 for the entire 2D flow area and 0.961 for the investigation area alone. Using the gap-filling methodology to align with that followed for the 2002 calibration event, the CSI for the 2013 validation event is 0.671 in the full 2D flow area. The gap filling procedure does not affect the CSI within the investigation area, which is measured at 0.844 for the 2013 event.

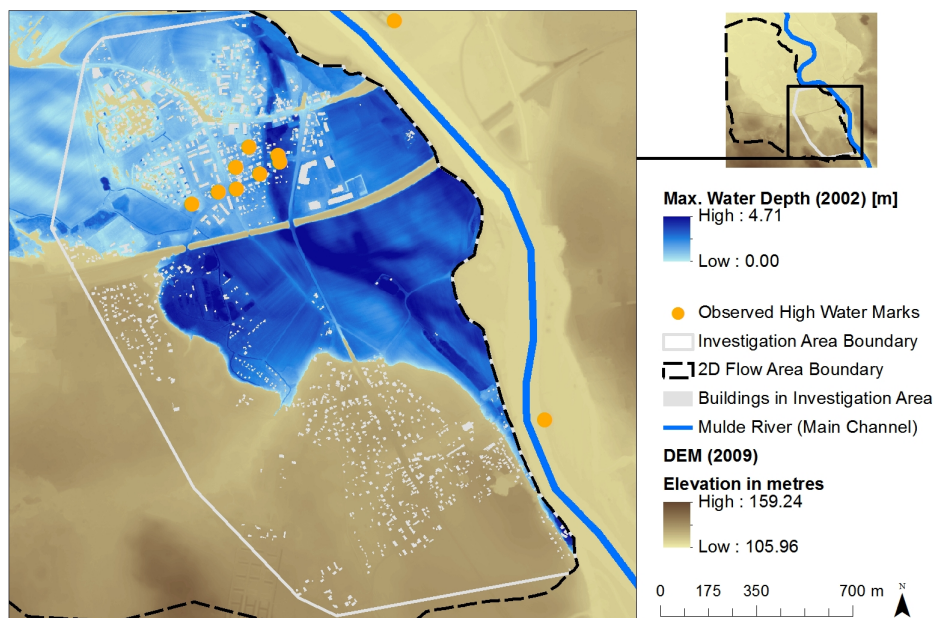
The maximum water surface elevation and maximum water depth results for 2002 and 2013 in the 2D flow area are presented in Figures 5.1 and 5.2. The maximum water surface elevation results for the 1D calibration events (2006, 2010, and 2011) are available in Appendix D, Figures D.1, D.2, and D.3, as there are no extent or observed water surface elevation data within the 2D flow area for any of these three events.

In Figure 5.1, it is evident that the maximum water surface elevation upstream of the train bridge is higher than that below the train bridge. In Figure 5.2, the water does not flood past the train bridge (the tunnels under the bridge were closed during this event), and there is no visible variation in water surface elevation within the flooded portion of the investigation area. Maximum water depth, however, varies based on variability in the DEM.

5. Results



a.



b.

Figure 5.1.: Maximum water surface elevation and maximum water depth in investigation area for 2002 event, simulated by calibrated 1D/2D unsteady flow HEC-RAS model

Darker blue indicates deeper maximum water surface elevation (a) or maximum water depth (b) over the course of the simulation. Orange points indicate the locations of the ten observed high water marks.

The Mulde River channel flows along the northeast boundary of the 2D flow area, from southeast to northwest.

5. Results

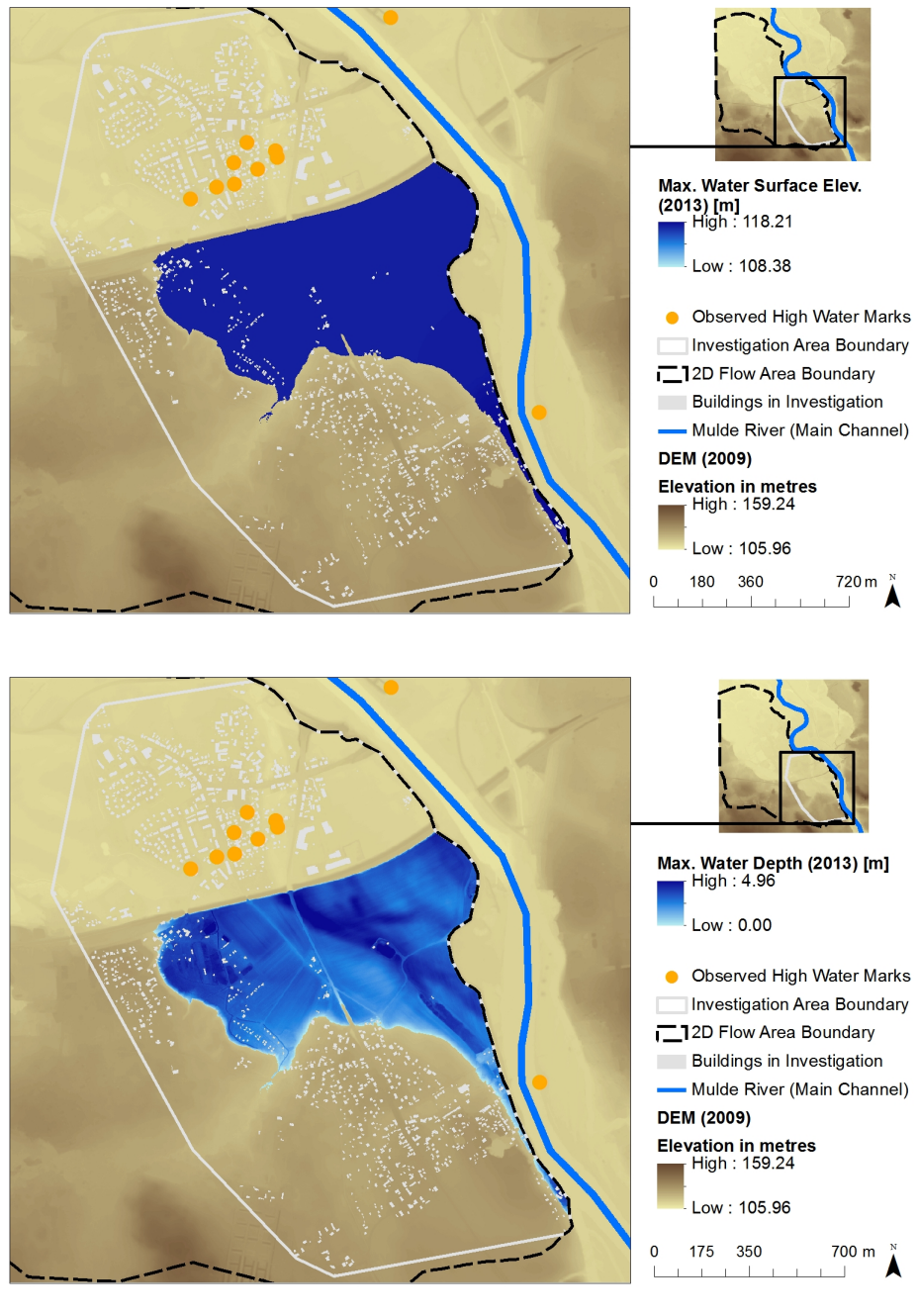


Figure 5.2.: Maximum water surface elevation and maximum water depth in investigation area for 2013 event, simulated by calibrated 1D/2D unsteady flow HEC-RAS model

Darker blue indicates deeper maximum water surface elevation (a) or maximum water depth (b) over the course of the simulation. Orange points indicate the locations of the ten observed high water marks.

The Mulde River channel flows along the northeast boundary of the 2D flow area, from southeast to northwest.

Figures 5.3 and 5.4 present the comparison between the simulated and observed flood extents for 2002 and 2013, respectively, within the investigation area. Both figures accurately represent the main community of Bennewitz (flooded in 2002, dry in 2013). As the edge of the investigation area controls the east, north, and northwest borders of the flood extent shapefiles, the comparison is focused on the south and southwest edges. The simulated 2002 flood extent appears more similar to the observed flood extent data than that of 2013. From a visual comparison, the 2002

5. Results

flood extent has an almost equal pixels which are false positives (simulated as wet, observed as dry) vs misses (simulated as dry, observed as wet), whereas the simulated 2013 flood extent errors are dominated by false positives (i.e. the model mostly overestimates the inundated area for the 2013 event).

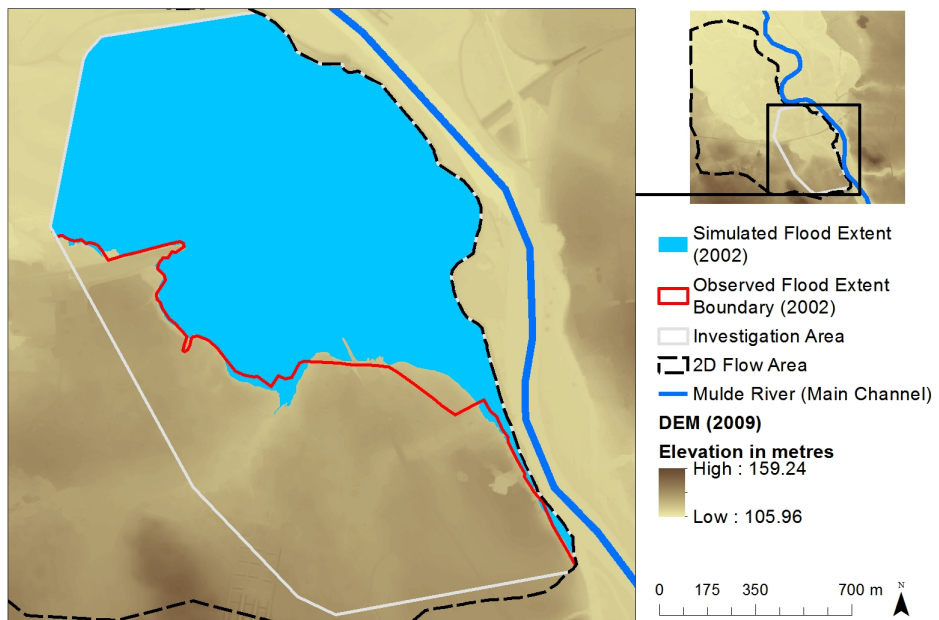


Figure 5.3.: Flood extent of 2002 event simulated by 1D/2D unsteady flow HEC-RAS model compared to observed flood extent

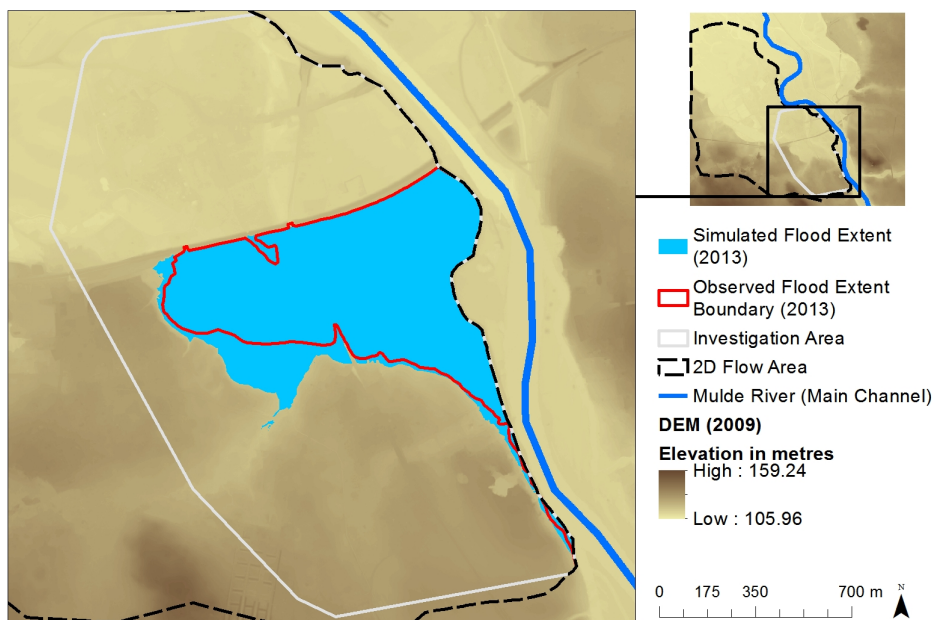


Figure 5.4.: Flood extent of 2013 event simulated by 1D/2D unsteady flow HEC-RAS model compared to observed flood extent

5. Results

Table 5.4 presents the simulated water surface elevations at high water marks for each of the four calibration events and the one validation event. Observed high water mark records were only available for the 2002 event. There was no record of flooding in the main community of Bennewitz in 2006, 2010, 2011, and 2013, and thus the water surface elevations for these eight marks are considered to be the same elevation as the DEM (resulting in error values of 0.00 m). All errors are calculated as simulated minus observed. For the 2002 event, maximum water surface elevation errors within the 2D flow area range from 0.00 to 0.32 m. That for the high water marks in the 1D model component (MB20 and LS6) range from -0.09 to 0.66.

Table 5.4.: Maximum water surface elevation error for calibrated 1D/2D unsteady flow model at high water marks

Type	Event	Maximum Water Surface Elevation Error [m]									
		BH20	RB15	ET7	RAT	AK4	AK13	ET25	ET28	MB20	LS6
Cal.	2002	-0.07	0.00	0.12	0.31	0.32	-0.33	-0.01	-0.16	-0.09	0.66
Cal.	2006	0.00	0.00	0.00	0.00	0.00	0.00	0.00	0.00	n/a	n/a
Cal.	2010	0.00	0.00	0.00	0.00	0.00	0.00	0.00	0.00	n/a	n/a
Cal.	2011	0.00	0.00	0.00	0.00	0.00	0.00	0.00	0.00	n/a	n/a
Val.	2013	0.00	0.00	0.00	0.00	0.00	0.00	0.00	0.00	n/a	n/a

Figure 5.5 presents the hydrographs of water surface elevation at each of the high water marks in the 2D flow area for the calibrated 2002 event simulation.

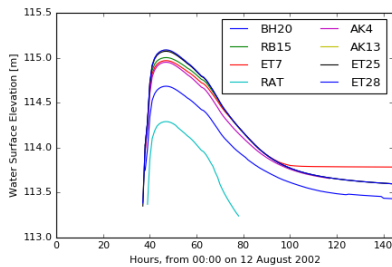


Figure 5.5.: Water surface elevation at the high water marks in the 2D flow area throughout the 2002 event, as simulated by 1D/2D HEC-RAS model

Table 5.5 presents the calibrated model's performance results in terms of stability, computational effort, and volume accounting. No individual simulation hit the number of maximum iterations allowed (20) more than seven times. The highest run time was just over an hour for the 2013 event, and the highest real minute per simulation day value was 7.67 minutes for the 2002 event. None of the models reached a 1% volume accounting error in the entire model (1D and 2D components) nor in the 2D flow area calculated separately. Discussion regarding these criteria, as well as discussion regarding ease-of-use, can be found in Section 6.

5. Results

Table 5.5.: Stability, computational effort, and volume accounting for calibrated 1D/2D HEC-RAS unsteady flow model

Type	Year	Stability	Computational Effort			Volume Error [%]	
		Max. It.	Run Time	Sim. Days	Real Min./Sim. Day	Entire Model	2D Area Only
Cal.	2002	6	0:46:00	6	7.67	0.002	0.456
Cal.	2006	2	0:26:23	10	2.64	0.040	0.066
Cal.	2010	1	0:15:00	7	2.14	0.023	0.463
Cal.	2011	1	0:27:47	10	2.78	0.098	0.285
Val.	2013	7	1:02:16	9	6.92	0.040	0.527

The column labelled "Max. It." indicates the number of times each simulation had a location and timestep which reached the maximum limit of 20 iterations to calculate the water surface elevation. Computation time is represented as real-time minutes required per simulation day, as the total run time is not comparable among events of different lengths. The column labelled "Volume Error" provides the percent error in water volume accounting (volume of water introduced into the model versus volume of water exiting or remaining in the model at the end of the simulation).

Table 5.6 presents the consistency of output of the calibrated model. The model was run ten separate trials for the 2002 event, with no changes to the input data or model settings. The maximum water surface elevation results showed no difference from one trial to the next. All trials reached the maximum number of iterations allowed (20) exactly six times. The run time for all events ranged from 40 minutes 24 seconds to 45 minutes 8 seconds (6.73 to 7.52 real minutes per simulation day). The volume accounting error, peak discharge magnitude at Golzern, and peak discharge timing at Golzern were all exactly the same for all trials.

Table 5.6.: Output consistency of calibrated 1D/2D HEC-RAS unsteady flow model, for the 2002 event

Trial	Stability	Computational Effort		Volume Error [%]		Peak Q at Golzern	
	Max. It.	Run Time	Real Min./Sim. Day	Entire Model	2D Flow Area Only	Sim. Q [m ³ /s]	Time Delay [hours]
1	6	0:43:20	7.22	0.002	0.456	2591.24	1
2	6	0:45:08	7.52	0.002	0.456	2591.24	1
3	6	0:44:51	7.48	0.002	0.456	2591.24	1
4	6	0:44:20	7.39	0.002	0.456	2591.24	1
5	6	0:44:36	7.43	0.002	0.456	2591.24	1
6	6	0:44:29	7.41	0.002	0.456	2591.24	1
7	6	0:42:05	7.01	0.002	0.456	2591.24	1
8	6	0:40:24	6.73	0.002	0.456	2591.24	1
9	6	0:40:24	6.73	0.002	0.456	2591.24	1
10	6	0:40:28	6.74	0.002	0.456	2591.24	1

The column labelled "Max. It." indicates the number of times each simulation had a location and timestep which reached the maximum limit of 20 iterations to calculate the water surface elevation. Computation time is represented with both total run time for a 6 day event and as real-time minutes required per simulation day, for comparison to Table 5.5. The column labelled "Volume Error" provides the percent error in water volume accounting (volume of water introduced into the model versus volume of water exiting or remaining in the model at the end of the simulation).

5. Results

5.1.3. Model Sensitivity

Tables 5.7, 5.8, and 5.9 present the results of the sensitivity analysis for the model, compared to the 2002 event.

The simulation using the 2D full momentum equation produced a large number of times where the computations reached their maximum number of allowed iterations, primarily in the 2D flow area, and this simulation was roughly twice as computationally expensive compared to the 2002 calibration simulation. In addition, this simulation produced higher volume accounting errors in comparison to the calibration simulation. The simulations varying upstream and downstream boundary conditions showed very little difference in stability, computational effort, and volume error, when compared to the calibration simulation.

The simulation using the full momentum equations in the 2D flow area made no difference in the peak at Golzern (which occurs in the upstream 1D portion of the model). However, the 2D full momentum equations produced a decrease of 5 to 16 cm in maximum water surface elevation in the 2D flow area, and an increase of 3 to 5 cm in maximum water surface elevation in the 1D component (see MB20 and LS6 in Table 5.8).

A 15% increase of the upstream discharge produced a sizeable increase in the magnitude of peak discharge at Golzern though the time delay remained the same. The maximum water surface elevations at the eight observation points in the 2D flow area increased 10-14 cm under this simulation, while the two points in the 1D component increased by 9 to 23 cm. A 15% decrease in upstream discharge produced a noticeable decrease in the peak discharge at Golzern, as well as decreases of 11 to 20 cm for all ten observation points.

Increasing the 1D downstream boundary by 20% increased the peak at Golzern by 1 cm. Other than this, changes to each the downstream boundary conditions showed no difference in peak Q at Golzern (magnitude or timing) and no difference in simulated maximum water surface elevation.

5. Results

Table 5.7.: Sensitivity of calibrated 1D/2D HEC-RAS unsteady flow model to equation sets and boundary conditions, for the 2002 event (1)

Variable Changed	Stability	Computational Effort		Entire Model	2D Flow Area Only	Peak Q, Golzern	Time Delay [hours]
		Max. It.	Run Time Real Min./Sim. Day				
2002 <i>Cal.</i> <i>Sim.</i>	6	0:46:00	7.67	0.002	0.456	2591.24	1
2D Full Moment.	11694 *	1:32:58	15.49	0.371	1.614	2591.24	1
1D US BCs +15%	12	0:47:21	7.89	0.084	0.330	2977.71	1
1D US BCs -15%	9	0:43:18	7.22	0.024	0.645	2205.76	1
1D DS BC +20%	5	0:47:34	7.93	0.033	0.456	2591.25	1
1D DS BC -20%	6	0:50:01	8.34	0.038	0.456	2591.24	1
2D N DS BC +20%	6	0:42:38	7.11	0.002	0.456	2591.24	1
2D N DS BC -20%	6	0:42:04	7.01	0.002	0.456	2591.24	1
2D W DS BC +20%	6	0:42:01	7.00	0.002	0.456	2591.24	1
2D W DS BC -20%	6	0:42:20	7.06	0.002	0.456	2591.24	1

The "Variable Changed" column indicates the component of the model being examined. In this column, "US" denotes upstream, "BC" denotes boundary condition(s), and the "N" and "W" indicate the location of the particular boundary (north or west, respectively) of the 2D flow area. The 2002 calibration simulation results are presented for comparison. The column labelled "Max. It." indicates the number of times each simulation had a location and timestep which reached the maximum limit of 20 iterations to calculate the water surface elevation. Computation time is represented with both total run time for a 6 day event and as real-time minutes required per simulation day, for comparison to Table 5.5. The column labelled "Volume Error" provides the percent error in water volume accounting (volume of water introduced into the model versus volume of water exiting or remaining in the model at the end of the simulation). Single asterisk indicates that only six of these computations were due to reaching the maximum number of iterations in the 1D portion of the model. The rest are from reaching the maximum number of iterations for individual cells in the 2D area.

5. Results

Table 5.8.: Sensitivity of calibrated 1D/2D HEC-RAS unsteady flow model to equation sets and boundary conditions, for the 2002 event (2)

Variable Changed	Simulated Maximum Water Surface Elevation [m]				
	BH20	RB15	ET7	RAT	AK4
2002 Cal. Sim.	114.68	115.00	114.97	114.30	114.95
2D Full Momentum	114.54	114.87	114.83	114.19	114.79
1D US BCs +15%	114.81	115.10	115.08	114.44	115.08
1D US BCs -15%	114.55	114.89	114.85	114.15	114.81
1D DS BC +20%	114.68	115.00	114.97	114.30	114.95
1D DS BC -20%	114.68	115.00	114.97	114.30	114.95
2D N DS BC +20%	114.68	115.00	114.97	114.30	114.95
2D N DS BC -20%	114.68	115.00	114.97	114.30	114.95
2D W DS BC +20%	114.68	115.00	114.97	114.30	114.95
2D W DS BC -20%	114.68	115.00	114.97	114.30	114.95

The "Variable Changed" column indicates the component of the model being examined. In this column, "US" denotes upstream, "BC" denotes boundary condition(s), and the "N" and "W" indicate the location of the particular boundary (north or west, respectively) of the 2D flow area. The 2002 calibration simulation results are presented for comparison.

Table 5.9.: Sensitivity of calibrated 1D/2D HEC-RAS unsteady flow model to equation sets and boundary conditions, for the 2002 event (3)

Variable Changed	Simulated Maximum Water Surface Elevation [m]				
	AK13	ET25	ET28	MB20	LS6
2002 Cal. Sim.	115.08	115.07	115.09	117.27	114.61
2D Full Momentum	114.94	114.93	114.94	117.32	114.64
1D US BCs +15%	115.22	115.20	115.22	117.50	114.69
1D US BCs -15%	114.94	114.94	114.95	117.03	114.40
1D DS BC +20%	115.08	115.07	115.09	117.27	114.61
1D DS BC -20%	115.08	115.07	115.09	117.27	114.61
2D N DS BC +20%	115.08	115.07	115.09	117.27	114.61
2D N DS BC -20%	115.08	115.07	115.09	117.27	114.61
2D W DS BC +20%	115.08	115.07	115.09	117.27	114.61
2D W DS BC -20%	115.08	115.07	115.09	117.27	114.61

The "Variable Changed" column indicates the component of the model being examined. In this column, "US" denotes upstream, "BC" denotes boundary condition(s), and the "N" and "W" indicate the location of the particular boundary (north or west, respectively) of the 2D flow area. The 2002 calibration simulation results are presented for comparison.

5.2. Task 2: Repeated Simulation with Changing Boundary Conditions

5.2.1. Extent of Automation of the Process of Changing Boundary Conditions

The process described in Section 4.3 and supported by Appendix G removes a significant portion of the manual effort otherwise required in order to prepare large numbers of simulations with varied upstream boundary conditions. The principle time-saving components are the creation of the unsteady flow files and plan files, the method for importing the unsteady and plan files to

5. Results

the project, and the method for extracting result TIF files from HEC-RAS after the simulation (introduced in Task 1, supported by Appendix B). The scripts for creating unsteady flow files and plan files, and that for extracting and renaming the TIF files take less than 5 seconds each for 81 discharge hydrographs (assuming proper configuration, correct paths, etc.). The method for importing unsteady files and plan files takes less than 1 minute total for 81 simulations. Additional thoughts regarding limitations and room for improvement will be presented in Section 6.2.1.

5.2.2. Sensitivity of Simulated Future Flood Characteristics to Changing Boundary Conditions

Table 5.10 presents descriptive statistics of extent (area in m^2) and of maximum water depth at the six points of interest (POIs). Only the maximum flood event from each 100-year hydrological discharge time series is included in the set of 81 total simulations.

Table 5.10.: Descriptive statistics of extent and of maximum water depth for future highest peak flood events simulated by 1D/2D HEC-RAS unsteady flow model under simulated future climate conditions

Model Comb.	Statistic	Extent [km^2]	Maximum Water Depth by Point of Interest [m]					
			POI1	POI2	POI3	POI4	POI5	POI6
All (81)	Min.	1.34	1.21	1.79	1.19	0.40	0.14	1.66
	Max.	1.41	2.39	2.96	1.71	0.96	0.46	2.36
	Range	0.07	1.18	1.17	0.52	0.57	0.31	0.70
	Mean.	1.38	1.76	2.33	1.42	0.64	0.26	1.97
	Std.	0.02	0.40	0.39	0.17	0.19	0.10	0.23
8, HadGEM2 (27)	Min.	1.36	1.46	2.04	1.29	0.50	0.18	1.80
	Max.	1.39	1.91	2.48	1.47	0.69	0.27	2.05
	Range	0.03	0.45	0.45	0.18	0.19	0.09	0.25
	Mean.	1.37	1.63	2.20	1.36	0.57	0.22	1.89
	Std.	0.01	0.16	0.16	0.06	0.07	0.03	0.09
9, ECHAM5 + RACMO (27)	Min.	1.34	1.21	1.79	1.19	0.40	0.14	1.66
	Max.	1.40	1.50	2.07	1.31	0.52	0.19	1.82
	Range	0.06	0.29	0.29	0.11	0.12	0.05	0.16
	Mean.	1.35	1.38	1.95	1.26	0.47	0.17	1.75
	Std.	0.01	0.11	0.11	0.04	0.05	0.02	0.06
10, ECHAM5 + REMO (27)	Min.	1.37	2.14	2.71	1.57	0.80	0.34	2.18
	Max.	1.41	2.39	2.96	1.71	0.96	0.46	2.36
	Range	0.04	0.25	0.25	0.14	0.16	0.11	0.18
	Mean.	1.40	2.27	2.84	1.64	0.88	0.40	2.27
	Std.	0.01	0.09	0.09	0.05	0.06	0.04	0.07

All descriptive statistics are based on the maximum water depth for each individual flood simulation. The column titled “Model Comb.” indicates the model combination (8, 9, 10, or all), as well as the number of simulations included, in parentheses.

Of all of the 81 simulations, the maximum flood extent comes from model combination 10, while the minimum comes from model combination 9. Model combination 9 also has the greatest range of the three model combinations. The standard deviation does not appear to vary greatly among the model combinations. The mean of model combinations 8 and 9 are both below the average for the entire group of 81 simulations. All of these findings are in accordance with the descriptive statistics of the 81 input hydrographs, presented in Section 4.3, Table 4.4 except the model combination with the greatest range. Of the input hydrographs, model combination 8 has

5. Results

the greatest range, whereas model combination 9 has the greatest range of flood extent area of the resulting hydrodynamic simulations.

Like flood extent, the minimum maximum water depth for each POI out of all 81 simulations is always one of the results from model combination 9, and the maximum maximum water depth for each POI out of all 81 simulations is always one of the results from model combination 10. The range of maximum water depth values is almost always highest for model combination 8, the only exception being for POI 5, for which model combination 10 has the greatest range. Like with flood extent, the mean of all 81 simulations is always higher than the mean for model combination 8 and model combination 9, but always lower than for model combination 10.

Figure 5.6 presents a histogram for the maximum water depth at each of the six POIs from all 81 simulations. The shapes of the POI histograms appear to be relatively consistent with one another.

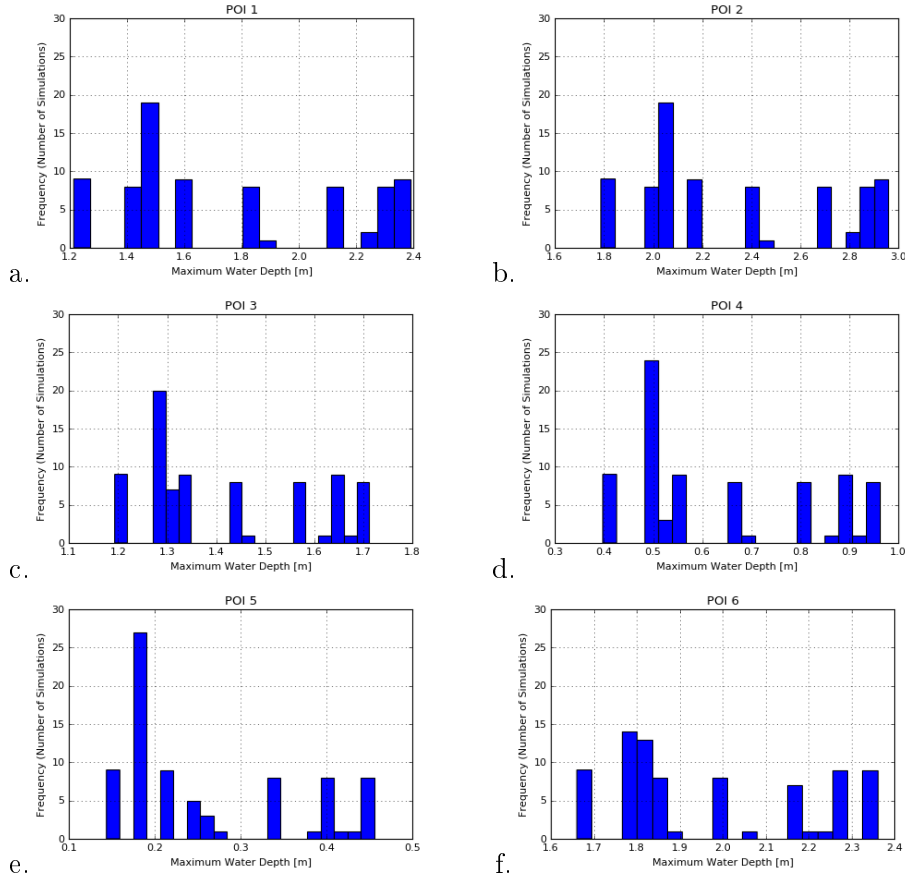


Figure 5.6.: Histograms of maximum water depth at each of the points of interest (POIs) in the 2D flow area of 1D/2D HEC-RAS model under changing boundary conditions

Each histogram was created with 20 bins.

5. Results

5.2.3. Uncertainty of Flood Extent

Figure 5.7 presents the percent of simulations that inundated each individual pixel. Much of the investigation area is flooded by 100% of the simulations.

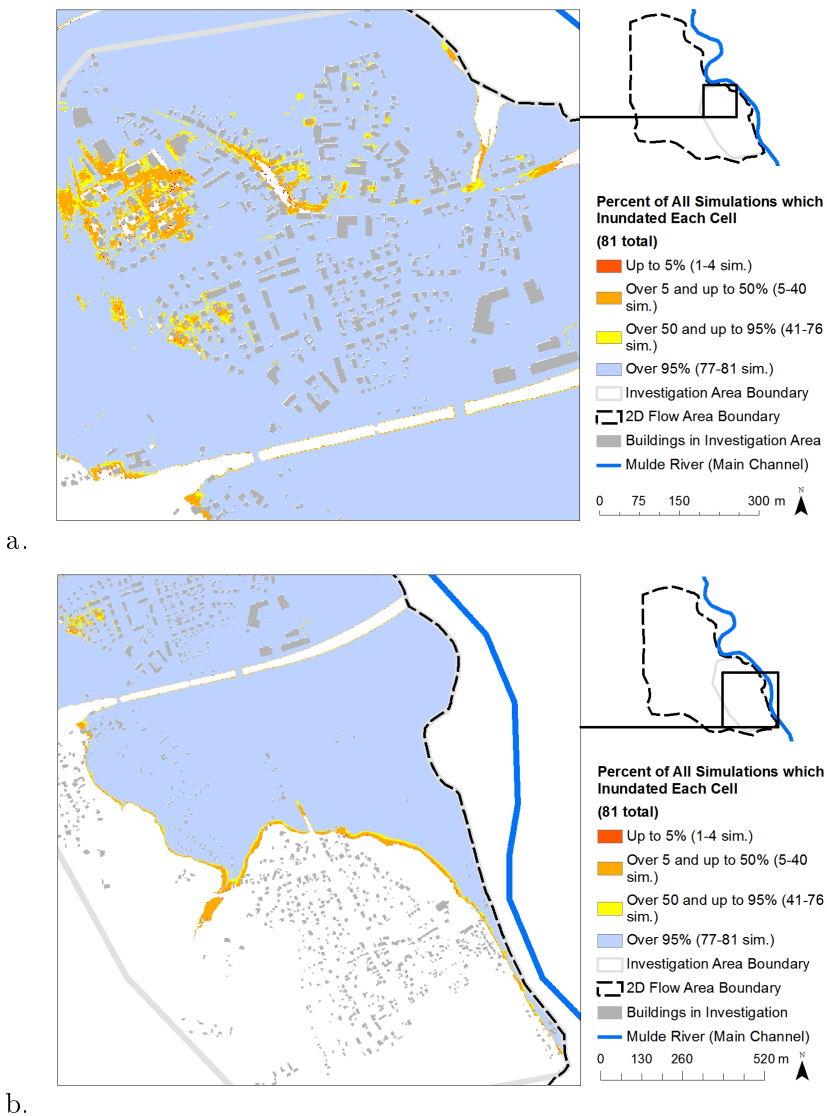


Figure 5.7.: Sensitivity of flood extent to the upstream boundary condition for all 81 1D/2D HEC-RAS unsteady flow simulations

For 81 distinct 101 year discharge time series produced by the model chain, the maximum peak discharge for each data set was fed into the 1D/2D HEC-RAS model, after the model's calibration and conditional validation for recent events. This figure presents the percent of 81 simulations that inundated each pixel in the main community of Bennewitz (a) and in the community of Schmölen (b).

Figures 5.8, 5.9, and 5.10 present the percent of simulations that inundated each individual pixel for the simulations by model combination 8, 9, and 10, respectively. Only the results for the main community of Bennewitz are included in this section.

5. Results

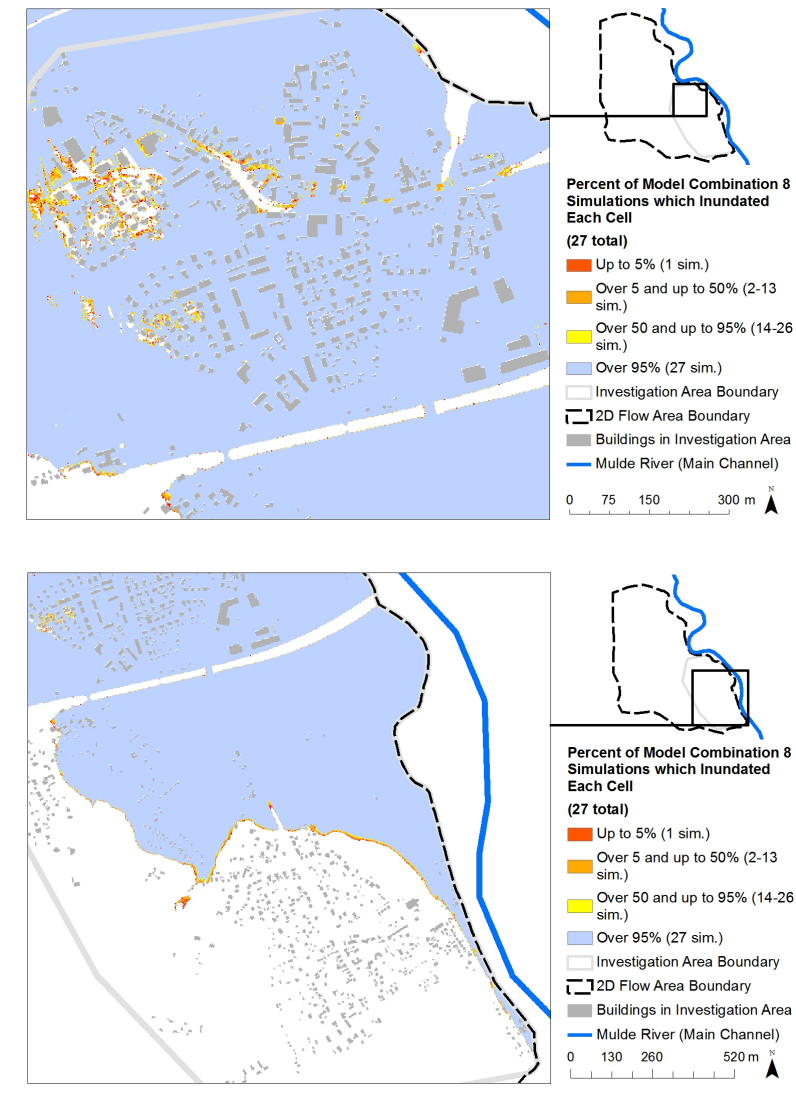


Figure 5.8.: Sensitivity of flood extent to the upstream boundary condition for the 27 model combination 8 1D/2D HEC-RAS unsteady flow simulations

For 27 distinct 101 year discharge time series produced by the model chain using model combination 8, the maximum peak discharge for each data set was fed into the 1D/2D HEC-RAS model, after the model's calibration and conditional validation for recent events. This figure presents the percent of 27 simulations that inundated each pixel in the main community of Bennewitz (a) and in the community of Schmölen (b). Model combination 8 consists of HadGEM2 (GCM) fed directly into WEREX V (ESD), without an intermediate RCM.

5. Results

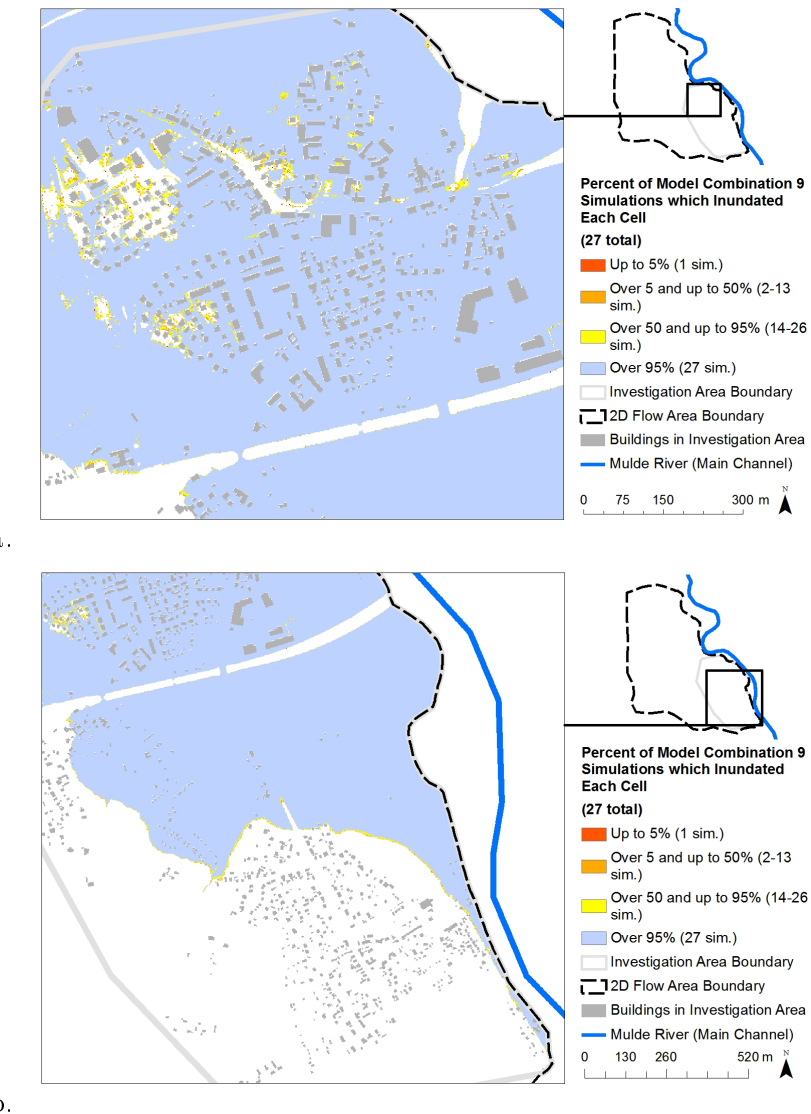


Figure 5.9.: Sensitivity of flood extent to the upstream boundary condition for the 27 model combination 9 1D/2D HEC-RAS unsteady flow simulations

For 27 distinct 101 year discharge time series produced by the model chain using model combination 9, the maximum peak discharge for each data set was fed into the 1D/2D HEC-RAS model, after the model's calibration and conditional validation for recent events. This figure presents the percent of 27 simulations that inundated each pixel in the main community of Bennewitz (a) and in the community of Schmölen (b). Model combination 9 consists of ECHAM5 (GCM) and RACMO (RCM) fed into WEREX V (ESD).

5. Results

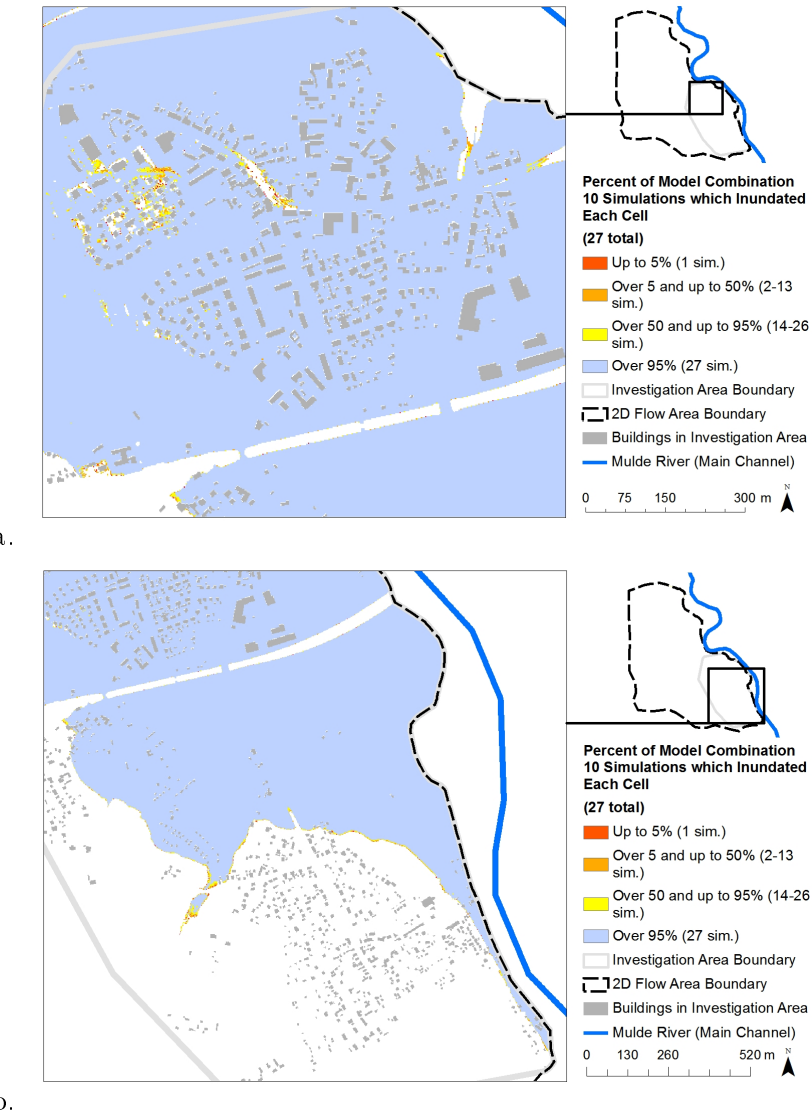


Figure 5.10.: Sensitivity of flood extent to the upstream boundary condition for the 27 model combination 9 1D/2D HEC-RAS unsteady flow simulations

For 27 distinct 101 year discharge time series produced by the model chain using model combination 10, the maximum peak discharge for each data set was fed into the 1D/2D HEC-RAS model, after the model's calibration and conditional validation for recent events. This figure presents the percent of 27 simulations that inundated each pixel in the main community of Bennewitz (a) and in the community of Schmölen (b). Model combination 10 consists of ECHAM5 (GCM) and REMO (RCM) fed into WEREX V (ESD).

Figures 5.7, 5.8, 5.9, and 5.10, show that there is more variety in extents when all three model combinations are included (i.e. greater uncertainty in flood extent in Figure 5.7). The implications of this result will be discussed in Section 6.3.

5.2.4. Uncertainty in Maximum Water Depth

Figure 5.11 presents descriptive statistics (minimum, mean, maximum) by pixel for maximum water depth for all 81 simulations in the main community of Bennewitz.

5. Results

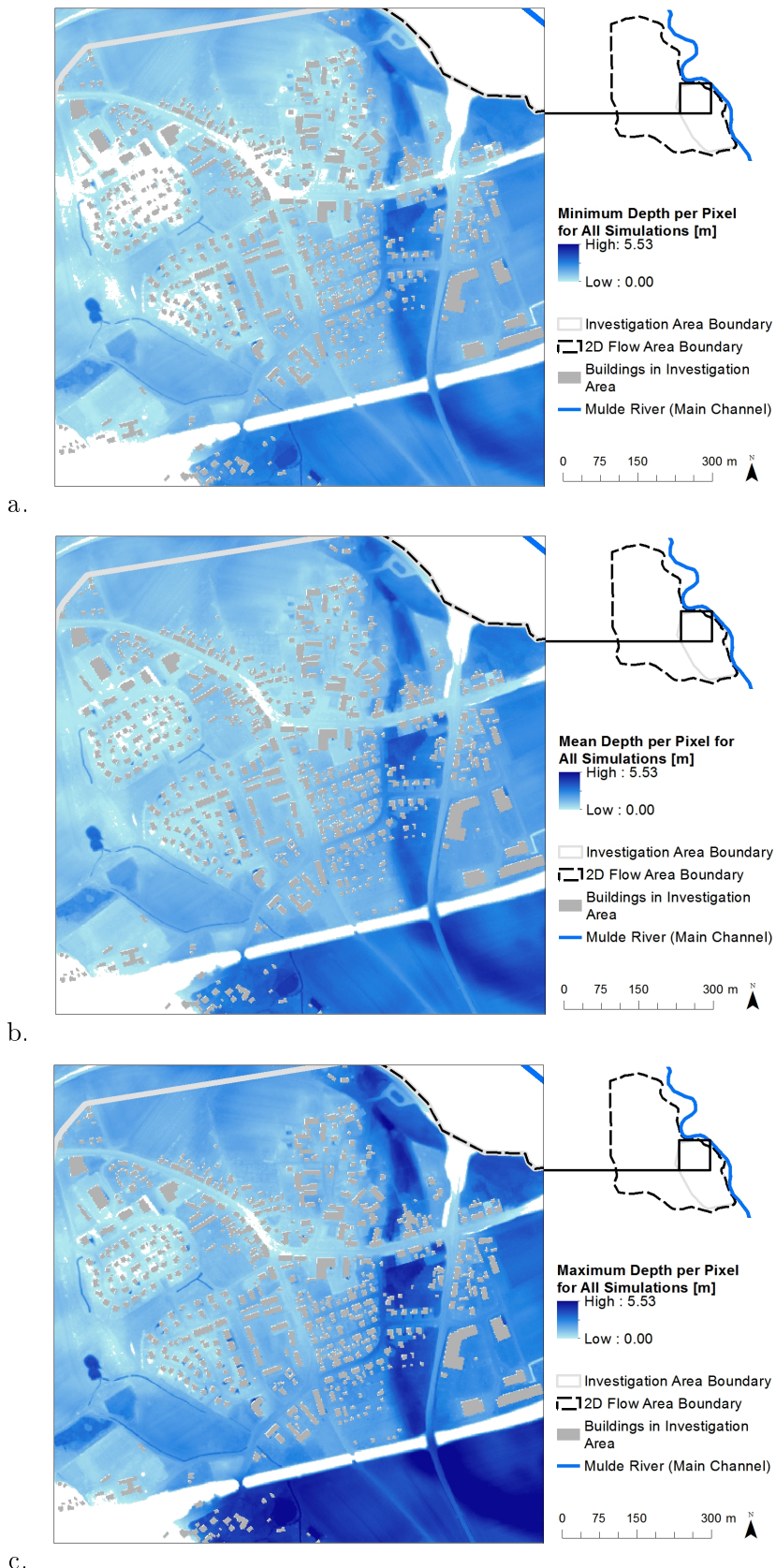


Figure 5.11.: Descriptive statistics of maximum water depth for all 81 1D/2D HEC-RAS unsteady flow simulations

For 81 distinct 101 year discharge time series produced by the model chain, the maximum peak discharge for each data set was fed into the 1D/2D HEC-RAS model, after the model's calibration and conditional validation for recent events. From 81 maximum water depth files, this figure presents the minimum (a), mean (b), and maximum (c), per cell, of all simulations.

5. Results

Figure 5.12 presents the standard deviation, per cell, of maximum water depths for all 81 simulations, and Figure 5.13 presents the same for only those simulations pertaining to model combination 8. Only model combination 8 was selected here, as this model combination had the greatest range and greatest standard deviation in water depths for all but one of the POIs (POI 5). The spatial patterns in standard deviation suggest that the variability in model combination 8 are quite similar to that of all 81 simulations. The train bridge appears to trap a large volume of water upstream, causing this water level to vary considerably in comparison to the main community of Bennewitz. Only a small few areas in between buildings in the main community of Bennewitz appear to get close to the magnitude of standard deviation experienced upstream of the train bridge.

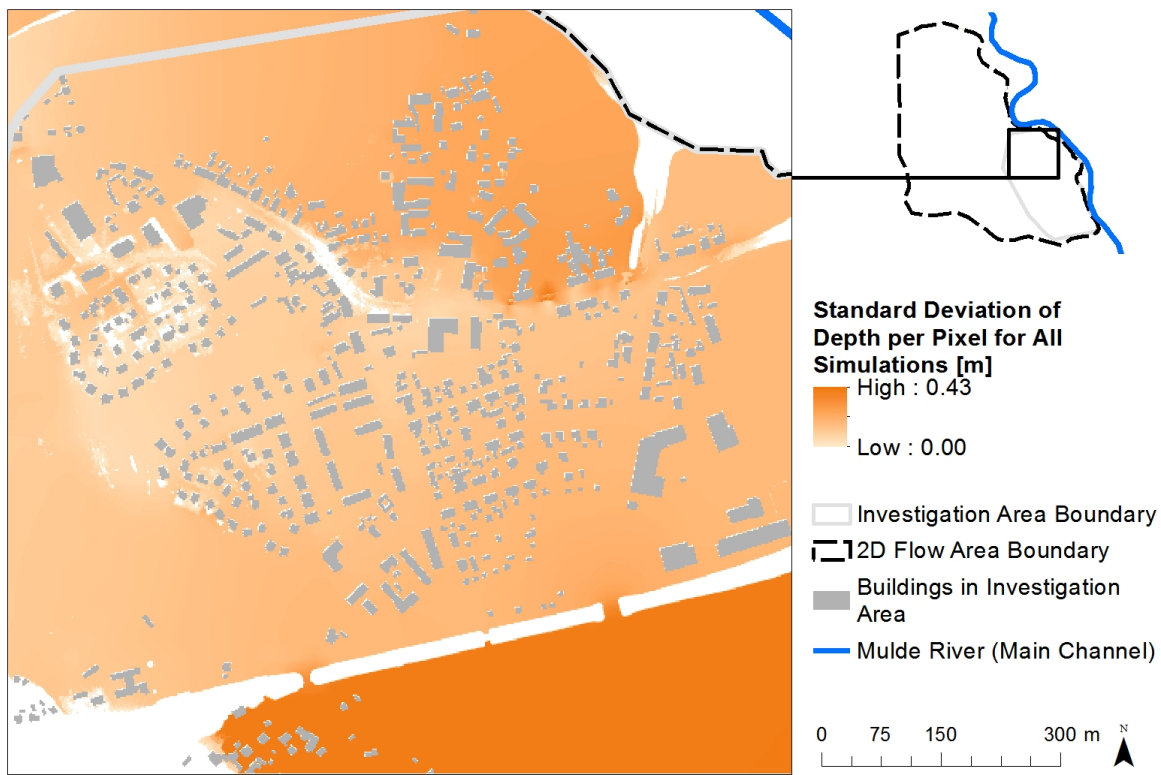


Figure 5.12.: Standard deviation per pixel of maximum water depth for all 81 1D/2D HEC-RAS unsteady flow simulations

For 81 distinct 101 year discharge time series produced by the model chain, the maximum peak discharge for each data set was fed into the 1D/2D HEC-RAS model, after the model's calibration and conditional validation for recent events. From 81 maximum water depth files, this figure presents the standard deviation, per cell, of all simulations.

5. Results

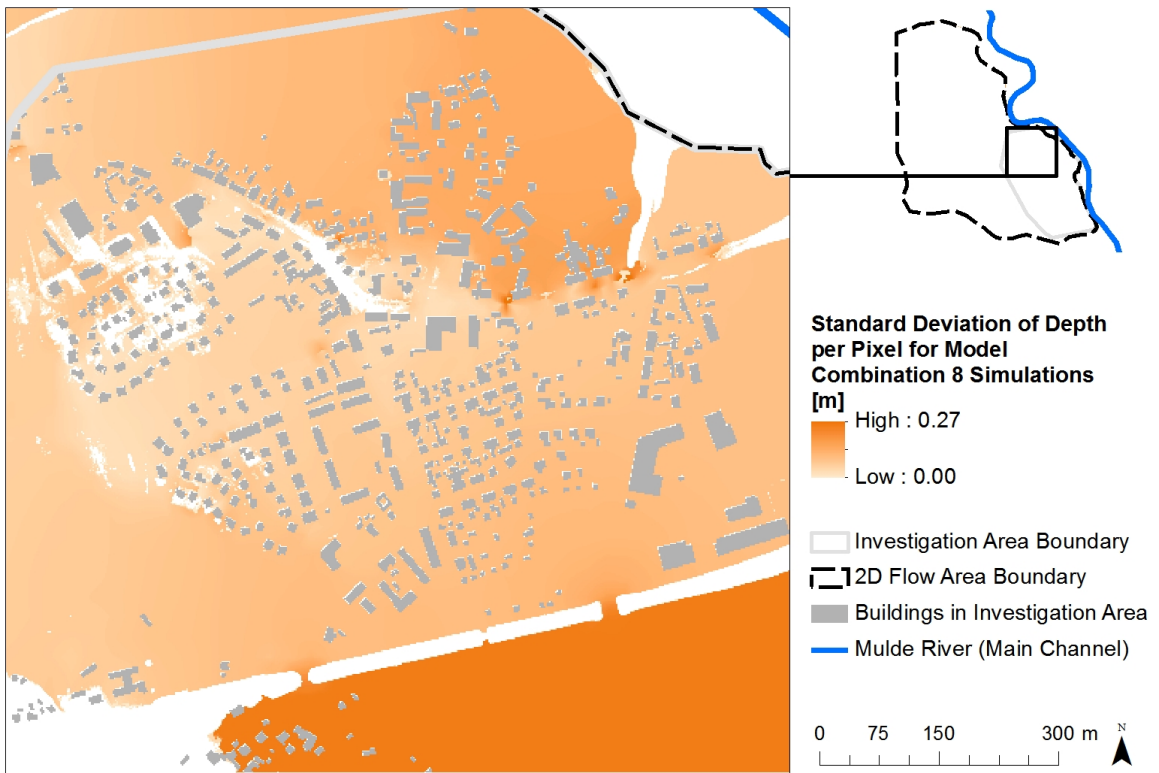


Figure 5.13.: Standard deviation per pixel of maximum water depth for model combination 8 1D/2D HEC-RAS unsteady flow simulations

For 27 distinct 101 year discharge time series produced by the model chain using model combination 8, the maximum peak discharge for each data set was fed into the 1D/2D HEC-RAS model, after the model's calibration and conditional validation for recent events. From 27 maximum water depth files, this figure presents the standard deviation, per cell, of all simulations. Model combination 8 consists of HadGEM2 (GCM) fed directly into WEREX V (ESD), without an intermediate RCM.

5.2.5. HEC-RAS Stability and Computation Effort

All but five of the 81 simulations completed successfully on the first attempt. Of the five which went unstable before finishing, two (both with model combination 8 and parameter set 9, realisation 11 and 22) successfully finished on the second attempt. The other three simulations (all from model combination 10 and realisation 11, parameter sets 1, 4, and 8) required an adjustment to the maximum headwater elevation at the train bridge in order to complete a full simulation without going unstable. For these three simulations, the maximum headwater elevation at the train bridge was increased from 118.5 to 120 m. The number of times in which a simulation reached the 20 allowable iterations for a computation ranged from 4 to 36 times, with a mean of 8 and a median of 7 times.

Computation effort of the HEC-RAS simulations ranged from 5.46 real minutes per simulation day (43 minutes 40 seconds for an 8 day simulation) to 8.56 real minutes per simulation day (1 hour 8 minutes 29 seconds for an 8 day simulation). The average was 6.74 and the median 6.76 real minutes per simulation day.

5.3. Task 3: Visualisation and Display

5.3.1. Mapping Uncertainty in Flood Extent

Figure 5.14 presents the percent of all 81 simulations as a continuous value compared to four percent categories.

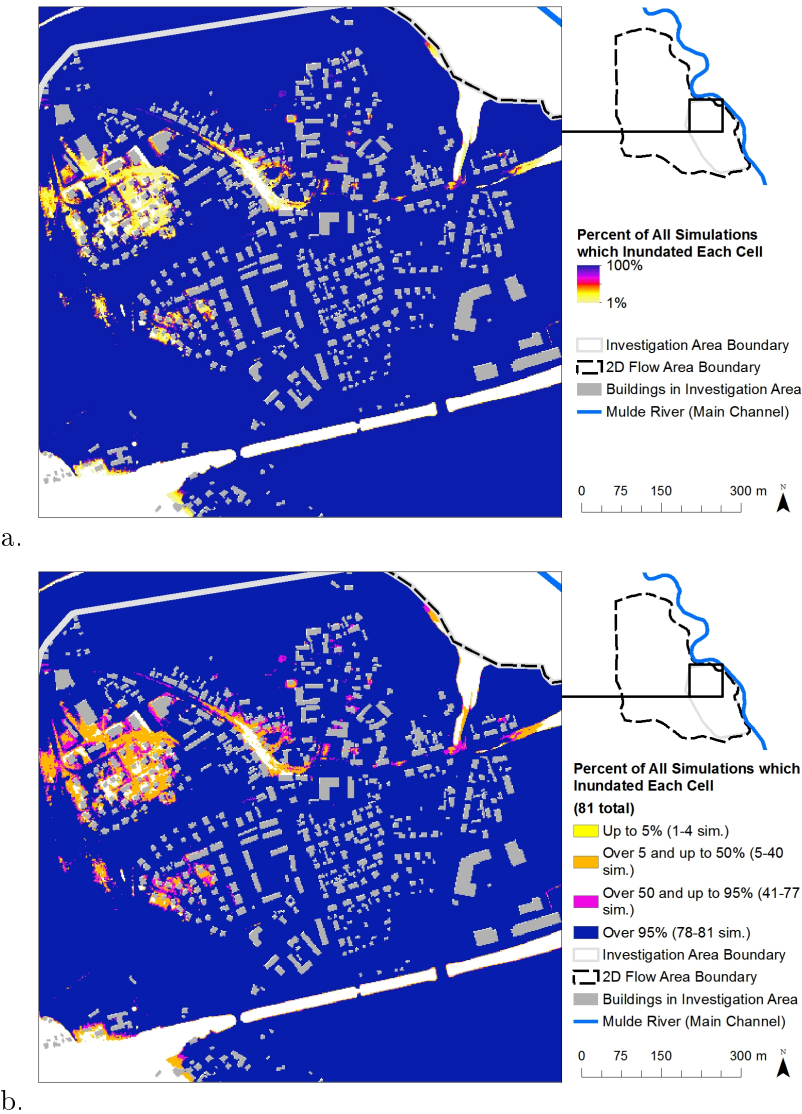


Figure 5.14.: Comparison of means of representing flood extent based on results from 1D/2D HEC-RAS unsteady flow model

Flood Extent Map 1 (a) presents the percent of simulations that wet each cell as a continuous value, whereas Flood Extent Map 2 (b) presents the percent of simulations that wets each cell in terms of four classes.

5.3.2. Mapping Uncertainty in Flood Depth

Figure 5.15 presents a comparison of the standard deviation of maximum water depth from the 27 simulations from model combination 8 under the two different scales.

5. Results

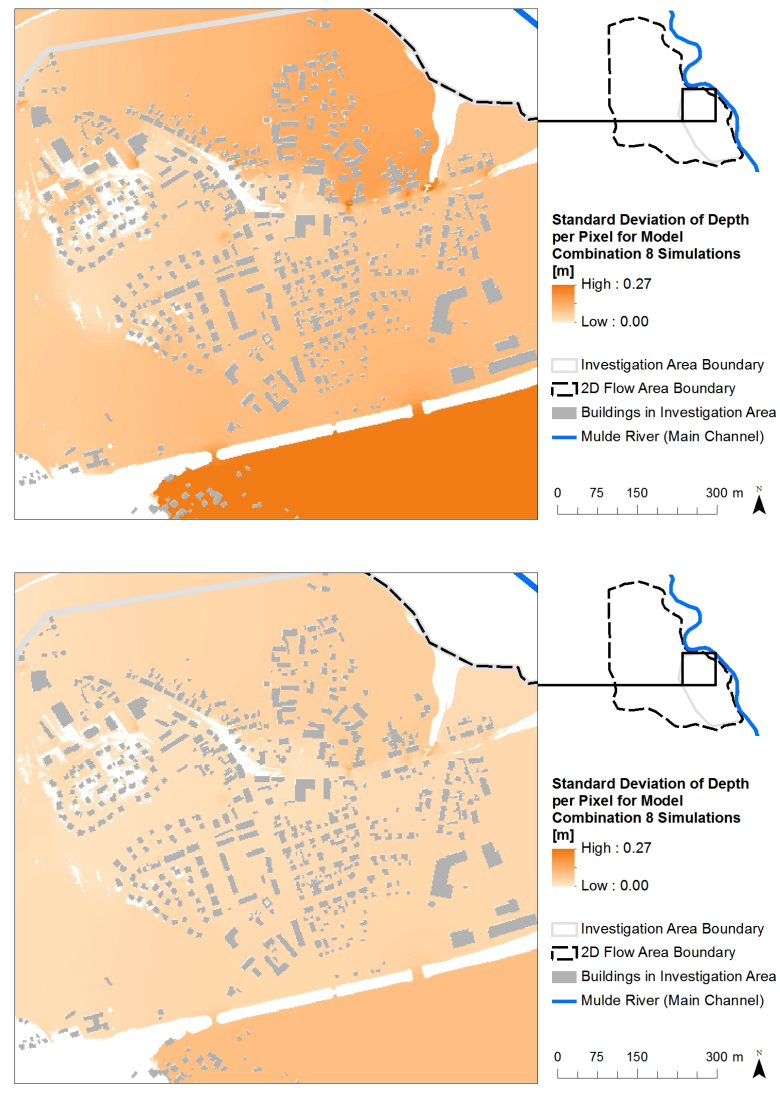


Figure 5.15.: Comparison of means of representing flood extent based on results from 1D/2D HEC-RAS unsteady flow model

Flood Depth Map 1 (a) presents the standard deviation of the maximum water depth per cell from the 27 simulations of model combination 8. Flood Depth Map 2 (b) presents the same information, but scaled to match the standard deviation of the maximum water depth per cell from all 81 simulations (all three model combinations).

6. Discussion

The discussion below is organised in terms of the five objectives presented in Section 1.3. Objective 1 discusses the results of Task 1. Objectives 2, 3, and 4 discuss the results of Task 2. Objective 5 discusses the results of Task 3.

6.1. Task 1: Model Set Up, Calibration, and Conditional Validation

Given the relatively recent release of HEC-RAS with 1D/2D capabilities (versions 5.0 and up), this task stands as one of the first evaluations of HEC-RAS 1D/2D capabilities to simulate a past flood event. Task 1 answers Research Question 1: *How accurately does the calibrated HEC-RAS 1D/2D model represent the flood extent and water surface elevation from recent flooding events?* In addition to an evaluation of model accuracy, the following discussion covers a qualitative assessment of model set up; an evaluation of model stability, computation time, and volume accounting; and model output consistency; and model sensitivity to a limited number of sources of uncertainty.

6.1.1. Model Set Up

There are many benefits of using a 1D/2D HEC-RAS model for flood inundation simulation. HEC-RAS is a popular tool for hydrodynamic simulation, and the advancements compared to past versions of the software continue to smooth the efficiency of set up time. However, compared to a 1D HEC-RAS model or 2D HEC-RAS model, one can imagine that the efficiency of the set up process is slightly reduced. The challenge of 1D/2D is that the user must set up the 1D component in addition to the 2D component, not to mention the management of issues related to the connection between the two model components. The most notable examples of challenges included:

- Creation, spacing, and adjustment of cross sections to capture the behaviour of the river and maintain stability (1D).
- Addressing errors related to the junction, a common issue with unsteady flow models in HEC-RAS (1D).
- Creation of bridges, manual entry of piers and stationing, and limited ability to save or copy bridge data when troubleshooting errors and instability issues (1D).
- Troubleshooting stationing issues regarding lateral structures (1D/2D connection).

6. Discussion

- Required manual adjustments to lateral structures whenever the 2D mesh changes (1D/2D connection).
- Troubleshooting stability issues when the 2D area is added to a previously functional model (2D).

For the 1D portion of this model, much of it was created in HEC-GeoRAS and exported to HEC-RAS, in order to leverage the tools of ArcGIS rather than the comparatively limited tools in RAS Mapper. However, RAS Mapper appears to have come a long way in a relatively short amount of time, allowing for more and more of the set up to be performed within HEC-RAS itself. The creation and manipulation of 1D geometry is not entirely efficient, but it appears to be at least fully possible, within RAS Mapper.

Regardless of the challenges faced and inefficiencies experienced, the overall impression of HEC-RAS 5.0.3 is that it is a strong tool for flood inundation modelling. It has a relatively intuitive user interface, state of the art visualisation capabilities, and is quite user-friendly in terms of extracting result data. In addition, there is a wealth of support documentation and resources for assisting with challenges of set up, simulation, or interpretation of results.

6.1.2. Accuracy

While the results from the calibrated model are subject to numerous uncertainties, the model produces strong results within the investigation area, as demonstrated below. Thus the model is considered conditionally validated for the observed past events within the investigation area.

Discharge at Golzern While Golzern falls outside of the investigation area, it is the closest gauge for which observed discharge data is available for the past events. In Section 5, Table 5.2 shows that all five of the events hit the discharge peak at Golzern within 15% of the observed value, and two of them were within 1% (2002 and 2006). As described in Section 4.2.7, the calibration process for the 1D component of the model was based on limited data. There were four calibration events, and only one gauge for which observed data was available for comparison to simulated values. Only one of these four calibration events included observed high water mark data in the 1D component of the model. As noted in Section 4.2.7, the calibration of 1D was primarily focused on the peak at Golzern. This was due to the recognition that, as the trials which showed a decrease in error for one high watermark typically showed an increase in the error of the other high watermark. Without additional information regarding which high water mark might be more reliable (less uncertain), and given that the high water marks were only available for 1 event, the focus remained on the discharge at Golzern. For most of the calibration trials, the model underestimated the discharge at Golzern in 2002 and 2006 (the lowest and highest events in this study) by as much as $114.25 \text{ m}^3/\text{s}$ and $21.08 \text{ m}^3/\text{s}$, respectively. For most of the same calibration trials, the model overestimated the discharge at Golzern in 2010 ad 2011 by as much as $67.00 \text{ m}^3/\text{s}$ and $110.32 \text{ m}^3/\text{s}$, respectively. Thus, the resulting model represents a compromise between satisfying the values for the two earlier events versus the two later events.

Over the course of the 11 years from 2002 to 2013, the river system experienced changes. The primary changes within Bennewitz are understood to be the shifting and slight raising of two portions of the left dike along the Mulde, instigated due to the aftermath of the 2002 event. These changes were accounted for to the extent possible through changes to the DEM, the levees, cross sections, and lateral structure. However, the model upstream of Bennewitz remained identical among all five events. In reality, one would expect there to be two types of differences in the model that would increase the uncertainty of the results from 1D routing. First, there may have been changes in storage and conveyance of flood waters for which data was unavailable. Towns and cities all along the Mulde experienced impacts from the 2002 flood. For example, in 2007, the LTV launched a flood protection project for Grimma, the most affected city in Saxony, with the goal being to protect it from a 1% annual chance flood (Spiegel Online, 2013). However, the

6. Discussion

project was not completed in time, and Grimma was hit hard again by the 2013 event, according to a Spiegel Online article titled "The flood is four years too early" ("Die Flut kommt vier Jahre zu früh") (Spiegel Online, 2013). However, most of these changes should have been captured by the 2009 DEM, with the exception of those between 2009 and each individual event year. Other than brief references to the project in Grimma, no data was available regarding other similar projects, much less their status at the time of each event.

Secondly, there were changes to the system during and as a result of some of the events. There is minimal data regarding dike breaches in 2002 and 2013, and no reference to breaches during any of the smaller events. In 2002 and 2013, the locations of the dike breaches are available, but the timing, depth, length, and other physical characteristics of the breaches are sparse or unavailable. As discussed in Section 4.2.3, initial attempts to represent breaches through storage areas and lateral structures did not produce promising results. Thus, the phenomenon of dike breaching introduces another source of uncertainty in the model.

Flood Extent In all four observed events during which the main community of Bennewitz was dry, the model accurately simulated them as such. The high Critical Success Indicator (CSI) for the 2002 event (0.961 in the investigation area; 0.977 for the entire 2D flow area) confirms a very good match in terms of extent (a CSI of 1.000 would represent model results which exactly match the observed data). However, as can be seen from the detailed 2D calibration results (see Appendix D, Tables D.9, D.12, and D.13), the CSI is not very sensitive to changes in roughness for this particular event. This is largely because the topography of the 2D flow area is relatively flat in the hinterland of the dike, then, after this low, flat valley, the elevation increases quickly until it reaches a plateau. Thus, if there is enough water to fill the lower elevations, the extent will not change very much with additional volume.

The CSI of 0.844 for the 2013 validation event within the investigation area is quite good. It is in line with the results from Aronica *et al.* (2002) in which the same calculation (referred to as performance measure $F^{(2)}$) produced values of 0.85 for a case study on the Imera River (Italy) and 0.72 for a case study on the River Thames (United Kingdom). The CSI for 2013 for the investigation area (0.844), as well as that calculated for the entire 2D flow area with gaps filled (0.671 with gaps filled) are both better than the same calculation (multiplied by 100 and referred to as measure of fit F) from a study on the River Severn (United Kingdom) by Horritt & Bates (2002), ranging from 63.81-65.88 for the 1998 event in 37.41-41.79 for the 2000 event under three separately calibrated hydrodynamic models.

As noted above, the CSI for the 2002 event was not very sensitive to changes in the roughness of the 2D flow area. However, the 2013 event falls in the window of discharge that is high enough to flood the 2D flow area below the train bridge and part of the area downstream of the train bridge, but low enough that it does not reach the edge of the steeper slopes. None of the calibration events fell within this range of discharge, and thus the lower CSI for 2013 for the whole 2D area is not entirely surprising. In addition, the 2013 event is that for which the error of peak discharge at Golzern was the highest. An additional 225 m³/s were flowing toward Bennewitz, and thus the flood extent was affected. However, it is suspected that uncertainty in the DEM (specifically with regard to the dike heights on both the Bennewitz and Wurzen sides) may play a strong role in the excess flooding in the 2D flow area for 2013. A detailed discussion can be found in Appendix E. However, it must also be noted that the shapefile representing observed flood extent for the 2013 event is not entirely congruent with the hard-copy representation of 2013 flood extent on display in an office of Bennewitz town hall (for which no shapefile was available). Thus, the accuracy of the observed 2013 extent data in the downstream portion of the 2D flow area is in question. However, the portion upstream of the train bridge appears to be consistent among the two. Thus, the flood extent for the 2013 event within the investigation area provides reliable validation data within the investigation area.

6. Discussion

Maximum Water Surface Elevation The accuracy of the 2D component of the model is best represented by the comparison of simulated and observed maximum water surface elevation data for the 2002 event. Of the eight high water marks in the 2D flow area, two of them are within 1 cm of the observed elevation, one is within 10 cm, two are within 20 cm, and the other three are just over 30 cm away from the observed elevation. Half of the marks are too high and other half are too low.

Combining this with knowledge of the means of observed data recording and collection, the errors are likely to be heavily influenced by uncertainty in the observed data. The high water marks were marked on the sides of buildings, and it is unknown who originally recorded the elevation or how close to the time of the flood it was recorded (for example, some of them may be estimates based on the homeowner's memory). The water mark at the town hall (RAT) was located in an area that has many changes in topography (one set of steps leading down to a lower level of the building, one ramp leading down to an entrance to the main floor of the building, and raised beds of grass and other vegetation as part of the landscaping). The maximum water surface elevation was derived from adding the observed depth above the ground to the DEM elevation, but there is no way to know which of these elevations was captured in the 2009 DEM. Additionally, and as described in Section 4.2.1, four of the high water marks were estimated from a number of metres away, as the project team did not have access to the property to take a closer measurement. All of these contribute to uncertainty in the observed water surface elevation data.

Of the ten high water marks, eight are located in the investigation area, which is fully within the 2D flow area. The model accurately portrayed all of these eight high water marks as being dry (maximum water depth of 0.00) for the 2013 event (as well as the other calibration events). In the absence of high water marks in the flooded area for the 2013 validation event, this is as close as this study can achieve in terms of validation of maximum water depth in the investigation area or 2D flow area.

6.1.3. Stability, Computational Effort, and Volume Accounting

For this study, the stability of the HEC-RAS model is evaluated in terms of the number of times the model reaches the maximum number of times the simulation hits the maximum allowable iterations (20). One must keep in mind that this is not a perfect indicator of stability. For example, the simulations that hit the maximum number of iterations more times don't always correlate to simulations that crash due to instability more often. Regardless, while recognising the imperfection of the indicator, the results suggests that the model is quite stable. In the five calibration or validation simulations, none of them had more than seven instances of reaching the maximum number of allowable iterations.

Computational effort, indicated by real minutes required per simulation day, is also an elusive criteria, particularly with only five model simulations to assess. According to Table 5.5, the model takes roughly 2 to 8 minutes of real time to run each simulation day. Though the low number of simulations to assess prohibit quantitatively significant evidence regarding what affects the computation time of a simulation, a couple of qualitative observations can be made. First, it seems that those simulations which more frequently hit the maximum number of iterations had higher run times. Second, the computation time of any given simulation over the course of the study was noticeably affected by certain other applications running on the same computer. For an anecdotal example, when the software called "pdflatex" (part of the TeX Distribution) was running at the same time as a particular HEC-RAS simulation, the simulation took more than twice as long (roughly 2.5 hours) as a repeat of the same simulation (roughly 45 minutes), initiated after the pdflatex software was closed.

The volume accounting in HEC-RAS indicates the difference between the amount of water introduced to the model compared to the amount of water which either exits the model over the course of the simulation or remains in the model at the end of the simulation. A low volume percent error suggests that a relatively low amount of water was either lost or gained erroneously

6. Discussion

as a result of the computational scheme in HEC-RAS. The volume percent error was below 1%, in both the entire model and the 2D flow area, for all five calibration or validation simulations. As recognised during the process of selecting the spacing and timestep for the model (see Section 4.2.6), the volume percent error appears to be most affected by the timestep selection. As the timestep increases, volume percent error increases as well. With the 6 second timestep of the calibrated model, volume accounting is maintained at a minimal level.

6.1.4. Output Consistency

As shown in Table 5.6, the model appears to be very consistent in terms of the peak discharge at Golzern (both timing and the discharge value itself) and maximum water surface elevation output when run multiple times with the exact same inputs. In addition, the volume accounting, as well as the number of times the model hits the maximum number of iterations, are remarkably consistent across the trials. The computation effort varies mildly. Thus, it appears that the model is quite consistent in terms of its output.

6.1.5. Model Sensitivity

Tables 5.7 and 5.8 suggest that the stability, computation time, and volume accounting for the model are sensitive to the selection of equation set for the 2D flow area. Most notably, the model took roughly twice as long to complete the simulation with the full momentum equation set in the 2D flow area. In addition, the volume accounting percent error for this simulation was the highest of all of the sensitivity analysis simulations.

The 2D full momentum equations are expected to more accurately capture the flow of the water, given that they account for local acceleration, advection, turbulence, and the Coriolis effect. The diffusion wave equations are expected to sufficiently capture the principle water dynamics in this case study, given that gravity and bottom friction terms are expected to be dominant for this particular area. However, the decrease of more than 10 cm in maximum water surface elevation when running the model with the full momentum equations suggests that further investigation may be needed in terms of whether the model could be substantially more accurate if re-calibrated using full momentum equations in the 2D area. Without re-calibrating, the simulation using the full momentum equation set produces higher errors in maximum surface elevation for six of the ten observation points (three of which are in the 2D flow area).

In terms of stability, computation time, and volume accounting, the model does not appear to be sensitive to changes in the upstream boundary condition. However, outside of these sensitivity analysis simulations, the model has been known to go unstable when the discharge in the channel is too low. Varying this particular event (the 2002 event), by 15%, this was not an issue. However, should the original event included a particularly low-flow series of discharge values, one would expect the lowering of the upstream discharge to negatively impact stability.

The upstream discharge had the anticipated impact on the peak at Golzern - an increase when upstream discharge was increased 15% and a decrease when discharge upstream was decreased 15%. The maximum water surface elevation results are noticeably, and expectedly, sensitive to the varying of upstream discharge. This component of sensitivity will be more fully explored in Task 2 of this thesis, though the results will not be directly comparable to the calibration and validation events, as they will represent artificially-generated discharge time series, and the model geometry will be slightly adjusted, as described in Section 4.3.3.

In all respects, the model is not particularly sensitive to the downstream boundary conditions. Stability, computation time, volume accounting, the peak at Golzern, and the maximum water surface elevations are all similar or exactly the same as the 2002 calibration simulation. This is considered a positive result, given that it suggests the downstream boundaries are far enough away from the main study area that they appear to have minimal impact.

6.1.6. Sources of Uncertainty

The model produced by Task 1 is a representation of reality subject to a number of sources of uncertainty. While by no means exhaustive, the following list highlights some of the most important sources of uncertainty to be aware of. This model is configured only for past events, rather than future predictions or design events of a particular recurrence interval. Therefore, all sources of uncertainty listed here would fall under the category of knowledge uncertainty, as described in Section 2.2.1.

Model selection Assumptions inherent in the use of the HEC-RAS software can be found (see Section 2.1 and Section 4.2.2), the following list details a number of assumptions specific to the process of building this model.

DEM accuracy The original 2009 DEM has an accuracy of +/- 0.2 m (Saechsisches Landesamt fuer Umwelt, Landwirtschaft und Geologie, 2016). In addition, small, thin, steep structures (such as a dike) can be difficult to capture with laser scanning techniques, and thus there may be additional uncertainty around the height of the dikes.

Representation of buildings The buildings in the 2D area are built into the DEM, and therefore water does not enter the building itself. Assuming some water entered buildings during the past events, this modelling decision introduces a level of uncertainty to the flow and inundation characteristics.

Changes in the flood risk system between 2002 and 2013 The only change considered in this project is the shifting of two portions of the Bennewitz dike and the closing of tunnels under the train bridge in 2013. The attempts to account for these changes (in the DEM, the levees, and the lateral structure) are uncertain, as they are based on limited data. In addition, there may have been other changes in the system that are unknown to the project team. Examples may include changes to the river bed elevations and location, land cover and structures in the overbanks and flooded areas, or flood protection measures (whether improvements or weakening mechanisms).

Routing simplifications As described in Section 4.2.5, the observed flow data of Großermuth and Erlln was routed from the gauges at Colditz and Leisnig (respectively). In addition, estimates of the lateral inflow are added in between and after the gauging stations for which observed data is available.

Selection of Manning's n values The process of calibration is designed to select the most appropriate Manning's n values to represent surface roughness. However, given limited time and resources, many assumptions are built into the process, such as the assumption that the Manning's n value is consistent throughout the entire channel; that the overbank Manning's n values are consistent on the left and right banks; that the Manning's n values of the overbanks in the tributaries (Zwickauer Mulde and Freiberger Mulde) are consistent with one another, but may be different than of the Vereinigte Mulde; and that variation of roughness of the 2D flow area is captured in the CORINE land cover classes. Even with significantly more time and higher data resolution (for example, of land cover classes), there would still remain uncertainty of the n values, though the relative influence of this source of uncertainty would likely decrease significantly.

6. Discussion

Accuracy of observed data Very little information is available about the origin and preparation of the observed data. The method for measuring hourly discharge is most likely based on stage-discharge relationships for each of the gauges. The accuracy of these rating curves can vary, and may not have been updated near the time of each event. It is unknown how long after the event each high water mark elevation was recorded, or what the source was (perhaps water stains on the building or the memory of a homeowner). Likewise, as the high water marks are measured from the ground, and added to the DEM to produce an observed maximum water surface elevation, the uncertainty of the DEM (+/- 0.2 m) would also be included in the high water mark elevation. It is unclear how the shapefiles representing flood extent for 2002 and 2013 were generated (perhaps based on a model of the event, extracted from aerial imagery, or based on descriptions or evidence of water damage assessed shortly after the event). It is suspected that the methodology for the 2002 shapefile was not exactly the same as that for the 2013, as discussed in Section 4.2.9. The bridge dimensions were based on a mixture of estimates and measurements, as survey data was not available.

Selection of coefficients HEC-RAS requires a number of coefficient values (contraction and expansion coefficients, weir coefficients for the bridges, weir coefficients for the lateral structure), all of which are informed estimates of the most appropriate value for this situation.

Cross sections to represent gauges HEC-RAS requires the assignment of each boundary condition in the 1D component of the model to a particular cross section. The cross sections meant to represent those aligned with the Colditz, Leisnig, and Golzern gauges are placed according to where the gauges appear to be located. However, they may not be aligned exactly with the gauge itself. The cross sections also capture a simplified version of the terrain (each cross section is limited to 500 stations, so the longer the cross section, the lower the resolution).

6.2. Task 2: Repeated Simulation with Changing Boundary Conditions

Task 2 covers Research Question 2: *How might one automate the simulation and/or post-processing of large numbers of flood events with changing upstream boundary conditions, and how efficient would it be to automate these processes?*; Research Question 3: *How sensitive are flood characteristics (flood extent and depth) to different simulated climate conditions within the A1B scenario?*; and Research Question 4: *How does the simulation of changing boundary conditions affect stability and computational effort of HEC-RAS?*

6.2.1. Assessment of Automation Tools and Methods for Modelling Changing Boundary Conditions

The methodology presented in Section 4.3 serves as a successful proof-of-concept for leveraging a handful of well-known tools to significantly reduce the manual effort of creating and running a medium-large number of simulations in HEC-RAS with changing boundary conditions. With the current setup of the scripts and procedural steps, the user has great flexibility in being able to check intermediate results, make small changes to certain tools to be able to repurpose them for slightly different needs, and to aid in the investigation of any unexpected results or errors. This flexibility was critical to the development of the methodology, though in order to make significant steps further in the automation of this process, the scripts and procedures would need to become more structured, directly connected, and polished. If performed properly, these improvements would not greatly inhibit the flexibility of the process, while continuing to reduce required intervention from the user.

6. Discussion

One particular tool which was not incorporated into this initial methodology is the HECRASController API. The HECRASController was considered to be an unnecessarily heavy lift for developing an initial methodology. In addition, it would likely require a higher level of comfortability with programming than the current methodology, which may limit its potential appeal and practicality for the time being.

Compared to the monotonous process of manually creating unsteady flow files and setting them up with plans, the current methodology proved very useful when the only component of the model to be changed was the upstream boundary condition. It is also relatively easy to adjust the scripts to manage multiple upstream boundary conditions. However, it would take additional effort to be able to adapt the script for changes controlled outside of the unsteady flow file or plan file. For example, the geometry file would require the editing of a hierarchical data format (HDF5) file through Python, which is not as straightforward as the unsteady flow and plan file formats.

The efficiency of the process depends on how many adjustments are needed in order to run the scripts for a particular need, and how comfortable the user is with making such adjustments. The methodology would be expected to be worth employing for as few as 5-20 simulations (5 for few adjustments and a user who is quite comfortable adjusting the scripts, 20 for a few more adjustments and/or a person who is less comfortable adjusting the scripts). Each run of the methodology can process up to 99 simulation files (as HEC-RAS can only handle 99 plans in one project). It is not difficult to set up multiple sets of 99 and run them in succession (or on multiple computers concurrently). Compared to the computation time of HEC-RAS to complete 99 simulations, the additional time needed to set up the batch of 99 is quite small. Therefore, the upper limit of this methodology's efficiency is more dependent on whether HEC-RAS is the most appropriate model for the task, as it runs simulations sequentially, in batches of up to 99, and with occasional failures to complete the simulation (discussed in Section 6.2.3).

6.2.2. Assessment of Sensitivity of Flood Characteristics to Changing Boundary Conditions

6.2.2.1. Flood Extent

Model combination 10 produces simulations with the largest flood extents, and model combination 9 produces the smallest flood extents, when considering the maximum, minimum, and mean for all three model combinations. These patterns reflect the comparison of the input discharge hydrographs, the statistics of which are presented in Section 4.3, Table 4.4. However, the model combination which produces flood simulations with the greatest range in flood extent is model combination 9 (58100 m^2), roughly one third greater range than model combination 10 and one half greater than model combination 8. According to the input hydrograph maximum discharge, model combination 8 has a far greater range than either of the other two model combinations, $933 \text{ m}^3/\text{s}$ for model combination 8 compared to $281 \text{ m}^3/\text{s}$ for model combination 9 and $323 \text{ m}^3/\text{s}$ for model combination 10. This may speak to the effect of Bennewitz's unique topography, and to the fact that the increase in discharge may flow to other areas of the model (for example, further downstream in the 2D flow area) rather than into the investigation area. Within certain ranges of the upstream boundary condition, it appears to have a greater impact on the flood extent in the investigation area. However, outside of those ranges, it has very little impact on the flood extent, even if the range is great. That being said, the overall impact on flood extent in the investigation area is relatively small, 5% of the mean of all 81 flood extent areas simulated.

In Section 5.2, Figures 5.7, 5.8, 5.9, and 5.10 suggest that, in this particular study area, the greatest uncertainty is confined to particular regions of the investigation area. Outside of those regions, the flood extent is not particularly sensitive to the range of boundary conditions introduced (i.e. all 81 simulations show these cells to be wet). This appears to be largely due

6. Discussion

to the topography of Bennewitz. It is a relatively flat valley until a certain point at which the ground elevation increases quickly. Once the water has filled to the edge of the steep slope, a large increase in volume or discharge does not appear to produce a significant increase in extent.

6.2.2.2. Flood Depth

The minimum, mean, and maximum flood depth maps provide a sense of the range of flood depth. However, in terms of uncertainty, the standard deviation map is perhaps more interesting. Looking at the whole 2D flow area, the maps and Table 5.10 suggest that the maximum water depth in the region upstream of the train bridge is particularly sensitive to changes in the upstream boundary condition. This is likely due to the train bridge itself. The tunnels under the bridge are open in these simulations, but the bridge still acts as a barrier and causes the water level upstream to rise. There is also a small region just to the east of Nepperwitz that appears relatively sensitive to the upstream boundary condition. This could be due to the height of the dike being at a particularly critical level for this range of upstream boundary conditions, or it could be due to the fact that this small region is slightly elevated compared to its surroundings.

The descriptive statistics of maximum flood depth at each of the points of interest (POIs) provide interesting insight into the uncertainty around flood depth, particularly with respect to model combinations. Looking at Table 5.10 model combination 9 appears to control the minimum value of all six POIs, and model combination 10 appears to control the maximum value of all six POIs. For five of the six POIs, model combination 8 has the highest standard deviation. The overall standard deviation, for all simulations, for each POI, is always higher than for any individual model combination. The range between the minimum and maximum for all simulations, for each POI, is also always larger than for any individual model combination. Assuming the range and standard deviation can be indicators of increased uncertainty, this suggests that water depths may be more heavily influenced by model combination than by the shuffle component which produces different realisations or than by the parameter sets of the hydrologic model.

6.2.3. Evaluation of HEC-RAS Model under Changing Boundary Conditions

In terms of stability, the HEC-RAS model performed relatively well under changing upstream boundary conditions. Of the 81 simulations, only five simulations failed to complete on the first attempt, and three of those five were due to the need to extend the headwater maximum on the train bridge. The primary concern when preparing to run a relatively large number of HEC-RAS simulations was that HEC-RAS might crash on a particular simulation and fail to continue to the next simulation. This behaviour, which was experienced occasionally during Task 1, has the potential to severely limit the efficiency of running large numbers of simulations with HEC-RAS. However, during Task 2, it did not cause any problems, even though the Task 2 simulations included higher maximum discharge events (see Section 4.3, Table 4.4).

In terms of computational effort, the HEC-RAS model performed as anticipated. The real minutes per simulation day required for each simulation was in the same ballpark as those for the 2002 and 2013 events from Task 1 (both of which are higher than the 2006, 2010, and 2013 events, all of which were significantly lower than the other two events).

6.2.4. Sources of Uncertainty

The purpose of this task was to examine the effect of changing upstream boundary conditions on the model. Though the discharge hydrograph at Golzern was the only input changed for each simulation, there are three sources of uncertainty that created these distinct hydrographs.

6. Discussion

GCM and RCM selection The A1B scenario served as the input to three distinct WEREX V model combinations (8, 9, and 10 in Table 1.1). Each of these model combinations simulate climatological characteristics in slightly different ways, and thus produce distinct results.

Realisations Each model combination was run with a shuffled component to produce ten different realisations, all still based on the A1B scenario. Of these ten realisations, three were selected for analysis in this research effort. Details regarding the specific shuffled component are not available, though each realisation is considered equally likely.

Parameter sets The optimisation algorithm used to calibrate the hydrologic model produced nine parameter sets which are equally likely to be the most appropriate for modelling the system. All nine parameter sets were considered for this research effort.

Because of the context in which they are under analysis, each of these sources of uncertainty lie on the border between knowledge uncertainty and inherent uncertainty (see Section 2.2). Taken out of the context of simulating future flood risk, all three of these sources of uncertainty would typically fall into the category of knowledge uncertainty. One could argue that, should you have enough data and sophisticated-enough technology, you would be able to identify which model combination (and with which realisation's shuffle component settings and which parameter set) was the best at simulating the conditions to produce a particular event. However, in the context of predicting future events, there is also an element of inherent uncertainty. There is no way to measure which model combination, realisation, or parameter set is the best at predicting future conditions or events, as future conditions are not yet fixed. This is one of the junctures at which the distinction between knowledge uncertainty and inherent uncertainty becomes blurred.

6.3. Task 3: Visualisation and Display

Task 3 covers Research Question 5: *How can the uncertainty of flood extent and depth be represented in a spatially distributed manner?*

Task 3 explores the representation of uncertainty of flood characteristics in a spatially distributed manner. The initial inspiration for the exploration of flood extent came from the prospect of combining a visual representation of knowledge uncertainty (e.g. model combination selection) and inherent uncertainty (e.g. the probability of an event). This vision cannot be further explored without set recurrence intervals. However, the exploration of how to present only the knowledge uncertainty of flood extent is valuable in itself.

The classification of flood extent results (i.e. batching the percentage into a number of classes) may make the data easier to digest. However, it may also unintentionally hide trends in the data. The creator of the map must use his or her discretion to determine what is most important for the viewer to understand, based on the particular data set. For example, if the map is presented as a high-level overview, classes may be needed, as it can be difficult to comprehend many different coloured pixels so small to the eye.

The presentation of standard deviation of maximum water depth was considered in terms of the scale. If the goal of the analysis is to understand the patterns within the standard deviation of the data set (for example, the northeast quadrant of the main community of Bennewitz appears to have a relatively high standard deviation both according to all 81 model combinations and the 27 model combination 8 simulations), then maintaining the original scale of the data set (i.e. map "a" in Figure 5.15) is preferable. The pattern is hardly visible in map "b" of Figure 5.15. However, if the goal is to examine whether there are any portions of the town for which model combination 8 appears to have a particular influence, then adjusting the scale to match that of the map for all 81 simulations (i.e. map "b" of Figure 5.15) would be preferable. Once again, it is up to the map maker's discretion what he or she intends to highlight in the data, and whether he or she can produce a map that is understandable to the target audience. Task

6. Discussion

3 is an exploratory effort, and would be considered only a brief skimming of the surface of a full investigation in to how to present uncertainty in flood characteristics through maps.

7. Conclusions and Recommendations

Task 1 of this research consists of the creation and evaluation of 1D/2D HEC-RAS model for flood inundation simulation in Bennewitz, Germany, conditionally validated for a particular investigation area within Bennewitz proper. The analysis of Task 2 provides insight into the sensitivity of this model to changing upstream boundary conditions, specifically with regards to modelling floods under distinct future climate conditions. Task 3 provides a limited exploration of the presentation of spatially distributed flood data.

The model produced by Task 1 of this research is conditionally valid for the investigation area. During calibration, it became clear that flood extent was not particularly sensitive to changes in the Manning's n values in the 2D flow area with the 2002 discharge hydrographs as the upstream boundary conditions. For the 2013 validation event, the model still produced strong flood extent results for the investigation area (CSI of 0.844). The extent results for the full 2D flow area were less satisfactory, and thus the model is considered conditionally valid specifically for the investigation area.

The high water marks within the 2D flow area are concentrated in the investigation area. The model accurately simulates all eight high water marks in the 2D flow area to be dry in the 2013 validation event. As there are no high water marks from the flooded areas in 2013, validation in terms of water depth is limited. However, under circumstances of limited data availability, and in combination with the strong flood extent results within the investigation area, the model can be expected to give meaningful results for the analysis conducted in Task 2.

Availability of observed data is proposed as the greatest limitation of the 1D/2D HEC-RAS model produced by Task 1. In particular, this includes conflicting data regarding the 2013 observed flood extent, the limited number of high water marks, the limited geographic and temporal distribution of high water marks, the limited access to measure the high water marks directly, and lack of information regarding who and how the marks were originally recorded.

Principle recommendations for future research regarding Task 1 include:

- Conduct additional efforts for observed data collection, both within the investigation area and outside of the investigation area. In particular, it would be valuable to acquire additional high water marks for both 2002 and 2013, especially in Schmölen, but anywhere within the model would be highly beneficial.
- Conduct additional efforts to obtain information about the height of the Wurzen and Bennewitz dikes, as they currently stand and as they were during previous floods.
- With additional data in hand, re-calibrate the 2D portion of the model. Before conducting this calibration, consider one of the following options: 1) the possibility of using observed

7. Conclusions and Recommendations

Golzern data as the upstream boundary, given challenges experienced in achieving accurate discharge values at Golzern gauge and the fact that the Task 2 analysis will start at the Golzern gauge as well; or 2) investigate further and address the causes of error in peak discharge at Golzern in the 1D portion of the model.

Task 2 suggests that, in the investigation area, flood extent is not sensitive to changing upstream boundary conditions, while flood depth appears to be quite sensitive. Of the 81 simulations of flood events under future climate conditions in Task 2, maximum flood depth had a range as low as 30 cm (POI 5) to 118 cm (POI 1) out of six points analysed. This suggests that, for flood hazard (and consequent flood risk) analyses in this area, uncertainty in future climate conditions should be considered.

Task 2 also provides the initial development and assessment of tools and a methodology for configuring and running many simulations with different upstream discharge hydrographs, using limited user intervention. The tools and methodology function as a proof of concept for using principally Python and ArcGIS to complete this task, though additional development and refinement is recommended.

Principle recommendations for future research regarding Task 2 include:

- If feasible in the model chain upstream of the HEC-RAS model, produce flood discharge hydrographs for each data set which are representative of flood events of a particular return period. This may be feasible by running the climatological and hydrological simulations for a longer period of time. Alternatively, a frequency analysis for each data set could produce a peak discharge magnitude for a given return period, and a representative flood event hydrograph shape could be scaled up or down to these peak discharge magnitudes.
- Perform the methodology for Task 2 using the results from all 12 model combinations and all realisations for additional insight into the uncertainty from these two sources.
- Continue the development, integration, and refinement of the scripts and methodology for running multiple simulations in HEC-RAS with changing the upstream boundary conditions. This should eventually eliminate the need for the user to edit Python scripts, and should require fewer user interventions in the process overall.

The exploratory effort conducted in Task 3 provides limited insight into the decisions a modeller makes when presenting uncertainty of results in a spatially distributed manner. The effort supports conclusions from mapping literature, that the decisions rely heavily on who the audience is and what specific component of the data is intended for communication to this audience. There is still much to be done in this realm.

Principle recommendations for future research regarding Task 3 include:

- Explore the possibility of combining particular sources of uncertainty with probability, such that a map could be a representation of the likelihood of flooding within a given number of years.
- Conduct focus groups and surveys of target audiences in terms of how well they understand the various means of representing uncertainty in a flood map and whether/how such a map might impact their personal or professional decisions.

Combining the work of all three tasks, this research has taken a modest but valuable step toward better understanding uncertainty in flood inundation mapping, and how to analyse and represent it in a spatially distributed manner. The practical implications of this work may vary greatly from place to place, but at the core this study supports the ongoing need to identify, attempt to quantify, and communicate flood hazard uncertainty with the goal of informing individuals and decision-makers as well as possible in their process of managing flood risk.

References

- Alfieri, L, Bisselink, B, Dottori, F, Naumann, G, de Roo, A, Salamon, P, Wyser, K, & Feyen, L. 2016. Global projections of river flood risk in a warmer world. *Earth's Future*.
- Apel, H., Thielen, A. H., Merz, B., & Bloschl, G. 2004. Flood risk assessment and associated uncertainty. *Natural Hazards and Earth System Sciences*.
- Aronica, G., Bates, P. D., & Horritt, M. S. 2002. Assessing the uncertainty in distributed model predictions using observed binary pattern information within GLUE. *Hydrological Processes*, **16**, 2001–2016.
- Bates, Paul D., Pappenberger, Florian, & Romanowicz, Renata J. 2014. *Applied Uncertainty Analysis for Flood Risk Management*. Imperial College Press. Chap. Uncertainty in Flood Inundation Modelling, pages 232–269.
- Bennett, Neil D, Croke, Barry FW, Guariso, Giorgio, Guillaume, Joseph HA, Hamilton, Serena H, Jakeman, Anthony J, Marsili-Libelli, Stefano, Newham, Lachlan TH, Norton, John P, Perrin, Charles, et al. 2013. Characterising performance of environmental models. *Environmental Modelling & Software*, **40**, 1–20.
- Bernhofer, Christian, Pluntke, Thomas, & Schaller, Andrea. 2016. *Witterungsexreme im WEREX-V-Ensemble: Analyse und Bewertung des WEREX-V-Ensembles hinsichtlich der Abbildung von Extremen in Sachsen*. Tech. rept. Landesamt fuer Umwelt Landwirtschaft un Geologie.
- Bilinski, W., Bohn, E., Buettner, U., Goerner, C., MÄŒller, I., Kardel, K., Rohde, S., Six, A., Walther, P., Wolf, E., Zander, K., Freier, K., Gerber, S., Jentsch, S., Kopp, T., Winkler, U., & Wundrak, P. 2015. *Ereignisanalyse Hochwasser Juni 2013*. Tech. rept. LfULG, Freistaat Sachsen.
- Blanco-Vogt, Angela, & Schanze, Jochen. 2014. High-Resolution Vulnerability Assessment Using Remote Sensing, GIS and Physical-Based Analysis Methods. *Natural Hazards and Earth System Sciences*, **14**(Aug), 2105–2117.
- Brunner, Gary, Jensen, Mark, Piper, Steven, Ackerman, Cameron, Kennedy, Alex, & Chacon, Ben. 2016 (APR). *2D Modeling and Mapping with HEC-RAS 5.0*. Presentation. Year estimated.
- Brunner, Gary W. 2016a (April). *Benchmarking of the HEC-RAS Two-Dimensional Hydraulic Modeling Capabilities*. Tech. rept. Hydrologic Engineering Center (HEC), U.S. Army Corps of Engineers Insitute for Water Resources Hydrologic Engineering Center (CEIWR-HEC) 609 Second Street Davis, CA 95616-4687.

References

- Brunner, Gary W. 2016b (February). *HEC-RAS River Analysis System Hydraulic Reference Manual Version 5.0*. U.S. Army Corps of Engineers Hydrologic Engineering Center (HEC), 609 Second Street Davis, CA 95616-4687.
- Brunner, Gary W. 2016c (Feb). *HEC-RAS River Analysis System User's Manual Version 5.0*. U.S. Army Corps of Engineers Institute for Water Resources Hydrologic Engineering Center (HEC), 609 Second Street Davis, CA 95616-4687.
- Chow, Ven Te. 1959. *Open channel hydraulics*. McGraw-Hill Book Company, Inc; New York.
- Cook, Aaron, & Merwade, Venkatesh. 2009. Effect of topographic data, geometric configuration and modeling approach on flood inundation mapping. *Journal of Hydrology*, **377**(1), 131–142.
- Copernicus Programme. 2017. *CLC 2012*.
- de Moel, H., van Alphen, J., & Aerts, J.C.J.H. 2009. Flood maps in Europe—methods, availability and use. *Natural Hazards and Earth System Sciences*, **9**(2), 289–301.
- Der Kiureghian, Armen, & Ditlevsen, Ove. 2009. Aleatory or epistemic? Does it matter? *Structural Safety*, **31**(2), 105–112.
- Di Baldassarre, Giuliano, Kooy, M, Kemerink, JS, & Brandimarte, L. 2013. Towards understanding the dynamic behaviour of floodplains as human-water systems. *Hydrology and Earth System Sciences*, **17**(8), 3235.
- Elmer, F, Hoymann, J, Düthmann, D, Vorogushyn, S, & Kreibich, H. 2012. Drivers of flood risk change in residential areas. *Natural Hazards and Earth System Sciences*, **12**(5), 1641–1657.
- European Union. 2007. Directive 2007/60/EC of the European Parliament and of the Council of 23 October 2007 on the Assessment and Management of Flood Risks. *Official Journal of the European Union*, **288**, 27–35.
- Fabio, P., Aronica, G. T., & Apel, H. 2010. Towards automatic calibration of 2-D flood propagation models. *Hydrology and Earth System Sciences*.
- Faghih, M., Mirzaei, M., Adamowski, J., Lee, J., & El-Shafie, A. 2017. Uncertainty estimation in flood inundation mapping: an application of non-parametric bootstrapping. *River Research and Applications*.
- Falter, Daniela, Vorogushyn, Sergiy, Lhomme, Julien, Apel, Heiko, Gouldby, Ben, & Merz, Bruno. 2013. Hydraulic model evaluation for large-scale flood risk assessments. *Hydrological Processes*, **27**, 1331–1340.
- Federal Agency for Cartography and Geodesy (Bundesamt fuer Kartographie und Geodäsie). 2017 (JAN). *Digital Landscape Model 1:250000 DLM250*.
- Gebrehiwot, Solomon Gebreyohannis, Seibert, Jan, GÃ¶rdenÃ¶s, Annemieke I., Mellander, Per-Erik, & Bishop, Kevin. 2013. Hydrological change detection using modeling: Half a century of runoff from four rivers in the Blue Nile Basin. *Water Resources Research*, **49**(6), 3842–3851.
- Gersonius, Berry, Ashley, Richard, Pathirana, Assela, & Zevenbergen, Chris. 2013. Climate change uncertainty: building flexibility into water and flood risk infrastructure. *Climatic Change*, **116**, 411–423.
- Gouldby, Ben, & Samuels, Paul. 2005 (March). *Language of Risk: Project Definitions*. FLOODsite.

References

- Hall, P.L., & Strutt, J.E. 2003. Probabilistic physics-of-failure models for component reliabilities using Monte Carlo simulation and Weibull analysis: a parametric study. *Reliability and System Safety*, **80**, 233–242.
- Hartmann, DL, Tank, AMGK, & Rusticucci, M. 2013. IPCC fifth assessment report, climate change 2013: The physical science basis. *IPCC AR5*, 31–39.
- Horritt, M.S., & Bates, P.D. 2002. Evaluation of 1D and 2D numerical models for predicting river flood inundation. *Journal of Hydrology*, **268**, 87–99.
- HR Wallingford. 2002. *Risk, Performance and Uncertainty in Flood and Coastal Defence - A Review (HR Wallingford Report SR587)*. Tech. rept. HR Wallingford.
- Intergovernmental Panel on Climate Change. 2016 (JUN). *Data Distribution Centre*.
- Jung, Younghun, & Merwade, Venkatesh. 2015. Estimation of uncertainty propagation in flood inundation mapping using 1-D hydraulic model. *Hydrological Processes*, **29**, 624–640.
- Jung, Younghun, Merwade, Venkatesh, Kim, Soojun, Kang, Narae, Kim, Yonsoo, Lee, Keonhaeng, Kim, Gilho, & Kim, Hung Soo. 2014. Sensitivity of subjective decisions in the GLUE Methodology for quantifying the uncertainty in the flood inundation map for Seymour Reach in Indiana, USA. *Water*, **6**, 2104–2126.
- Kalyanapu, Alfred, Judi, David R., Mcpherson, Timothy N., & Burian, Steven J. 2011. Monte Carlo-based flood modelling framework for estimating probability weighted flood risk. *Journal of Flood Risk Management*.
- Knight, Frank H. 1921. *Risk, Uncertainty, and Profit*. Library of Economics and Liberty.
- Koehler, Albrecht. 2016. *Possibilities of a backward analysis of levee failures - The case study of failures during the 2013 flood in Saxony*. Tech. rept. Technical University of Dresden, Faculty of Civil Engineering, Institute for Water Engineering and Technical Hydromechanics.
- Kosztra, Barbara, & Arnold, Stephan. 2014 (JAN). *Proposal for enhancement of CLC nomenclature guidelines*. Tech. rept. European Environment Agency.
- Kreienkamp, Frank, Spekat, Ame, & Enke, Wolfgang. 2011. *WEREX V: Regionale Klimaprojektionen fuer Sachsen*. Tech. rept. Landesamt fuer Umwelt Landwirtschaft un Geologie.
- Lehner, Bernhard, Döll, Petra, Alcamo, Joseph, Henrichs, Thomas, & Kaspar, Frank. 2006. Estimating the impact of global change on flood and drought risks in Europe: a continental, integrated analysis. *Climatic Change*, **75**(3), 273–299.
- Lins, HF. 2012. A note on stationarity and non-stationarity. *CHy Advisory Working Group*.
- LVZ [author unknown]. 2002. Das Muldental versinkt: Hunderte Menschen verlieren ihr Zuhause. *Leipziger Volkszeitung*, AUG. 14.08.2002.
- Martini, F, & Loat, R. 2007. *Handbook on good practices for flood mapping in Europe. European exchange circle on flood mapping (EXCIMAP)*, Paris/Bern.
- Melillo, Jerry M., Richmond, Terese (T.C.), & Yohe, Gary W. (eds). 2014. *Climate Change Impacts in the United States: The Third National Climate Assessment*. Washington, D.C.: U.S. Government Printing Office.

References

- Merwade, Venkatesh, Olivera, Francisco, Arabi, Mazdak, & Edleman, Scott. 2008. Uncertainty in flood inundation mapping: current issues and future directions. *Journal of Hydrologic Engineering*, **13**(7), 608–620.
- Merz, Bruno, Apel, Heiko, Dung, Nguyen Viet, Falter, Daniela, Hundecha, Yeshewatesfa, Kreibich, Heidi, Schroeter, Kai, & Vorogushyn, Sergiy. 2016. Large-scale flood risk assessment using a coupled model chain. In: *FLOODrisk 2016 - 3rd European Conference on Flood Risk Management*.
- Milly, P.C.D., Betancourt, Julio, Falkenmark, Malin, Hirsch, Robert M., Kundzewicz, Zbigniew W., Lettenmaier, Dennis P., & Stouffer, Ronald J. 2008. Stationarity Is Dead: Whither Water Management? *Science*, **319**(02), 573–574.
- Milly, PCD, Betancourt, Julio, Falkenmark, Malin, Hirsch, Robert M, Kundzewicz, Zbigniew W, Lettenmaier, Dennis P, Stouffer, Ronald J, Dettinger, Michael D, & Krysanova, Valentina. 2015. On critiques of "Stationarity is dead: whither water management?". *Water Resources Research*, **51**(9), 7785–7789.
- Morss, Rebecca E, Wilhelm, Olga V, Downton, Mary W, & Grunfest, Eve. 2005. Flood risk, uncertainty, and scientific information for decision making: lessons from an interdisciplinary project. *Bulletin of the American Meteorological Society*, **86**(11), 1593–1601.
- Muis, Sanne, Güneralp, Burak, Jongman, Brenden, Aerts, Jeroen CJH, & Ward, Philip J. 2015. Flood risk and adaptation strategies under climate change and urban expansion: A probabilistic analysis using global data. *Science of the Total Environment*, **538**, 445–457.
- Nakicenovic, Nebojsa, Alcamo, Joseph, Davis, Gerald, de Vries, Bert, Fenmann, Joergen, Gaffin, Stuart, Gregory, Kermeth, Griibler, Amulf, Jung, Tae Yong, Kram, Tom, Rovere, Emilio Lebre La, Michaelis, Laurie, Mori, Shunsuke, Morita, Tsuneyuki, Pepper, William, Pitcher, Hugh, Price, Lynn, Riahi, Keywan, Roehrl, Alexander, Rogner, Hans-Holger, Sankovski, Alexei, Schlesinger, Michael, Shukla, Priyadarshi, Smith, Steven, Swart, Robert, van Rooijen, Sascha, Victor, Nadejda, & Dadi, Zhou. 2000. *IPCC Special Report on Emissions Scenarios*. Cambridge University Press.
- National Research Council. 2000. *Risk Analysis and Uncertainty in Flood Damage Reduction Studies*. Washington, D.C.: The National Academies Press.
- New, Mark, Lopez, Ana, Dessai, Suraje, & Wilby, Rob. 2007. Challenges in using probabilistic climate change information for impact assessments: an example from the water sector. *Philosophical Transactions of the Royal Society of London A: Mathematical, Physical and Engineering Sciences*, **365**(1857), 2117–2131.
- Nicholls, Robert J, Hoozemans, Frank MJ, & Marchand, Marcel. 1999. Increasing flood risk and wetland losses due to global sea-level rise: regional and global analyses. *Global Environmental Change*, **9**, S69–S87.
- Olivier, Linsey Brooke. 2017. *Hydrodynamic Simulations of the Prototype Mississippi River and Expanded Small-Scale Physical Model to Investigate Impact of Sea Level Rise*. M.Phil. thesis, Louisiana State University Agricultural and Mechanical College.
- Opperman, Jeffrey J, Galloway, Gerald E, Fargione, Joseph, Mount, Jeffrey F, Richter, Brian D, & Secchi, Silvia. 2009. Sustainable floodplains through large-scale reconnection to rivers. *Science*, **326**(5959), 1487–1488.
- Pappenberger, F., & Beven, K. J. 2006. Ignorance or bliss: Or seven reasons not to use uncertainty analysis. *Water Resources Research*, **42**.

References

- Quiroga, V. Moya, Kure, S., Udo, K., & Mano, A. 2016. Application of 2D numerical simulation for the analysis of the February 2014 Bolivian Amazonia flood: Application of the new HEC-RAS version 5. *RIBAGUA - Revista Iberoamericana del Agua*, **3**(Feb), 25–33.
- Quiroga, Vladimir Moya, Kure, Schuichi, Udo, Keiko, & Mano, Akira. 2015. *Automating HEC-RAS input data and execution for improved hydraulic analysis: The Bolivian Amazonia 2014 flood*. IAHR World Congress Proceedings Website.
- Romanowicz, Renata, & Beven, Keith. 2003. Estimation of flood inundation probabilities as conditioned on event inundation maps. *Water Resources Research*, **39**(3).
- Saechsisches Landesamt fuer Umwelt, Landwirtschaft und Geologie. 2016. *Geoportal Sachsenatlas, Metadaten Portal*.
- Saechsisches Landesamt fuer Umwelt, Landwirtschaft und Geologie. 2017. *Wasser, Wasserwirtschaft: Geodaten download des Fachbereichs Wasser*.
- Saechsisches Landesamt fuer Umwelt und Geologie. 2004. *Event Analysis - August 2002 flood in the watercourses of the Osterzgebirge mountains Management Report*. Tech. rept. Freistaat Sachsen.
- Schanze, Jochen. 2006. *Flood Risk Management: Hazards, Vulnerability and Mitigation Measures*. NATO Science Series, vol. 67. Springer. Chap. Flood risk management: a basic framework, pages 1–20.
- Schanze, Jochen. 2012. Dealing with future change in flood risk management. *Journal of Flood Risk Management*, **5**(1), 1–2.
- Schanze, Jochen, Schwarze, Robert, Horlacher, Hans-Burkhard, & Deilmann, Clemens (eds). 2015. *Veraenderung und Management der Risiken extremer Hochwasserereignisse in grossen Flussgebieten - am Beispiel der Elbe*. Schweizerbart.
- Serinaldi, Francesco, & Kilsby, Chris G. 2015. Stationarity is undead: Uncertainty dominates the distribution of extremes. *Advances in Water Resources*, **77**, 17–36.
- Smemoe, Christopher M., Nelson, E. James, Zundel, Alan K., & Miller, A. Woodruff. 2007. Demonstrating floodplain uncertainty using flood probability maps. *Journal of the American Water Resources Association*, **43**(2), 359–371.
- Spiegel Online. 2013. Die Flut kommt vier Jahre zu frueh. *Spiegel Online*, Jun.
- Statistisches Landesamt des Freistaat Sachsen. 2014 (Jan). *Kleinraeumiges Gemeindeblatt Zensus 2011 Bevoelkerung, Haushalte, Familien und deren Wohnsituation am 9. Mai 2011 Grunddaten und Indikatoren Bennewitz*.
- Statistisches Landesamt des Freistaat Sachsen. 2016a (JAN). *Datenblatt 6. Regionalisierte Bevoelkerungsvorausberechnung fÃœr den Freistaat Sachsen 2015 bis 2030: Ausgewahlte Ergebnisse fuer Gemeinde Bennewitz*.
- Statistisches Landesamt des Freistaat Sachsen. 2016b. *Statistischer Bericht: Bodennutzung im Freistaat Sachsen Agrarstrukturerhebung*.
- Swedish Meteorological and Hydrological Institute. 2017. *HBV*. Website. Accessed 21 July 2017.
- Tingsanchali, T. 2012. Urban flood disaster management. *Procedia engineering*, **32**, 25–37.
- Traver, Robert (ed). 2014. *Flood Risk Management: Call for a National Strategy*. 1801 Alexander Bell Drive Reston, Virginia 20191-4382: American Society of Civil Engineers.

References

- UNISDR. 2015. *Sendai Framework for Disaster Risk Reduction 2015-2030*. Geneva: UNISDR.
- van der Linden, P., & Mitchell, J.F.B. (eds). 2009. *ENSEMBLES: Climate Change and its Impacts: Summary of research and results from the ENSEMBLES project*. FitzRoy Road, Exeter EX1 3PB, UK.: Met Office Hadley Centre.
- van Waveren, R.H., Groot, S., Scholten, H., van Geer, F.C., Woesten, J.H.M., Koeze, R.D., & Noort, J.J. 1999. *Good Modelling Practice Handbook*. STOWA/RWS-RIZA.
- Vause, Richard. 2013 (Aug). *End-user Specific Flood Uncertainty Mapping: Effective Map Design from the Perspective of the English Public*. M.Phil. thesis, Technical University of Dresden.
- Visser, Ubbo. 2005. *Intelligent information integration for the Semantic Web*. Vol. 3159. Springer.
- Walther, Petra. 2004 (July). *Event Analysis - August 2002 flood in the watercourses of the Osterzgebirge mountains*. Tech. rept. Saxon State Office for Environment and Geology.
- Weichel, T., Pappenberger, F., & Schulz, K. 2007. Sensitivity and uncertainty in flood inundation modelling - concept of an analysis framework. *Advances in Geosciences*, **11**(12), 31–36.
- Wood, Nathan. 2011. *Understanding Risk and Resilience to Natural Hazards*. U.S. Geological Survey Fact Sheet.
- Yan, Kun, Baldassarre, Giuliano Di, Solomatine, Dimitri P., & Schumann, Guy J.-P. 2015. A review of low-cost space-borne data for flood modelling: topography, flood extent and water level. *Hydrological Processes*, **29**, 3368–3387.
- Young, Peter, Parkinson, Stuart, & Lees, Matthew. 1996. Simplicity out of complexity in environmental modelling: Occam's razor revisited. *Journal of Applied Statistics*, **23**(2-3), 165–210.

Appendices

A. Geometric Data

Figure A.1 presents a screenshot of the Task 1 geometric data as stored in HEC-RAS. The water flows from the bottom two tributaries (Zwickauer on the left, Freiberger on the right) up and alongside the 2D region. Green lines indicate cross sections. Red dots indicate bank stations on each cross section. Magenta dots indicate levees on cross sections. The blue-outline polygon indicates the border of the 2D region. Red lines within the 2D region indicate breaklines.



Figure A.1.: HEC-RAS 1D/2D model geometric data for Task 1

A. Geometric Data

The geometric data for the shortened version of the model, used in Task 2, is presented in Figure A.2.

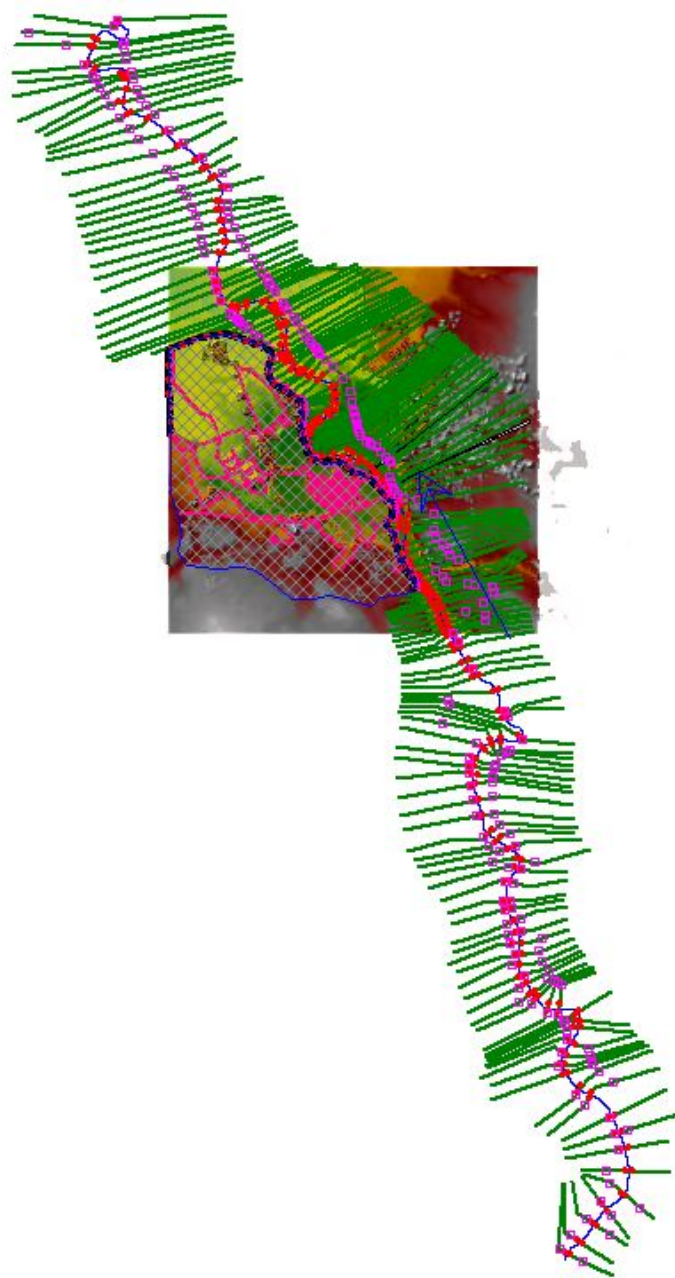


Figure A.2.: HEC-RAS 1D/2D model geometric data for Task 2

B. Extracting and Processing Data from HEC-RAS

The purpose of including this level of detail here is to 1) support continued use of this particular model set up in the ScaDS project, and 2) provide transparency into the processes used to support this work. However, it must be recognised that the processes here represent varying levels of sophistication and polish, given the time and resource constraints available for this particular thesis work. These steps are intended to follow the completion of a batch of HEC-RAS simulations.

Note that the steps and tools presented here are built on basic Python functions and ArcGIS tools. For future work, it may be desirable to organise and re-combine them into cleaner and more efficient collections of functions and tools, perhaps using the ArcPy package. Supporting scripts are available at https://github.com/mhearn11/MSc_floodtools.

Extraction

Check the status of the result maps in RAS Mapper. If the elevation maps for the plans (i.e. simulations) of interest are not yet stored (i.e. they are still dynamic maps that are only viewable through RAS Mapper), follow the sequence below.:

- Close HEC-RAS (not required, but avoids potential conflict).
- Open the RASMAP file (extension .rasmap, will be located in the same folder as the HEC-RAS project) in a simple text editor (e.g. Notepad, etc.).
- Use the Replace tool to replace all instances of *MapType="elevation"* *OutputMode="Dynamic Surface"* with *MapType="elevation"* *LayerName="WSE"* *OutputMode="Stored Current Terrain"* in the text.
- Save and close.
- Within HEC-RAS, open the project and RAS Mapper.
- Right click on the "Results" header and select "Manage Results Maps".
- Highlight each of the stored maps and click the "Compute/Update Stored Maps" button.
- Now HEC-RAS will have stored the individual TIF files in separate folders, one for each project, and the name of each file will be "WSE (Max)" along with an indication of the terrain file name. The next step is to get all of the files into one place and give them unique names (note - names will be based on the name of the plan). Run a script which will:

B. Extracting and Processing Data from HEC-RAS

- Iterate through each folder in the HEC-RAS project directory.
- Iterate through each TIF file within each folder.
- Copy each TIF file to an assigned destination location and rename it with the folder name (i.e. the name of the plan).
- Follow this by running a second script that truncates the names of the TIF files. Spaces will already have been removed by the previous code, but having a very short name will assist when using the ArcGIS Extract Multi Values to Points Tool in later steps. The script will:
 - Iterate through files in an assigned directory.
 - Rename each file by truncating a number of characters from an assigned portion of the file name (for example, remove the first eight characters of the name).

Creating Extent Polygon and Calculating CSI

This description is for comparison to the 2002 event (i.e. for calibration). The process will require adjustment or other purposes.

First transform the TIF files (after extraction from HEC-RAS using the process outlined above) into polygon shapefile format, matching the observed 2002 data. This can be achieved for many result files at once using an ArcGIS ModelBuilder tool as shown in Figure B.1.

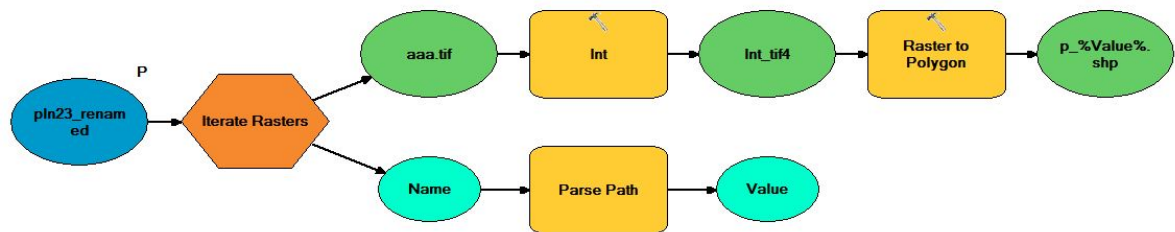


Figure B.1.: ArcGIS ModelBuilder tool to convert TIFs to polygons

Once the results are in shapefile format, the gaps (caused by building footprints, small portions of elevated ground surrounded by water) within the extent must be filled so as not to erroneously lower the calculation of the Critical Success Indicator. In addition, the result file must be clipped to the extent of the 2D flow area, as the extent of interest is focused on Bennewitz and not the 1D portion of the model. This can be achieved for many result files at once using an ArcGIS ModelBuilder tool as shown in Figure B.2. In order for gaps to be filled (see Section 4.2.1), the check box in the Union tool called "Gaps Allowed" must be unchecked. In addition, for this particular model, the result file must be merged with a small patch polygon to connect the 2D flow area to the downstream 1D portion, otherwise the space between the 2D area and the 1D area will not be recognised as gaps to be filled.

B. Extracting and Processing Data from HEC-RAS

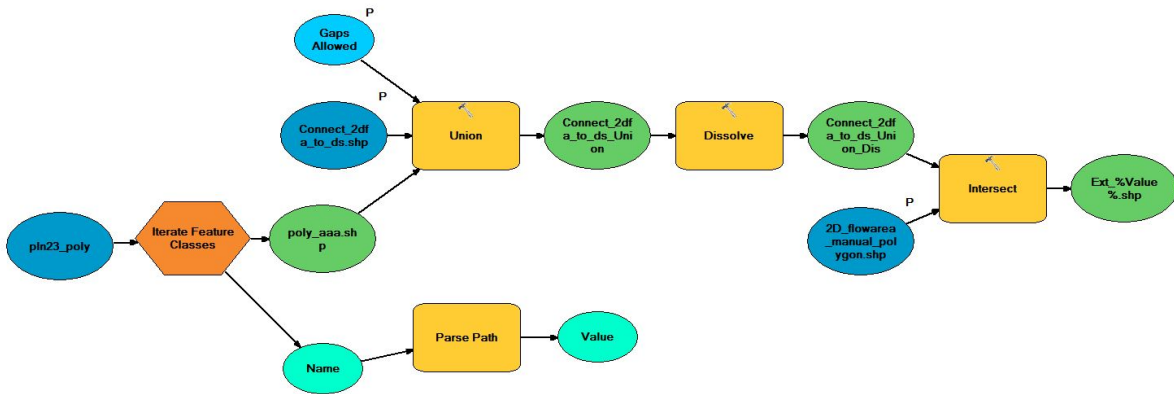


Figure B.2.: ArcGIS ModelBuilder tool to fill gaps and clip to 2D area

Now that the extent of each result file has been saved as a gap-filled polygon clipped to the edge of the 2D area, the hits, misses, and false positives must be calculated (see Table 4.2) for the CSI. Hits are represented by the overlap (intersection) between the the simulation extent and the observed extent, calculated using the Intersect tool. Misses are represented by the area of the observed extent minus the area of the simulated extent, calculated using the Erase tool. False positives are represented by the area of the simulated extent minus the area of the observed extent, also calculated using the Erase tool. This can be achieved for many result files at once using an ArcGIS ModelBuilder tool as shown in Figure B.3. The end of this ModelBuilder tool includes the Union tool again so as to end with a shapefile that includes all three values in one attribute table.

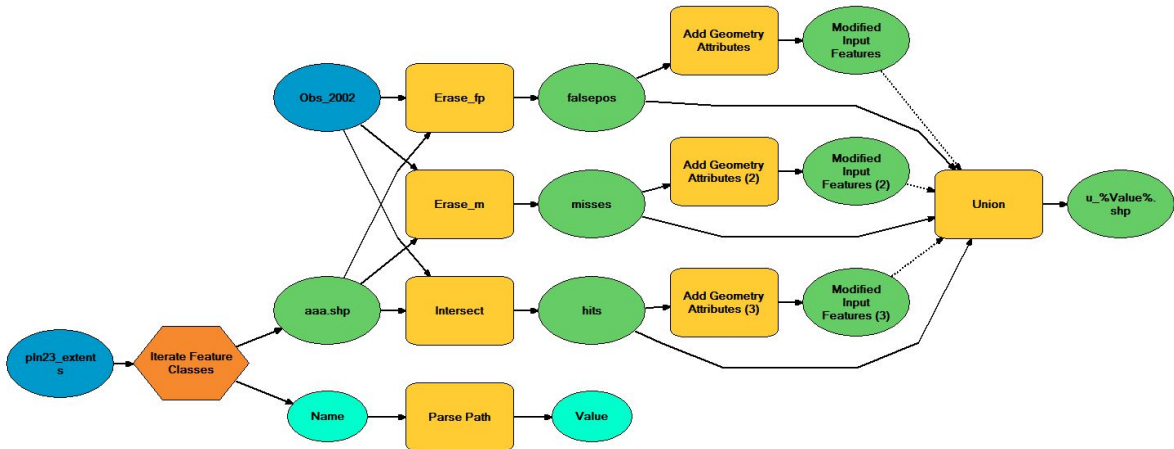


Figure B.3.: ArcGIS ModelBuilder tool to calculate hits, misses, and false positives to support the CSI calculation

Once the hits, misses, and false positives have been stored in attribute tables, one for each simulation, the tables require extraction from ArcGIS. For this, a very simple ArcGIS ModelBuilder tool was created for the purpose of iterating through multiple files, as shown in Figure B.4.

B. Extracting and Processing Data from HEC-RAS

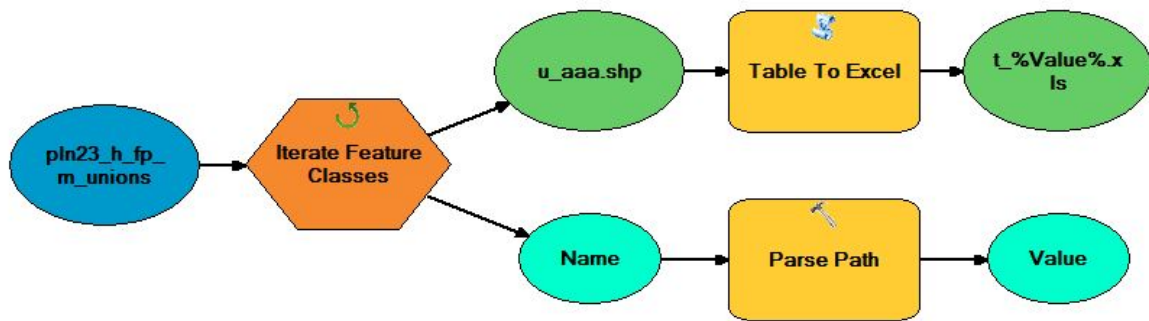


Figure B.4.: ArcGIS ModelBuilder tool to extract tables for CSI calculation.

Finally, the CSI for each table is calculated using a brief Python script which will:

- Create a dataframe in Python pandas.
- Open each of the tables created by B.4.
- Identify the cells with the total area (in square metres) for hits, false positives, and misses, and store these values in the dataframe.
- Calculate CSI (using the equation from Section 4.2.7.2, Equation 4.6), and store this value in the dataframe.

Identification of Maximum Water Surface Elevation Results at Each High Water Mark

This is accomplished using the Extract Multi Points to Feature tool in ArcGIS. If all of the TIF files have short, unique filenames, the user avoids the need to manually assign unique, identifiable names to each individual TIF for extraction. The same function will serve for any of the other TIF outputs from HEC-RAS (water depth, velocity duration, etc.).

C. Data Sources for Task 1

Figures C.1, C.2, and C.3 present the original 2009 DEM, the DEM with adjustments for 2002, and the DEM with adjustments for 2013. These figures are zoomed into the area where the changes occurred, which includes two portions along the left dike, before and after the bridges (for the 2002 adjustments), and the closing of the tunnels under the overland train bridge (for the 2013 adjustments). The 2002-adjusted DEM was also used for the 2006 calibration event, and the 2013-adjusted DEM was used for the 2010 and 2011 events.

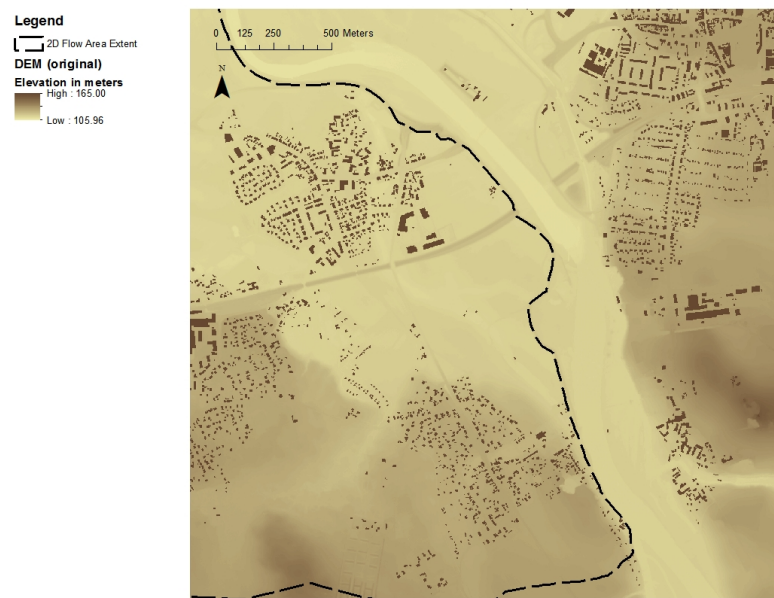


Figure C.1.: DEM of Bennewitz from 2009, with building footprints added

C. Data Sources for Task 1

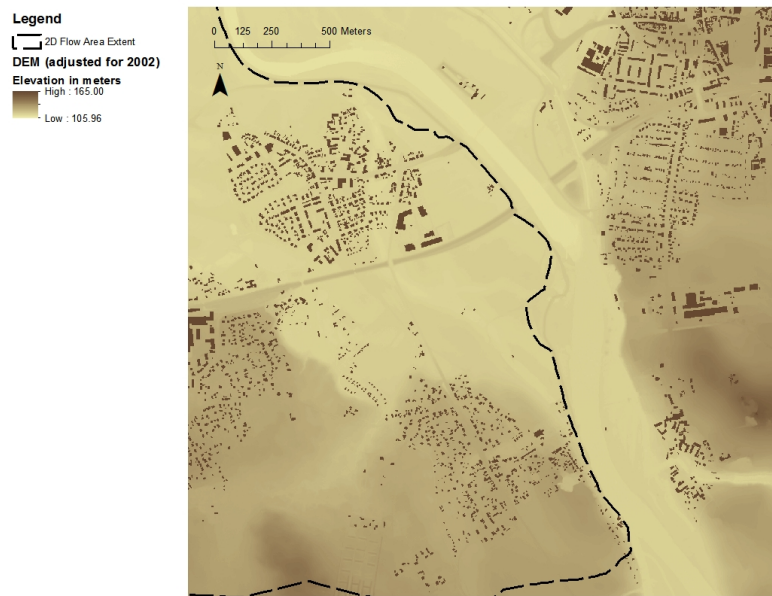


Figure C.2.: DEM of Bennewitz adjusted to better represent elevation during the flood event of 2002

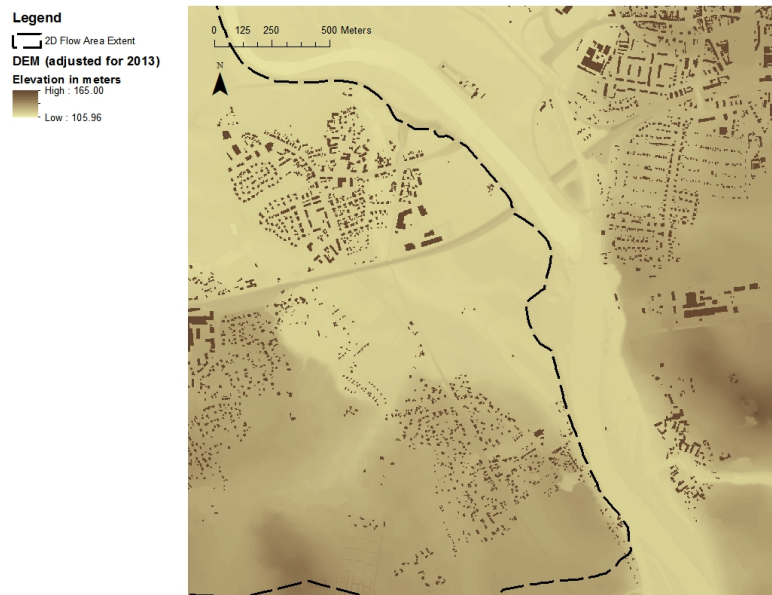


Figure C.3.: DEM of Bennewitz adjusted to better represent elevation during the flood event of 2002

Table C.1 presents the eight high water marks from the 2002 event collected from a visit to Bennewitz on 23 May 2017 (marks 1-8) as well as two high water marks from the 2002 event available in digital format from the Free State of Saxony's geodata download section for water data (Saechsisches Landesamt fuer Umwelt, Landwirtschaft und Geologie, 2017) (marks 9-10). All spatial references refer to Universal Transverse Mercator (UTM), Zone 33N, and are given in metres (rounded to the nearest metre). The height above ground for each of the marks 1-8 was added to the elevation given in the DEM in order to derive the water surface elevation, and for marks 9-10 the elevation was subtracted from the water surface elevation to derive the height above ground.

C. Data Sources for Task 1

Table C.1.: Observed high water marks in Bennewitz from the flood event of 2002

#	Easting	Northing	Height above Ground [m]	Water Surface Elevation [m]	Address	Key
1	340689	5692129	1.33	114.75	Bahnhofstraße 20	BH20
2	340799	5692293	1.35	115.00	Rudolf-Breitscheidstraße 15	RB15
3	340753	5692219	1.09	114.85	Ernst-Thälmann-Straße 7	ET7
4	340593	5692085	1.14	113.99	Rathaus Rückseite	RAT
5	340755	5692141	1.00	114.63	Albert-Kunst-Strasse 4	AK4
6	340839	5692195	2.00	115.41	Albert-Kunst-Strasse 13	AK13
7	340905	5692263	2.00	115.08	Ernst-Thälmann-Straße 25	ET25
8	340913	5692239	2.00	115.25	Ernst-Thälmann-Straße 28	ET28
9	341881	5691297	3.55	117.36	Am Mühlbach 20, Fährhaus	MB20
10	341331	5692753	0.87	113.95	Leipziger Strasse 6, Schützenverein	LS6

Figure C.4 presents the shift of one of the high water mark near the citizen protection centre (LS6).

C. Data Sources for Task 1

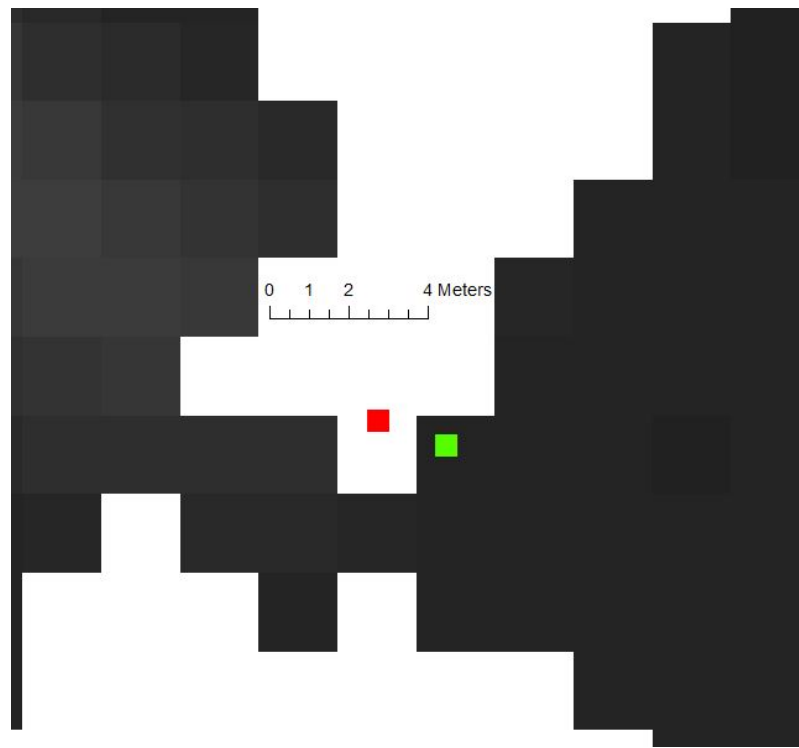


Figure C.4.: Shift of the location of the LS6 observed high water mark

Red represents the old location (directly on top of the building); green represents the new location (just next to the building, where water surface elevation data will be available). The dark cells represent lower elevations in the DEM, white cells represent high cells (buildings) in the DEM.

Figures C.5 and C.6 present the original observed flood extents for 2002 and 2013, as they were available from the Free State of Saxony geodata download website. Figure C.7 presents the 2013 with gaps filled, so as to be consistent with the methodology for the 2002 event.

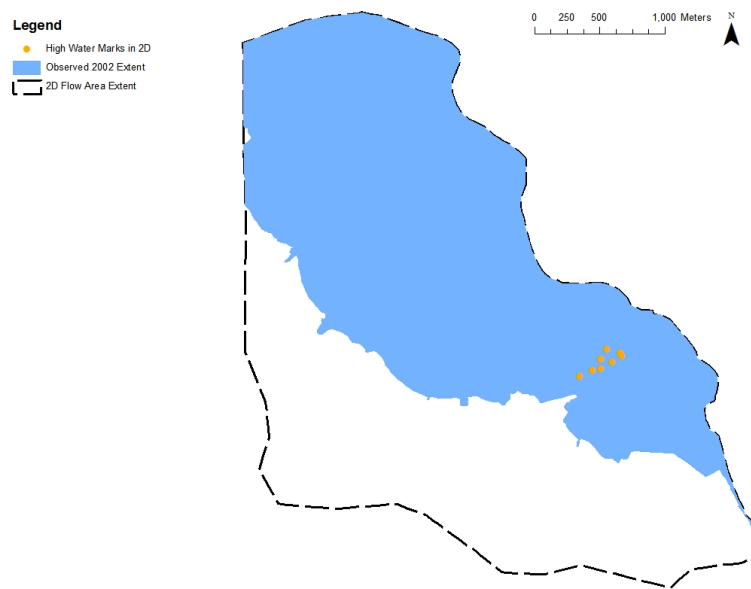


Figure C.5.: Observed 2002 flood extent for calibration of 1D/2D HEC-RAS unsteady flow model

C. Data Sources for Task 1



Figure C.6.: Observed 2013 flood extent for calibration of 1D/2D HEC-RAS unsteady flow model, with no gaps filled.



Figure C.7.: Observed 2013 flood extent for calibration of 1D/2D HEC-RAS unsteady flow model, with gaps filled.

D. Additional Results from Task 1

Table D.1 presents the alignment of model component regions with their respective Manning's n values, taking into account a variety of reference materials. Each model region is aligned with a CORINE Land Cover class (Kosztra & Arnold, 2014). Initial n values used for the determination of an appropriate mesh size and timestep were based on Fabio *et al.* (2010), in which the authors tested a number of optimisation methods for calibrating roughness for a 2D flood propagation model in Eilenburg, a city downstream of Bennewitz on the Mulde River (referred to in the table as the "Eilenburg Study"). The ranges for calibration of the 1D components were based principally on the guidance for calibration in the HEC-RAS Hydraulic Reference Manual, while those of the 2D area are based principally on Chow (1959). The first exception was in the selection of the maximum calibration n value for the overbanks. For this, the value from the Eilenburg study was selected (0.158), as it was very near the HEC-RAS maximum recommendation (0.16). The second exception was for the roughness values of the 2D urban areas. No category in HEC-RAS or Chow indicated a range specific to urban areas, and so the minimum was based on minimum values for lined and constructed channels, and the maximum was based on maximum values for floodplains.

Table D.2 presents data used to identify the most appropriate mesh size (25 m x 25 m) for this study. Tables D.3 and D.4 present data used to identify the most appropriate timestep (6 s) for this study. Table D.5 presents data from Stage 1 of the 1D calibration process. These results informed the selection of 0.0316 as the Manning's n value for the main channel throughout the model.

Table D.1.: Roughness value ranges for 1D/2D HEC-RAS unsteady flow model calibration

Desc.	Model Comp.	Cal. Min.	Cal. Max.	CLC Code	CLC Desc.	CLC Class	Eilenburg Study Desc.	Eilenburg Study Strickler k Value	Eilenburg Study n value ($n = 1/k$)
Channel	1D	0.0250	0.0750	511	Water courses	Wetlands	Channel	31.64	0.0316
Overbanks	1D	0.0500	0.1580	N/A	N/A	N/A	Floodplain	6.33	0.1580
Urban	2D	0.0100	0.1600	112	Discontinuous Urban Fabric	Artificial Areas	Urban Area	12.94	0.0773
Agricultural	2D	0.0200	0.1600	211	Non-irrigated Arable Land				
				231	Pastures				
Woodland	2D	0.0300	0.1600	311	Broad-leaved Forest	Forest and Semi-natural Areas	Woodland	6.33	0.1580
				312	Coniferous Forest				
				313	Mixed Forest				

"Desc." indicates the description. "Model Comp." indicates the model component to which the Manning's n value (or range) is applied. "Cal. Min." and "Cal. Max." indicate the minimum Manning's n value and maximum Manning's n value for calibration, respectively. "CLC" refers to the CORINE land cover classification system. The Eilenburg Study refers to Fabio et al. (2010).

Table D.2.: 1D/2D HEC-RAS model performance under varying mesh size

Trial	Mesh Size [m]	Max. It.	Computation Time		Volume Error [%]		Maximum Depth Error [m]							
			Run Time	Real Min/Sim. Day	Entire Model	2D Area Only	BH20	RB15	ET7	RAT	AK4	AK13	ET25	ET28
1	40	2	0:29:39	3.0	0.447	0.120	-0.22	-0.23	-0.10	0.39	0.08	-0.60	-0.28	-0.44
2	35	2	0:32:21	3.2	0.130	0.071	-0.14	-0.17	-0.05	0.36	0.13	-0.54	-0.22	-0.38
3	30	2	0:41:14	4.1	0.071	0.693	-0.21	-0.20	-0.08	0.33	0.07	-0.58	-0.25	-0.42
4	25	2	1:00:52	6.1	0.072	0.541	-0.25	-0.25	-0.13	0.33	0.05	-0.63	-0.30	-0.46
5	20	3	1:57:17	11.7	0.028	0.032	-0.20	-0.25	-0.12	0.39	0.07	-0.61	-0.28	-0.45
6	15	2	2:37:18	15.7	0.016	0.054	-0.17	-0.22	-0.11	0.38	0.08	-0.60	-0.27	-0.44
7	10	179	9:18:36	55.9	9.093	23.660	0.11	0.02	0.14	0.66	0.34	-0.34	-0.01	-0.17

The column labelled "Max. It." indicates the number of times each simulation had a location and time which reached the maximum limit of 20 iterations to calculate the water surface elevation. The column labelled "Computation Time" includes the total time for the entire 10-day simulation, as well as a representation of real-time minutes required per simulation day, for comparison to simulations beyond this table. The column labelled "Volume Error" provides the percent error in water volume accounting (volume of water introduced into the model versus volume of water exiting or remaining in the model at the end of the simulation). The column labelled "Maximum Depth Error" represents the error at each of the eight high water marks available in the 2D area. All simulations were conducted with consistent Manning's n values (see Eilenburg Study n values in Table D.1), a 10-day run of the 2002 event, and a 6 second timestep. The column labelled "Mesh Size" indicates the user-entered value for the spacing of both dx and dy in the creation of the computational mesh.

D. Additional Results from Task 1

Table D.3.: 1D/2D HEC-RAS model performance under varying timestep (1)

Trial	dt [s]	Courant No. in 2D Flow	Max. It.	Computation Time		Volume Error [%]	
				Run Time	Real Min/Sim. Day	Entire Model	2D Area Only
1	0.5	0.62	7	7:09:24	42.9	0.296	1.516
2	1	0.04	7	3:52:41	23.3	0.307	1.967
3	2	0.08	8	2:15:42	13.6	0.198	0.829
4	3	0.13	4	1:35:27	9.5	0.118	0.660
5	4	0.17	3	1:18:13	7.8	0.094	0.611
6	5	0.21	3	1:05:15	6.5	0.068	0.557
7	6	0.25	2	1:02:22	6.2	0.072	0.541
8	10	0.42	2	0:40:51	4.1	0.989	3.633
9	12	0.50	2	0:40:06	4.0	3.841	16.340
10	15	0.63	0	0:34:04	3.4	12.150	28.250

The column labelled "dt" indicates the timestep in seconds. The Courant number was calculated using the equation in Section 4.2.6, with wave speed as recommended for practical applications in the HEC-RAS Hydraulic Reference Manual (average maximum velocity * 1.5). The column labelled "Max. It." indicates the number of times each simulation had a location and time which reached the maximum limit of 20 iterations to calculate the water surface elevation. The column labelled "Computation Time" includes the total time for the entire 10-day simulation, as well as a representation of real-time minutes required per simulation day, for comparison to simulations beyond this table. The column labelled "Volume Error" provides the percent error in water volume accounting (volume of water introduced into the model versus volume of water exiting or remaining in the model at the end of the simulation). All simulations were conducted with consistent Manning's n values (see Eilenburg Study n values in Table D.1), a 10-day run of the 2002 event, and a mesh size of 25 by 25 metres.

Table D.4.: 1D/2D HEC-RAS model performance under varying timestep (2)

Trial	dt [s]	Maximum Depth Error [m]							
		BH20	RB15	ET7	RAT	AK4	AK13	ET25	ET28
1	0.5	-0.24	-0.24	-0.12	0.34	0.06	-0.62	-0.29	-0.45
2	1	-0.24	-0.24	-0.12	0.34	0.06	-0.62	-0.29	-0.46
3	2	-0.24	-0.24	-0.12	0.33	0.06	-0.62	-0.29	-0.46
4	3	-0.24	-0.24	-0.12	0.34	0.06	-0.62	-0.29	-0.46
5	4	-0.24	-0.24	-0.13	0.33	0.06	-0.62	-0.29	-0.46
6	5	-0.24	-0.25	-0.13	0.33	0.05	-0.62	-0.30	-0.46
7	6	-0.25	-0.25	-0.13	0.33	0.05	-0.63	-0.30	-0.46
8	10	-0.22	-0.23	-0.11	0.35	0.07	-0.60	-0.27	-0.44
9	12	-0.18	-0.19	-0.07	0.40	0.12	-0.56	-0.23	-0.40
10	15	-0.15	-0.15	-0.04	0.43	0.15	-0.52	-0.19	-0.36

The column labelled "dt" indicates the timestep in seconds. The column labelled "Maximum Depth Error" represents the error at each of the eight high water marks available in the 2D area. All simulations were conducted with consistent Manning's n values (see Eilenburg Study n values in Table D.1), a 10-day run of the 2002 event, and a mesh size of 25 by 25 metres.

D. Additional Results from Task 1

Table D.5.: 1D/2D HEC-RAS unsteady flow model 1D calibration intermediate results, Stage 1

Trial	n Channel	n Overbanks		Event	Peak Q Golzern				WSEL Error	
		Zw. and Fr.	Ve.		Error [m]	MAE	RMSE	Time Delay [hrs]	MB20	LS6
1	0.0250	0.0500	0.0500	2002	7.52	46.62	63.61	0	-0.33	0.44
				2006	6.00			4	n/a	n/a
				2010	62.64			1	n/a	n/a
				2011	110.32			3	n/a	n/a
2	0.0250	0.0630	0.0630	2002	4.81	45.75	63.40	0	-0.25	0.49
				2006	-3.71			3	n/a	n/a
				2010	67.00			2	n/a	n/a
				2011	107.48			3	n/a	n/a
3	0.0250	0.1580	0.1580	2002	-26.67	45.78	57.64	2	-0.08	0.76
				2006	-9.54			6	n/a	n/a
				2010	44.32			3	n/a	n/a
				2011	102.58			5	n/a	n/a
4	0.0320	0.0500	0.0500	2002	7.83	44.17	61.98	0	-0.09	0.62
				2006	0.47			4	n/a	n/a
				2010	60.46			2	n/a	n/a
				2011	107.92			3	n/a	n/a
5	0.0320	0.0630	0.0630	2002	2.00	41.73	60.37	0	0.00	0.69
				2006	-2.86			5	n/a	n/a
				2010	54.22			3	n/a	n/a
				2011	107.83			3	n/a	n/a
6	0.0320	0.1580	0.1580	2002	-41.89	45.64	56.56	3	0.23	0.86
				2006	-9.00			8	n/a	n/a
				2010	32.00			5	n/a	n/a
				2011	99.68			6	n/a	n/a
7	0.0750	0.1580	0.1580	2002	-114.25	57.22	71.76	5	1.45	1.13
				2006	-21.08			13	n/a	n/a
				2010	-9.84			11	n/a	n/a
				2011	83.70			10	n/a	n/a

All simulations were performed using a 6 second timestep and a 25 metre computational mesh size.

Details regarding the high water mark keys can be found in Table C.1. WSEL stands for water surface elevation.

Tables D.6 and D.7 present data from Stage 2 of the 1D calibration process. These results informed the selection of 0.158 as the Manning's n value in the overbanks of the Zwickauer and Freiberger Mulde and 0.0632 as the Manning's n value for the overbanks of the Vereinigte Mulde. With only four events per trial, MAE and RMSE were not considered statistically valid indicators, but rather simple tools to aid in the digesting and comparing of data.

D. Additional Results from Task 1

Table D.6.: 1D/2D HEC-RAS unsteady flow model 1D calibration intermediate results, Stage 2 (1)

Trial	n Overbanks		Event	Peak Q at Golzern				WSEL Error	
	Zw. and Fr.	Ve.		Error [m]	MAE	RMSE	Time Delay [hrs]	MB20	LS6
1	0.0500	0.0500	2002	7.83	44.17	61.98	0	0.62	-0.09
			2006	0.47			4	n/a	n/a
			2010	60.46			2	n/a	n/a
			2011	107.92			3	n/a	n/a
2	0.0500	0.0632	2002	6.08	43.86	61.33	0	0.70	0.02
			2006	-3.72			4	n/a	n/a
			2010	57.57			2	n/a	n/a
			2011	108.07			3	n/a	n/a
3	0.0500	0.1110	2002	-8.06	42.88	59.27	1	0.79	0.22
			2006	-5.43			5	n/a	n/a
			2010	51.9			3	n/a	n/a
			2011	106.13			4	n/a	n/a
4	0.0500	0.1580	2002	-21.06	45.07	58.46	2	0.89	0.32
			2006	-6.76			6	n/a	n/a
			2010	48.28			3	n/a	n/a
			2011	104.17			5	n/a	n/a
5	0.0632	0.0500	2002	4.53	43.26	61.36	0	0.62	-0.10
			2006	-2.74			5	n/a	n/a
			2010	57.47			2	n/a	n/a
			2011	108.31			3	n/a	n/a
6	0.0632	0.0632	2002	2	41.73	60.37	0	0.69	0.00
			2006	-2.86			5	n/a	n/a
			2010	54.22			3	n/a	n/a
			2011	107.83			3	n/a	n/a
7	0.0632	0.1110	2002	-11.99	43.00	58.72	1	0.79	0.22
			2006	-4.75			5	n/a	n/a
			2010	49.58			3	n/a	n/a
			2011	105.67			4	n/a	n/a
8	0.0632	0.1580	2002	-24.13	45.19	58.18	2	0.89	0.31
			2006	-6.67			6	n/a	n/a
			2010	46.09			4	n/a	n/a
			2011	103.86			5	n/a	n/a

All simulations were performed using a 6 second timestep, a 25 metre computational mesh size, and a Manning's n value of 0.316 in the channel throughout the model.

D. Additional Results from Task 1

Table D.7.: 1D/2D HEC-RAS unsteady flow model 1D calibration intermediate results, Stage 2 (2)

Trial	n Overbanks		Event	Peak Q at Golzern				WSEL Error	
	Zw. and Fr.	Ve.		Error [m]	MAE	RMSE	Time Delay [hrs]	MB20	LS6
9	0.1110	0.0500	2002	-3.07	41.81	58.52	0	0.61	-0.10
			2006	-9.33			5	n/a	n/a
			2010	49.03			3	n/a	n/a
			2011	105.82			4	n/a	n/a
10	0.1110	0.0632	2002	-5.82	41.63	57.71	1	0.70	0.01
			2006	-9.56			6	n/a	n/a
			2010	45.74			3	n/a	n/a
			2011	105.38			4	n/a	n/a
11	0.1110	0.1110	2002	-20.61	43.88	56.64	2	0.79	0.21
			2006	-10.72			6	n/a	n/a
			2010	41.33			4	n/a	n/a
			2011	102.87			5	n/a	n/a
12	0.1110	0.1580	2002	-35.25	46.28	56.89	2	0.89	0.30
			2006	-11.55			7	n/a	n/a
			2010	37.53			4	n/a	n/a
			2011	100.8			6	n/a	n/a
13	0.1580	0.0500	2002	-10.8	41.11	57.01	1	0.61	-0.11
			2006	-5.74			6	n/a	n/a
			2010	43			3	n/a	n/a
			2011	104.88			4	n/a	n/a
14	0.1580	0.0632	2002	-12.73	40.99	56.34	1	0.70	0.00
			2006	-6.29			6	n/a	n/a
			2010	40.91			4	n/a	n/a
			2011	104.02			4	n/a	n/a
15	0.1580	0.1110	2002	-27.37	43.03	55.61	2	0.79	0.21
			2006	-7.68			7	n/a	n/a
			2010	35.64			4	n/a	n/a
			2011	101.44			5	n/a	n/a
16	0.1580	0.1580	2002	-41.89	45.64	56.56	3	0.86	0.23
			2006	-9			8	n/a	n/a
			2010	32			5	n/a	n/a
			2011	99.68			6	n/a	n/a

All simulations were performed using a 6 second timestep, a 25 metre computational mesh size, and a Manning's n value of 0.316 in the channel throughout the model.

Tables D.8, D.9, and D.10 present data from Stage 1 of the 2D calibration process. These results informed the selection of 0.1600 as the Manning's n value in the woodland areas, a finer look into Manning's n values between 0.0773 and 0.1600 for the urban areas, and the continued consideration of 0.0550, 0.0900, and 0.1600 for agricultural areas.

D. Additional Results from Task 1

Table D.8.: 1D/2D HEC-RAS unsteady flow model 2D calibration Manning's values for Stage 1

Trial	Manning's n		
	Urban	Agri.	Wood.
1	0.0100	0.0200	0.0300
2	0.0100	0.0200	0.0625
3	0.0100	0.0200	0.0950
4	0.0100	0.0200	0.1600
5	0.0100	0.0550	0.0300
6	0.0100	0.0550	0.0625
7	0.0100	0.0550	0.0950
8	0.0100	0.0550	0.1600
9	0.0100	0.0900	0.0300
10	0.0100	0.0900	0.0625
11	0.0100	0.0900	0.0950
12	0.0100	0.0900	0.1600
13	0.0100	0.1600	0.0300
14	0.0100	0.1600	0.0625
15	0.0100	0.1600	0.0950
16	0.0100	0.1600	0.1600
17	0.0375	0.0200	0.0300
18	0.0375	0.0200	0.0625
19	0.0375	0.0200	0.0950
20	0.0375	0.0200	0.1600
21	0.0375	0.0550	0.0300
22	0.0375	0.0550	0.0625
23	0.0375	0.0550	0.0950
24	0.0375	0.0550	0.1600
25	0.0375	0.0900	0.0300
26	0.0375	0.0900	0.0625
27	0.0375	0.0900	0.0950
28	0.0375	0.0900	0.1600
29	0.0375	0.1600	0.0300
30	0.0375	0.1600	0.0625
31	0.0375	0.1600	0.0950
32	0.0375	0.1600	0.1600
33	0.0773	0.0200	0.0300
34	0.0773	0.0200	0.0625
35	0.0773	0.0200	0.0950
36	0.0773	0.0200	0.1600
37	0.0773	0.0550	0.0300
38	0.0773	0.0550	0.0625
39	0.0773	0.0550	0.0950
40	0.0773	0.0550	0.1600
41	0.0773	0.0900	0.0300
42	0.0773	0.0900	0.0625
43	0.0773	0.0900	0.0950
44	0.0773	0.0900	0.1600
45	0.0773	0.1600	0.0300
46	0.0773	0.1600	0.0625
47	0.0773	0.1600	0.0950
48	0.0773	0.1600	0.1600
49	0.1600	0.0200	0.0300
50	0.1600	0.0200	0.0625
51	0.1600	0.0200	0.0950
52	0.1600	0.0200	0.1600
53	0.1600	0.0550	0.0300
54	0.1600	0.0550	0.0625
55	0.1600	0.0550	0.0950
56	0.1600	0.0550	0.1600
57	0.1600	0.0900	0.0300
58	0.1600	0.0900	0.0625
59	0.1600	0.0900	0.0950
60	0.1600	0.0900	0.1600
61	0.1600	0.1600	0.0300
62	0.1600	0.1600	0.0625
63	0.1600	0.1600	0.0950
64	0.1600	0.1600	0.1600

D. Additional Results from Task 1

Table D.9.: 1D/2D HEC-RAS unsteady flow model 2D calibration intermediate results, Stage 1 (1)

Trial	Maximum Water Surface Elevation Error [m]								RMSE	MAE	CSI
	BH20	RB15	ET7	RAT	AK4	AK13	ET25	ET28			
1	-0.64	-0.60	-0.46	-0.27	-0.31	-1.01	-0.67	-0.84	0.64	0.60	0.976
2	-0.64	-0.60	-0.46	-0.27	-0.31	-1.01	-0.67	-0.84	0.64	0.60	0.976
3	-0.64	-0.60	-0.46	-0.27	-0.31	-1.01	-0.67	-0.84	0.64	0.60	0.976
4	-0.64	-0.60	-0.46	-0.27	-0.31	-1.01	-0.67	-0.84	0.64	0.60	0.976
5	-0.69	-0.72	-0.57	-0.07	-0.41	-1.13	-0.80	-0.97	0.74	0.67	0.980
6	-0.69	-0.72	-0.57	-0.07	-0.41	-1.13	-0.80	-0.97	0.74	0.67	0.980
7	-0.69	-0.72	-0.57	-0.07	-0.41	-1.13	-0.80	-0.97	0.74	0.67	0.980
8	-0.69	-0.72	-0.57	-0.07	-0.41	-1.13	-0.80	-0.97	0.74	0.67	0.980
9	-0.69	-0.78	-0.63	0.00	-0.46	-1.19	-0.86	-1.03	0.78	0.71	0.982
10	-0.69	-0.78	-0.63	0.00	-0.46	-1.19	-0.86	-1.03	0.78	0.71	0.982
11	-0.69	-0.78	-0.63	0.00	-0.46	-1.19	-0.86	-1.03	0.78	0.71	0.982
12	-0.69	-0.78	-0.63	0.00	-0.46	-1.19	-0.86	-1.03	0.78	0.71	0.982
13	-0.75	-0.88	-0.73	-0.03	-0.55	-1.29	-0.96	-1.13	0.87	0.79	0.983
14	-0.75	-0.88	-0.73	-0.03	-0.55	-1.29	-0.96	-1.13	0.87	0.79	0.983
15	-0.75	-0.88	-0.73	-0.03	-0.55	-1.29	-0.96	-1.13	0.87	0.79	0.983
16	-0.75	-0.88	-0.73	-0.03	-0.55	-1.29	-0.96	-1.13	0.87	0.79	0.983
17	-0.23	-0.15	-0.03	0.11	0.15	-0.51	-0.18	-0.34	0.25	0.21	0.977
18	-0.23	-0.15	-0.03	0.11	0.15	-0.51	-0.18	-0.34	0.25	0.21	0.977
19	-0.23	-0.15	-0.03	0.11	0.15	-0.51	-0.18	-0.34	0.25	0.21	0.977
20	-0.23	-0.15	-0.03	0.11	0.15	-0.51	-0.18	-0.34	0.25	0.21	0.977
21	-0.36	-0.31	-0.19	0.12	-0.02	-0.70	-0.37	-0.53	0.38	0.33	0.980
22	-0.36	-0.31	-0.19	0.12	-0.02	-0.70	-0.37	-0.53	0.38	0.33	0.980
23	-0.36	-0.31	-0.19	0.12	-0.02	-0.70	-0.37	-0.53	0.38	0.33	0.980
24	-0.36	-0.31	-0.19	0.12	-0.02	-0.70	-0.37	-0.53	0.38	0.33	0.980
25	-0.42	-0.41	-0.29	0.15	-0.12	-0.81	-0.48	-0.64	0.47	0.41	0.981
26	-0.42	-0.41	-0.29	0.15	-0.12	-0.81	-0.48	-0.64	0.47	0.41	0.981
27	-0.42	-0.41	-0.29	0.15	-0.12	-0.81	-0.48	-0.64	0.47	0.41	0.981
28	-0.42	-0.41	-0.29	0.15	-0.12	-0.81	-0.48	-0.64	0.47	0.41	0.981
29	-0.47	-0.53	-0.40	0.19	-0.22	-0.94	-0.61	-0.77	0.57	0.52	0.982
30	-0.47	-0.53	-0.40	0.19	-0.22	-0.94	-0.61	-0.77	0.57	0.52	0.982
31	-0.47	-0.53	-0.40	0.19	-0.22	-0.94	-0.61	-0.77	0.57	0.52	0.982
32	-0.47	-0.53	-0.40	0.19	-0.22	-0.94	-0.61	-0.77	0.57	0.52	0.982

All simulations were performed using a 6 second timestep, a 25 metre computational mesh size, and the Manning's n values selected from the 1D calibration process (0.0316 in the channel, 0.0158 in the overbanks of the Zwickauer and Freiberger Mulde, and 0.0632 in the overbanks of the Vereinigte Mulde). All simulations are for the 2002 event, as that is the only event for which observed high water marks are available. With only eight high water marks per trial, MAE and RMSE were not considered statistically valid indicators, but rather simple tools to aid in the digesting and comparing of data.

D. Additional Results from Task 1

Table D.10.: 1D/2D HEC-RAS unsteady flow model 2D calibration intermediate results, Stage 1 (2)

Trial	Maximum Water Surface Elevation Error [m]								RMSE	MAE	CSI
	BH20	RB15	ET7	RAT	AK4	AK13	ET25	ET28			
33	0.01	0.08	0.21	0.32	0.42	-0.22	0.09	-0.05	0.22	0.17	0.976
34	0.01	0.08	0.21	0.32	0.42	-0.22	0.09	-0.05	0.22	0.17	0.976
35	0.01	0.08	0.21	0.32	0.42	-0.22	0.09	-0.05	0.22	0.17	0.976
36	0.01	0.08	0.21	0.32	0.42	-0.22	0.09	-0.05	0.22	0.17	0.976
37	-0.14	-0.08	0.04	0.26	0.23	-0.42	-0.10	-0.26	0.22	0.19	0.979
38	-0.14	-0.08	0.04	0.26	0.23	-0.42	-0.10	-0.26	0.22	0.19	0.979
39	-0.14	-0.08	0.04	0.26	0.23	-0.42	-0.10	-0.26	0.22	0.19	0.979
40	-0.14	-0.08	0.04	0.26	0.23	-0.42	-0.10	-0.26	0.22	0.19	0.979
41	-0.24	-0.19	-0.07	0.23	0.11	-0.55	-0.23	-0.39	0.29	0.25	0.980
42	-0.24	-0.19	-0.07	0.23	0.11	-0.55	-0.23	-0.39	0.29	0.25	0.980
43	-0.24	-0.19	-0.07	0.23	0.11	-0.55	-0.23	-0.39	0.29	0.25	0.980
44	-0.24	-0.19	-0.07	0.23	0.11	-0.55	-0.23	-0.39	0.29	0.25	0.980
45	-0.33	-0.32	-0.20	0.23	-0.03	-0.71	-0.38	-0.55	0.40	0.34	0.982
46	-0.33	-0.32	-0.20	0.23	-0.03	-0.71	-0.38	-0.55	0.40	0.34	0.982
47	-0.33	-0.32	-0.20	0.23	-0.03	-0.71	-0.38	-0.55	0.40	0.34	0.982
48	-0.33	-0.32	-0.20	0.23	-0.03	-0.71	-0.38	-0.55	0.40	0.34	0.982
49	0.25	0.28	0.44	0.53	0.69	0.07	0.35	0.22	0.40	0.35	0.975
50	0.25	0.28	0.44	0.53	0.69	0.07	0.35	0.22	0.40	0.35	0.975
51	0.25	0.28	0.44	0.53	0.69	0.07	0.35	0.22	0.40	0.35	0.975
52	0.25	0.28	0.44	0.53	0.69	0.07	0.35	0.22	0.40	0.35	0.975
53	0.11	0.16	0.29	0.45	0.52	-0.11	0.19	0.05	0.28	0.23	0.978
54	0.11	0.16	0.29	0.45	0.52	-0.11	0.19	0.05	0.28	0.23	0.978
55	0.11	0.16	0.29	0.45	0.52	-0.11	0.19	0.05	0.28	0.23	0.978
56	0.11	0.16	0.29	0.45	0.52	-0.11	0.19	0.05	0.28	0.23	0.978
57	0.00	0.05	0.18	0.38	0.39	-0.26	0.06	-0.09	0.23	0.18	0.980
58	0.00	0.05	0.18	0.38	0.39	-0.26	0.06	-0.09	0.23	0.18	0.980
59	0.00	0.05	0.18	0.38	0.39	-0.26	0.06	-0.09	0.23	0.18	0.980
60	0.00	0.05	0.18	0.38	0.39	-0.26	0.06	-0.09	0.23	0.18	0.980
61	-0.14	-0.09	0.02	0.32	0.22	-0.44	-0.12	-0.28	0.24	0.20	0.981
62	-0.14	-0.09	0.02	0.32	0.22	-0.44	-0.12	-0.28	0.24	0.20	0.981
63	-0.14	-0.09	0.02	0.32	0.22	-0.44	-0.12	-0.28	0.24	0.20	0.981
64	-0.14	-0.09	0.02	0.32	0.22	-0.44	-0.12	-0.28	0.24	0.20	0.981

All simulations were performed using a 6 second timestep, a 25 metre computational mesh size, and the Manning's n values selected from the 1D calibration process (0.0316 in the channel, 0.0158 in the overbanks of the Zwickauer and Freiberger Mulde, and 0.0632 in the overbanks of the Vereinigte Mulde). All simulations are for the 2002 event, as that is the only event for which observed high water marks are available. With only eight high water marks per trial, MAE and RMSE were not considered statistically valid indicators, but rather simple tools to aid in the digesting and comparing of data.

The small open water region (CLC code 512) to the northwest of the main community of Bennewitz was erroneously set to a Manning's n value of 0.3 for Stage 1 of the 2D calibration process. As this was expected to have relatively little impact on the intermediate calibration results (given its distance from the high water marks and the edge of the extent), the value was corrected for Stage 2, but Stage 1 trials were not re-run. For Stage 2, the value for this region was set to match the corresponding areas in 1D that would be in the open water category (Manning's

D. Additional Results from Task 1

value of 0.0316).

Table D.11 presents the Manning's n values used for Stages 2 and 3 of 2D calibration. Table D.12 presents data from Stage 2 of the 2D calibration process. The results informed the selection of 0.098 for urban areas and 0.055 in agricultural areas for Stage 3 of 2D calibration.

Table D.11.: 1D/2D HEC-RAS unsteady flow model 2D calibration Manning's n values for Stages 2 and 3

Stage 2 Trial	Manning's n			Stage 3 Trial	Manning's n		
	Urban	Agri.	Wood.		Urban	Agri.	Wood.
1	0.0773	0.0550	0.1600	1	0.0830	0.0470	0.1600
2	0.0773	0.0900	0.1600	2	0.0830	0.0510	0.1600
3	0.0773	0.1600	0.1600	3	0.0830	0.0550	0.1600
4	0.0980	0.0550	0.1600	4	0.0830	0.0590	0.1600
5	0.0980	0.0900	0.1600	5	0.0830	0.0630	0.1600
6	0.0980	0.1600	0.1600	6	0.0910	0.0470	0.1600
7	0.1200	0.0550	0.1600	7	0.0910	0.0510	0.1600
8	0.1200	0.0900	0.1600	8	0.0910	0.0550	0.1600
9	0.1200	0.1600	0.1600	9	0.0910	0.0590	0.1600
10	0.1400	0.0550	0.1600	10	0.0910	0.0630	0.1600
11	0.1400	0.0900	0.1600	11	0.0980	0.0470	0.1600
12	0.1400	0.1600	0.1600	12	0.0980	0.0510	0.1600
13	0.1600	0.0550	0.1600	13	0.0980	0.0550	0.1600
14	0.1600	0.0900	0.1600	14	0.0980	0.0590	0.1600
15	0.1600	0.1600	0.1600	15	0.0980	0.0630	0.1600
				16	0.1050	0.0470	0.1600
				17	0.1050	0.0510	0.1600
				18	0.1050	0.0550	0.1600
				19	0.1050	0.0590	0.1600
				20	0.1050	0.0630	0.1600
				21	0.1130	0.0470	0.1600
				22	0.1130	0.0510	0.1600
				23	0.1130	0.0550	0.1600
				24	0.1130	0.0590	0.1600
				25	0.1130	0.0630	0.1600

D. Additional Results from Task 1

Table D.12.: 1D/2D HEC-RAS unsteady flow model 2D calibration intermediate results, Stage 2

Trial	Maximum Water Surface Elevation Error [m]								RMSE	MAE	CSI
	BH20	RB15	ET7	RAT	AK4	AK13	ET25	ET28			
1	-0.14	-0.08	0.04	0.26	0.23	-0.42	-0.10	-0.26	0.22	0.19	0.978
2	-0.24	-0.19	-0.07	0.23	0.11	-0.56	-0.23	-0.39	0.29	0.25	0.979
3	-0.33	-0.32	-0.20	0.23	-0.03	-0.71	-0.38	-0.55	0.40	0.34	0.981
4	-0.07	0.00	0.12	0.31	0.32	-0.33	-0.01	-0.16	0.21	0.16	0.977
5	-0.17	-0.11	0.00	0.27	0.19	-0.46	-0.14	-0.30	0.24	0.21	0.979
6	-0.28	-0.25	-0.13	0.25	0.05	-0.63	-0.30	-0.46	0.34	0.29	0.980
7	0.00	0.07	0.19	0.36	0.40	-0.24	0.07	-0.08	0.22	0.18	0.977
8	-0.10	-0.04	0.07	0.31	0.27	-0.38	-0.06	-0.22	0.22	0.18	0.978
9	-0.22	-0.19	-0.07	0.27	0.12	-0.55	-0.23	-0.39	0.29	0.25	0.980
10	0.06	0.12	0.25	0.41	0.46	-0.17	0.14	-0.01	0.25	0.20	0.977
11	-0.05	0.01	0.13	0.35	0.33	-0.31	0.00	-0.15	0.22	0.17	0.978
12	-0.18	-0.14	-0.02	0.30	0.17	-0.49	-0.17	-0.33	0.26	0.22	0.980
13	0.11	0.16	0.29	0.44	0.52	-0.11	0.19	0.05	0.28	0.23	0.976
14	0.00	0.05	0.18	0.38	0.39	-0.26	0.06	-0.09	0.22	0.18	0.978
15	-0.14	-0.09	0.02	0.32	0.22	-0.44	-0.12	-0.28	0.24	0.20	0.979

All simulations were performed using a 6 second timestep, a 25 metre computational mesh size, the Manning's n values selected from the 1D calibration process (0.0316 in the channel, 0.0158 in the overbanks of the Zwickauer and Freiberger Mulde, and 0.0632 in the overbanks of the Vereinigte Mulde), and a Manning's value of 0.16 for woodland areas in the 2D portion of the model. With only eight high water marks per trial, MAE and RMSE were not considered statistically valid indicators, but rather simple tools to aid in the digesting and comparing of data.

Table D.13 presents data from Stage 3 of the 2D calibration process. The results of this stage confirmed the selection of 0.098 for urban areas and 0.055 in agricultural areas as the final Manning's n values in the model, thus ending the calibration process and providing results regarding the sensitivity of the model with regard to the roughness values.

D. Additional Results from Task 1

Table D.13.: 1D/2D HEC-RAS unsteady flow model 2D calibration intermediate results, Stage 3

Trial	Maximum Water Surface Elevation Error [m]								RMSE	MAE	CSI
	BH20	RB15	ET7	RAT	AK4	AK13	ET25	ET28			
1	-0.09	-0.02	0.09	0.29	0.29	-0.35	-0.03	-0.19	0.21	0.17	0.977
2	-0.11	-0.04	0.08	0.28	0.27	-0.37	-0.05	-0.21	0.21	0.18	0.978
3	-0.12	-0.05	0.06	0.27	0.26	-0.39	-0.07	-0.23	0.22	0.18	0.978
4	-0.13	-0.07	0.05	0.27	0.24	-0.41	-0.09	-0.25	0.22	0.19	0.978
5	-0.15	-0.08	0.03	0.26	0.22	-0.43	-0.11	-0.26	0.23	0.19	0.978
6	-0.06	0.01	0.13	0.31	0.33	-0.31	0.00	-0.15	0.21	0.16	0.977
7	-0.08	-0.01	0.11	0.30	0.31	-0.34	-0.02	-0.17	0.21	0.17	0.977
8	-0.09	-0.02	0.09	0.29	0.29	-0.36	-0.04	-0.19	0.21	0.17	0.978
9	-0.11	-0.04	0.08	0.29	0.27	-0.37	-0.05	-0.21	0.21	0.18	0.978
10	-0.12	-0.05	0.06	0.28	0.26	-0.39	-0.07	-0.23	0.22	0.18	0.978
11	-0.04	0.03	0.15	0.33	0.36	-0.28	0.03	-0.12	0.21	0.17	0.977
12	-0.05	0.02	0.13	0.32	0.34	-0.30	0.01	-0.14	0.21	0.16	0.977
13	-0.07	0.00	0.12	0.31	0.32	-0.33	-0.01	-0.16	0.21	0.16	0.977
14	-0.08	-0.01	0.10	0.31	0.30	-0.34	-0.03	-0.18	0.21	0.17	0.978
15	-0.09	-0.03	0.09	0.30	0.29	-0.36	-0.04	-0.20	0.21	0.17	0.978
16	-0.01	0.06	0.18	0.35	0.39	-0.25	0.06	-0.09	0.22	0.17	0.977
17	-0.03	0.04	0.16	0.34	0.37	-0.28	0.04	-0.11	0.21	0.17	0.977
18	-0.04	0.02	0.14	0.33	0.35	-0.30	0.02	-0.13	0.21	0.17	0.977
19	-0.06	0.01	0.13	0.32	0.33	-0.31	0.00	-0.15	0.21	0.16	0.977
20	-0.07	-0.01	0.11	0.32	0.31	-0.33	-0.02	-0.17	0.21	0.17	0.978
21	0.01	0.08	0.20	0.37	0.42	-0.22	0.09	-0.06	0.23	0.18	0.977
22	0.00	0.06	0.18	0.36	0.39	-0.24	0.07	-0.08	0.22	0.17	0.977
23	-0.02	0.05	0.17	0.35	0.38	-0.27	0.05	-0.10	0.22	0.17	0.977
24	-0.03	0.03	0.15	0.34	0.36	-0.28	0.03	-0.12	0.21	0.17	0.977
25	-0.05	0.02	0.14	0.33	0.34	-0.30	0.01	-0.14	0.21	0.17	0.978

All simulations were performed using a 6 second timestep, a 25 metre computational mesh size, the Manning's n values selected from the 1D calibration process (0.0316 in the channel, 0.0158 in the overbanks of the Zwickauer and Freiberger Mulde, and 0.0632 in the overbanks of the Vereinigte Mulde), and a Manning's value of 0.16 for woodland areas in the 2D portion of the model. The Manning's n values were varied up to 15% higher and lower than the values selected from Stage 2. With only eight high water marks per trial, MAE and RMSE were not considered statistically valid indicators, but rather simple tools to aid in the digesting and comparing of data.

Figures D.1, D.2 and D.3 present the maximum water surface elevation results from the calibrated model for 2006, 2010, and 2013, respectively. In all three of these simulations, flooding in the 2D flow area is minimal and restricted to the upstream portion of the flow area (the southeast corner, near Schmölen).

D. Additional Results from Task 1

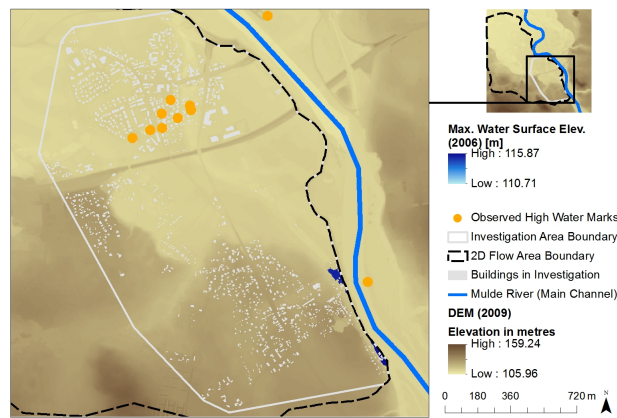


Figure D.1.: Simulated maximum water surface elevation in 2D flow area of 1D/2D HEC-RAS unsteady flow model for flood event in 2006

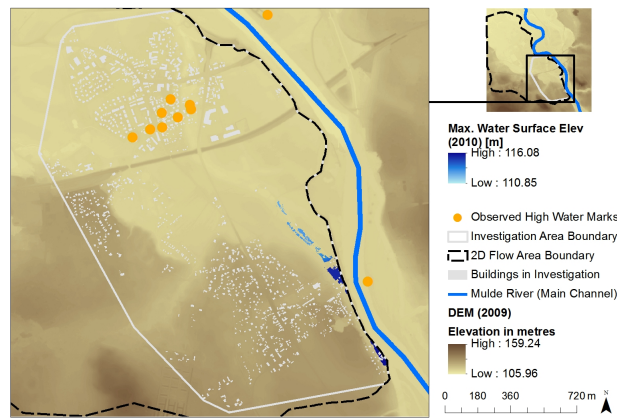


Figure D.2.: Simulated maximum water surface elevation in 2D flow area of 1D/2D HEC-RAS unsteady flow model for flood event in 2010

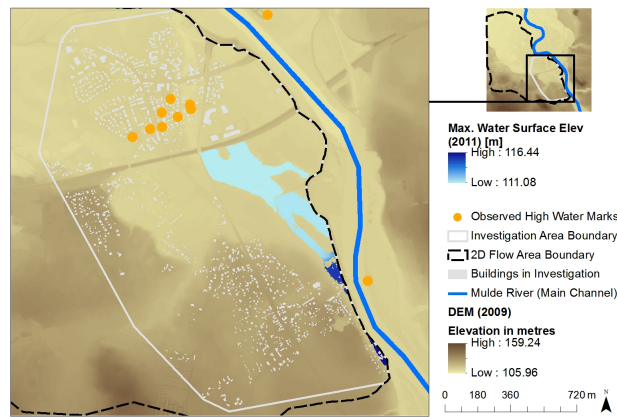


Figure D.3.: Simulated maximum water surface elevation in 2D flow area of 1D/2D HEC-RAS unsteady flow model for flood event in 2011

E. Additional Discussion Regarding the Influence of DEM Uncertainty on Flood Extent Results from Task 1

When taking a closer look at where and when excess flood water (i.e. flooding in an area that is not expected to be flooded in 2013) enters the 2D flow area in the simulation of the 2013 event, it appears that it first breaches the dike near a community called Grubnitz. The simulated first breach at this location occurs at 05:00 on 3 June 2013. According to Koehler (2016), the dike was not breached at this location in 2013, though later in the simulation, the model does accurately portray a breach further downstream, near Nepperwitz. Thus, this begs the question whether the inaccurate breach at Grubnitz is due principally to the excess flow (i.e. the additional 225 m³/s at Golzern) or due to inaccuracies in the 2009 DEM representation of the levee height in this region. The vertical uncertainty of laser scan data for DEMs should be roughly 15-20 cm. However, with a relatively small, steep topographical feature, such as a dike, the uncertainty may be greater. To investigate this issue further the inflow at the upstream end of the model was artificially reduced until the dike at Grubnitz no longer experienced a breach. It appears that if 500 m³/s is removed from the peak of the upstream boundary conditions (250 m³/s from Leisnig, 250 m³/s from Colditz, gradually introduced to the peak of the hydrograph), the dike no longer breaches at Grubnitz. Removing 400 m³/s from the peak, the dike still breaches at Grubnitz, though it then fails to breach near Nepperwitz. Both of these artificial reductions far exceed the excess discharge experienced at Golzern (producing a peak of 1781 m³/s for the former and 1881 m³/s for the latter). Thus the most likely cause for uncertainty in this breach at Grubnitz appears to be vertical elevation error in the DEM.

While the focus of this study is on the investigation area, the 1D portion of the model also includes Wurzen. For the simulated 2002 and 2013 events (but not the 2006, 2010, and 2011 events), the dikes breach on the Wurzen side of the Mulde. To examine what effect this might have on Bennewitz, the 2002 event was run with a large artificial levee placed along the DEM dike alignment adjacent to Wurzen, preventing any water from flowing into Wurzen. In this simulation, four of ten available high water marks were slightly improved compared to the observed data, while the other six were slightly worse. Subtracting the raster data within the 2D flow area of the "no-wall" results from the "with-wall" results, the average difference among cells was 4 cm, and the standard deviation was 2 cm. This is considered another source of uncertainty in the model results, though it may be due to vertical elevation errors in the DEM, as suggested for the erroneous breach near Grubnitz.

F. Data Sources for Task 2

The nine parameter sets produced by the optimisation procedure for the calibration of the HBV model, performed by Ms. Verena Maleska, are presented in Table F.1.

Table F.1.: Optimal parameter sets for HBV hydrologic model

	Set 1	Set 2	Set 3	Set 4	Set 5	Set 6	Set 7	Set 8	Set 9
FC	211.247	220.796	222.476	222.605	222.621	222.621	225.332	225.815	594.549
LP	0.786	0.784	0.781	0.788	0.781	0.781	0.781	0.781	1.757
BETA	1.233	1.000	1.221	1.000	1.000	1.000	1.000	1.000	2.363
UZL	9.996	9.996	9.330	10.000	10.000	10.000	10.000	10.000	9.718
PERC	0.129	0.129	0.129	0.144	0.129	0.129	0.129	0.129	0.388
K0	0.015	0.015	0.015	0.016	0.015	0.015	0.015	0.015	0.025
K1	0.015	0.015	0.015	0.015	0.015	0.015	0.015	0.015	0.007
K2	0.128	0.128	0.150	0.150	0.150	0.150	0.150	0.150	0.020
MAXBAS	31	32	32	32	32	32	32	32	33
CFMAX	0.938	0.938	0.938	0.938	0.938	0.938	0.938	0.938	1.299
TT	-1.552	-1.449	-1.449	-1.449	-1.595	-1.449	-1.449	-1.449	-1.445

Column labels indicate the parameter set. FC represents the maximum soil moisture storage, or the parameter version of field capacity. LP represents a soil moisture value above which evapotranspiration reaches its potential value (mm). BETA is a coefficient which determines the proportion of precipitation contributed to the response function or soil moisture storage. UZL is the maximum threshold parameter at which water is retained in the upper box. K0, K1, and K2 are the recession coefficients for peak flow, subsurface flow, and base flow, respectively. MAXBAS is the parameter function for equilateral triangular weighting function. CFMAX is the degree-day factor, used to calculate the melt rate using the degree-day method. TT represents the threshold temperature for melting, to distinguish snow from rainfall. The above descriptions of the parameters were informed by Gebrehiwot et al. (2013) and Swedish Meteorological and Hydrological Institute (2017).

G. Python Tools for Task 2

Two scripts were created for preparing files to be imported into HEC-RAS, one for the unsteady flow file and another for the plan file. The scripts are available at https://github.com/mhearn11/MSc_floodtools.

The script for creating the unsteady flow file is requires that a template unsteady flow file is created, with brackets inserted where the data is to be inserted. The script will:

- Iterate through the CSV files in an assigned directory.
- Read the CSV file (which provides the discharge hydrograph) and write the time series into a dataframe (one column for date and time, one column for discharge).
- Copy the dataframe and convert the string discharge values to float.
- Apply a threshold to the discharge values (any values below the threshold will be raised to the threshold value), and re-insert the thresholded float values as string values to the original dataframe.
- Remove the excess simulation days before and after the desired 8 day simulation period.
- Create a string list of the discharge values.
- Format the list as a string with each value being 8 characters long and to print in lines of 10 values to a row, and store it as an object called "hydrograph_str"
- Identify the name of the original file and store it as an object called "title"
- Open the template unsteady flow file and insert the title and hydrograph_str into the template to replace the brackets.
- Save the file named as the title with ".uXX" as the extension, but with the "XX" being a 2-character number counting up from "01" for each iterated CSV file.

The script for creating the plan file, which also requires a plan template, is very similar to the last steps of that for the unsteady flow file. The script will:

- Iterate through the CSV files in an assigned directory.
- Identify the name of the original file and store it as object called "title".
- Identify the ".uXX" extension to be matched with the file (2-character number counting up from "01" for each iterated CSV file).
- Open the template plan file and insert the title (for the title and for what is called the short ID) and the unsteady flow file extension into the template to replace the brackets.

H. Additional Results from Task 2

In order to ensure that the shortening of the 1D component of the model (starting at Golzern rather than at Leisnig and Colditz) did not have a great impact on the results, the original model from Task 1 was compared to the shortened model from Task 2 for the 2013 event. The difference between the maximum water surface elevation for each cell was very small. The absolute mean of the differences was less than 0.5 mm, and the standard deviation was 1.6 mm. The maximum absolute difference was 13 cm, but this occurred far from the main study area (the main town of Bennewitz).

This Task 2 model, starting at Golzern, was tested both with and without an artificially increased "wall" on the Wurzen side of the river, using the simulated 2013 flow hydrograph and the original DEM (i.e. same as 2013, but with the tunnels under the train bridge remaining open). The simulation with a wall along Wurzen produced maximum water surface elevations that were 2-3 cm higher at each of the eight observation points in the 2D flow area, compared to the simulation without the wall along Wurzen. The maximum water surface elevation at MB20 was also 2 cm, though that at LS6 was significantly higher, reaching 18 cm. Figure H.1 presents the differences in maximum water surface elevation for the simulation with the wall minus that without the wall.

H. Additional Results from Task 2

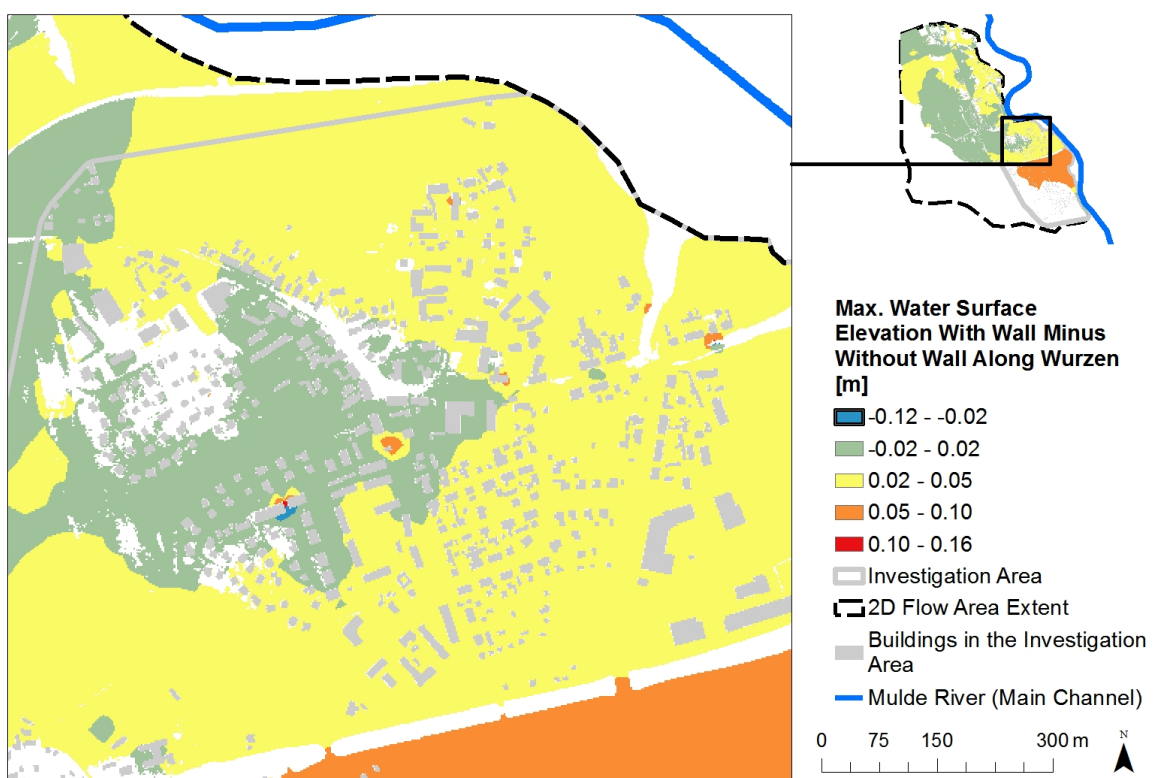


Figure H.1.: 1D/2D HEC-RAS unsteady flow model effect of wall along Wurzen on simulated maximum water surface elevation

Difference in elevation is calculated using the results from the simulation with the wall minus the simulation results without the wall.